LV-2013-017

Landsvirkjun

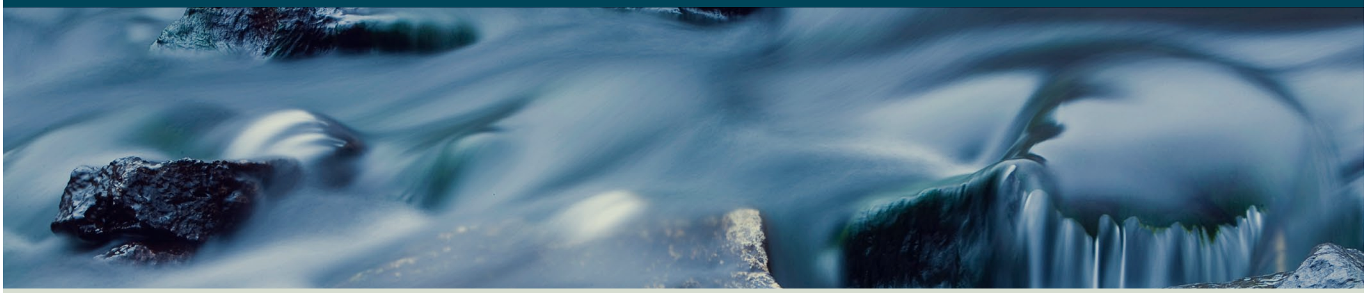

Urriðafoss HEP Lower Þjórsá Numerical Model Investigation of a Juvenile Fish Passage System

Landsvirkjun

Key page

LV report no:	LV-2013-017	Date:	March 2013

Number of pages: 94	Copies: 20	Distribution:	☒ On www.lv.is ☒ Open ☐ Limited until

Title: Urriðafoss HEP Lower Þjórsá
Numerical Investigation of a Juvenile Fish Passage System

Authors / Company: Gunnar Guðni Tómasson / Reykjavík Univ., Sigurður Magnús Garðarsson / Univ. of Iceland, Ágúst Guðmundsson / Univ. of Iceland and Andri Gunnarsson / Univ. of Iceland

Project manager: Helgi Jóhannesson

Prepared for: Landsvirkjun

Co operators: Verkís, Mannvit and Icelandic Maritime Administration

Abstract: In this report results of a numerical model investigation of the Urriðafoss HEP surface flow outlet (SFO) type juvenile fish passage system are presented. The approach flow conditions in the intake pond and the flow conditions inside the SFO conveyance channel are investigated to ensure safe and timely passage of juvenile salmon through the system. The numerical model used was the free surface model of ANSYS-CFX software. Improvements and technical optimizations of the original reference design are described. The results are compared with the results from a physical model built at a scale of 1:40. Description of the physical model investigation of the juvenile fish passage system is presented in a separate report LV-2013-016. This report is based on Ágúst Guðmundsson M.Sc. thesis, Gudmundsson (2013).

Keywords: Þjórsá, Urriðafoss, juvenile fish passage, numerical model, ANSYS-CFX.

ISBN no:

Approved by Landsvirkjun's project manager:

Helgi Jóhannesson

LV-2013-017

Urriðafoss HEP Lower Þjórsá
Numerical Model Investigation
of a Juvenile Fish Passage System

March 2013

Summary

The National Power Company of Iceland (LV), is planning to construct three power plants in the Lower Þjórsá River, Hvammur Hydro Electric Project (HEP), Holt HEP and Urriðafoss HEP. The projects are run of the river power plants with small intake ponds. Urriðafoss HEP is the lowest of the three projects utilizing the head between elevations of 50 m a.s.l. and 9.4 m a.s.l. The design discharge is 370 m^3/s providing installed capacity of approximately 128 MW, and energy-generating capacity of 980 GWh/a with two Kaplan turbines.

The University of Iceland and Reykjavík University joined forces in performing model tests at a scale of 1:40 to investigate and optimize the design of the spillway, downstream conditions and juvenile fish passage facility. In addition to the physical model study the flow characteristics of the intake pond and a Surface Flow Outlet (SFO) type juvenile bypass system were investigated using a 3D computational fluid dynamics (CFD) model and a 1:40 scale physical model. In addition the flow conditions inside SFO conveyance channel were evaluated in a separate CFD model. The intake pond and juvenile bypass system are a part of proposed hydroelectric power plant in the Lower Þjórsá River in Southern Iceland which is located in the migratory pathway of the North Atlantic Salmon. The approach flow conditions in the intake pond and flow conditions inside the SFO conveyance channel were investigated to ensure safe and timely passage of juvenile salmon through the system. Three cases of operational conditions were investigated for the approach flow conditions in the reservoir while the conveyance channel was evaluated with regard to four different discharge rates. The numerical model used was the free surface model of ANSYS-CFX software with a standard κ-ε turbulence model. The numerical results were compared and validated with the physical model results by comparison of velocity profiles from an Acoustic Doppler Velocimeter (ADV), particle tests, dye tests and visual observations from the physical model study. In general the SFO design and approach flow conditions prove to be effective in providing a safe and timely passage of juvenile salmon through the system. There is a good agreement between the results of the physical and the numerical models closest to the intake and spillway structures. Further upstream the results between the physical and numerical model started to differ due to minor inconsistencies between numerical and physical model topography.

Contents

List of figures

List of tables

1. Introduction

1.1. General Introduction

Of the river systems in Iceland the Þjórsá and Tungnaá river system has the greatest hydropower potential providing 27% of all economically viable hydroelectric energy in the country. The drainage area of the system is 7530 km^2 were 1200 km^2 are covered by glaciers characterising the river mainly as a surface runoff river with glacial and spring influences.

The development of the Þjórsá and Tungná river system started with commission of the Búrfell hydroelectric project (HEP) in 1969. Four additional power plants and extensive diversion systems in the uppermost part of the river system have been commissioned since then making the river highly regulated. In late 2013 the fifth power plant Búðarháls HEP will start operation utilizing the head between Hrauneyjafoss HEP and Sultartangi HEP.

Landsvirkjun is preparing construction of three hydroelectric power plants in the Lower Þjórsá River, Hvammur HEP 81 MW, Holt HEP 53 MW and Urriðafoss HEP 128 MW, shown in Figure 1.1. Because of the highly regulated characteristics of the Lower Þjórsá River no additional storage is needed for the projects.

The project furthest downstream, Urriðafoss HEP, utilizes the head difference between elevations of 50 m.a.s.l. and 9.4 m.a.s.l. The design discharge at Urriðafoss is 370 m^3/s with energy generating capacity of about 980 GWh/year.

The layout of the Urriðafoss HEP, shown in Figure 1.2, is in sense typical for a run of the river hydro electric plant with the exception of additional structures to aid the migration of salmon through the project. The additional structures to aid salmon migration are a Surface Flow Outlet (SFO) type juvenile fish bypass system, upstream fishway and a mandatory release structure to provide constant 10 m^3/s discharge in to the riverbed downstream of the dam. The powerhouse will be equipped with two minimum gap Kaplan turbines which are considered to be fish friendly (Gudjonsson & Johannesson, 2009).

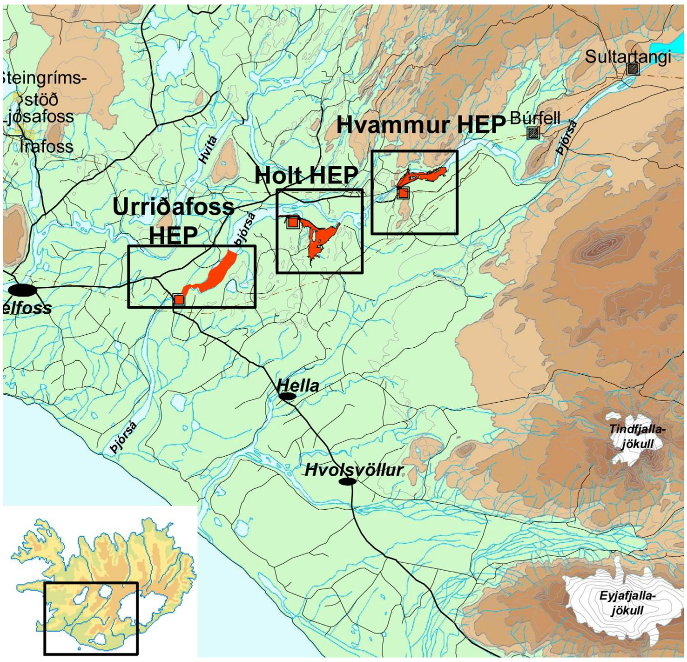

Figure 1.1: Overview of the Lower Þjórsá River hydroelectric projects (Landsvirkjun, 2010).

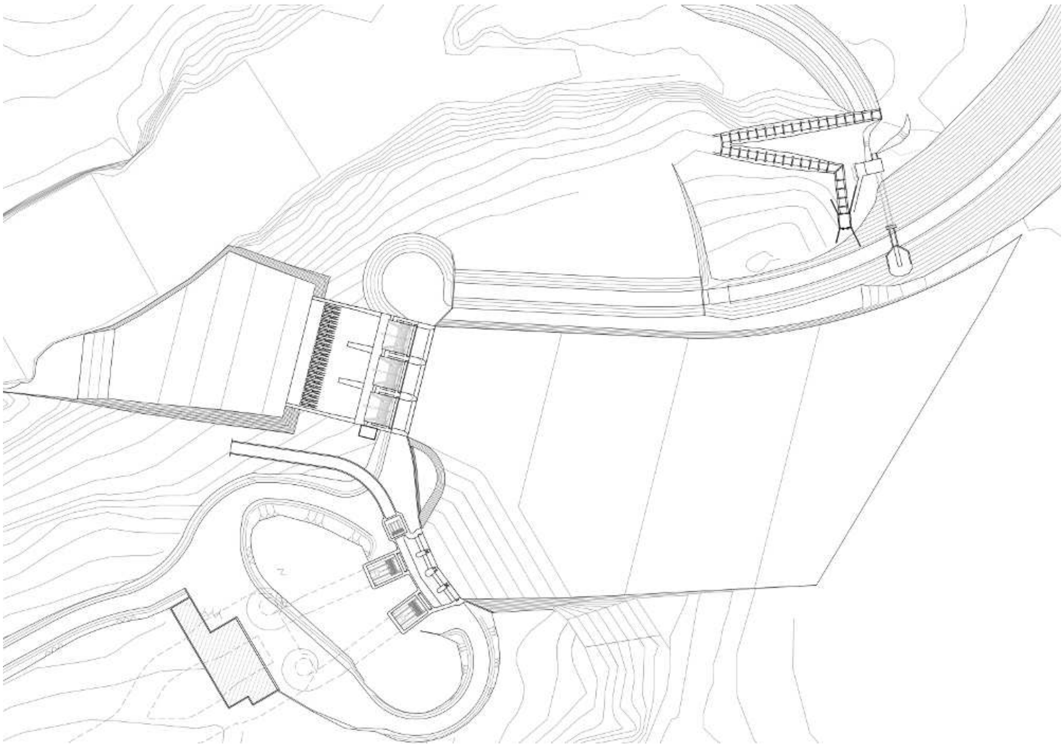

Figure 1.2: Overview of Urriðafoss hydroelectric project (Landsvirkjun, 2010).

A small 9 km^2 intake pond, Heiðarlón reservoir, is formed at Heiðartangi point with 7.5 km long dykes lying along the west bank of the river. Normal Reservoir Water Level (NRWL) is 50 m a.s.l. but during the design flood event the High Reservoir Water Level (HRWL) is 51.5 m a.s.l. The spillway structure consists of three radial gates with a roller bucket type energy dissipator.

The SFO is located above the turbine intake as shown in Figure 1.3 and has four 5.95 m wide entrances, each with a smooth rounded crest at an elevation of 49.1 m a.s.l. providing an estimated discharge of 40 m^3/s at NRWL. From the crest the water from the four entrances is united in a single sideway channel and routed through a 4.5 m wide concrete channel 90 m downstream of the dam to the original riverbed. The elevation difference between the entrance of the SFO and outfall is 8 m. The SFO is designed to transport the uppermost 1 m layer of water and to create favourable conditions to attract juvenile salmon towards the SFO entrance.

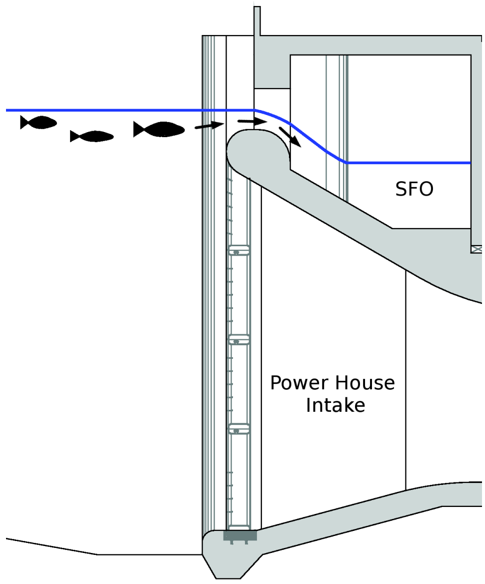

Figure 1.3: Schematic longitudinal view of SFO and power intake structures.

1.2. Motivation

In recent years environmental issues associated with the construction and operation of hydroelectric power plants have been receiving more and more attention. With the proposed Lower Þjórsá River hydroelectric projects outmigration of juvenile salmon becomes a factor in the design not encountered before in Icelandic hydroelectric projects. The limited experience provides ground for expanding the local knowledge base by seeking out global successes and factors necessary for a successful design. By identifying factors influencing the response of juvenile salmon to unnatural flow features associated with the operation of hydroelectric power plants necessary measures can be made to ensure successful operation and thus limit the overall impact of the project.

In the environmental impact assessment for the Lower Þjórsá River projects from 2003 mitigation measures are listed that are intended to sustain the natural salmon stock of the Þjórsá River. The mitigation measures consist of a mandatory release structure intended to maintain a minimum flow of 10 m^3/s (environmental flow) to the original riverbed downstream of the dam, an upstream fishway and a juvenile fish bypass structure for downstream migration of juvenile salmon.

The study presented in this report is part of the physical model study of the Lower Þjórsá River projects Hvammur HEP and Urriðafoss HEP carried out at the hydraulic laboratories of the Icelandic Marine Administration in Kópavogur, Iceland. The project is a collaboration of Landsvirkjun, the University of Iceland, the Reykjavík University, the Icelandic Marine Administration and the designers Mannvit and Verkís consulting engineers. The first phase of the project, the Hvammur HEP physical model, was built and tested through out the year 2011 (Tomasson et al., 2012). The model was the first physical model study to be conducted in Iceland in over twenty years. The second phase, the Urriðafoss HEP model test, was built and tested from February to August 2012. As part of the project three master thesis are carried out at the University of Iceland. From first phase Andri Gunnarsson carried out a study of the spillway at Hvammur (Gunnarsson, 2012), from that followed a full technical report (Tomasson et al., 2012) and a conference article (Gunnarsson et al., 2012). From the second phase two master thesis are carried out, a master thesis on the juvenile fish bypass facility carried out by Ágúst Guðmundsson (Gudmundsson, 2013) and a master thesis on the roller bucket type energy dissipator carried out by Gísli Steinn Pétursson. In addition from the second phase a full technical report on the physical model study (Tomasson et al., 2013) and a conference article (Gudmundsson et al., 2012) were released.

As a further expansion of the physical model study a numerical model of the juvenile bypass system and pond at Urriðafoss HEP was built. The numerical model and physical model are intended to compliment each other with the numerical model shedding light on delicate features in the approach flow and other features which are hard to quantify in the physical model. The results from both models represent a realistic indication of flow conditions expected on a prototype scale. Description of the physical model investigation is presented in a separate report LV-2013-016 (Tomasson et al., 2013).

1.3. Objective

The objective of this study is to evaluate the design of the proposed Surface Flow Outlet (SFO) type juvenile fish bypass system at Urriðafoss HEP using two models, a physical model and a numerical model. The models are compared and validated by various methods including comparison of velocity profiles and general flow behaviour from particle tests from the physical model study. The validated numerical model is in addition used to look into features hard or impossible to measure in the physical model which are important for evaluation of the design with regard to the juvenile salmon. The evaluation is mainly focused on approach flow conditions upstream of the SFO entrances and flow conditions inside the SFO conveyance channel where conditions are evaluated to ensure safe and timely passage of juvenile salmon.

1.4. Co-ordination Groups

Two co-ordination groups where established during the physical model study. The first group, the contractor group, was responsible for co-ordination of the model construction and time schedule for the project:

- Dr. Helgi Jóhannesson, Landsvirkjun.
- Prof. Sigurður Magnús Garðarsson, University of Iceland.
- Dr. Gunnar Guðni Tómasson, Reykjavík University.
- Mr. Pétur Sveinbjörnsson, Icelandic Maritime Administration.
- Mr. Andri Gunnarsson, Head of Laboratory.
- Mr. Gísli Steinn Pétursson, Laboratory Researcher.
- Mr. Ágúst Guðmundsson, Laboratory Researcher.

The second group was responsible for review of the physical model results of the SFO and suggest improvements. The group consisted of participants from the client, modelling group, designers and fisheries consultants:

- Dr. Helgi Jóhannesson, Landsvirkjun.
- Prof. Sigurður Magnús Garðarsson, University of Iceland.
- Dr. Gunnar Guðni Tómasson, Reykjavík University.
- Ms. Ólöf Rós Káradóttir, Verkís Engineering.
- Mr. Þorbergur S. Leifsson, Verkís Engineering.
- Mr. Einar Júlíusson, Mannvit Engineering.
- Dr. Sigurður Guðjónsson, Institute of Freshwater Fisheries.
- Mr. Andri Gunnarsson, Head of Laboratory.
- Mr. Gísli Steinn Pétursson, Laboratory Researcher.
- Mr. Ágúst Guðmundsson, Laboratory Researcher.

1.5. Literature Review

1.5.1. Behavior of Migrating Juvenile Salmon

The migration down river to sea is one of the major events in the life cycle of salmon. While still in freshwater juvenile salmon undergoes a transformation from freshwater dwelling parr to saltwater adapted smolt, a process known as smoltification (Seear et al., 2010). As juvenile salmon migrate downstream they tend to locate themselves in the middle of the stream where boundary effects are at a minimum and flow velocities are high to minimize delay, injury and the threat of predation (Goodwin et al., 2001). Migrating juvenile salmon are surface oriented and locate themselves in the uppermost part of the water column (Karadottir & Gudjonsson, 2009).

Migration of juvenile salmon in Icelandic rivers can take place from mid May to early August. The onset, duration and magnitude of the migration is highly dependent on environmental factors. Juvenile salmon migrate mainly, when light intensities are low, at night early in the summer or early in the day late in summer. In the south western part of Iceland increased flow in rivers, usually associated with warm southerly winds and rain, can stimulate the emigration of juvenile salmon. However in the rivers in the northern part of Iceland increased flow is usually associated with cold northerly winds which may in turn depress the juvenile salmon emigration. During colder years in the north fewer juvenile salmon may migrate and migration can be delayed until August. Juvenile salmon is generally older when it migrates in the north of Iceland and has a greater variety in annual mean length than in the south. The large variety of environmental conditions in Iceland is reflected in large variations of the size of juvenile salmon, timing and magnitude of juvenile salmon runs (Antonsson & Gudjonsson, 2002).

In the Lower Þjórsá river system migration of juvenile salmon begins annually in the middle of May and continues to the middle of June. Timing of migration differs between years because of environmental factors (Johannsson et al., 2002).

In an unregulated river the natural hydraulic cues that guide juvenile salmon to the optimum zone in the rivers cross section can separate from the bulk flow near dams where large, deep, slow eddies and sharp shear zones exist. As juvenile salmon enters the forebay of a dam it can become disoriented relative to the direction and depth of bulk flow (Goodwin et al., 2001). If juvenile salmon are delayed in the forebays of dams it can have adverse effect on their survival. The onset of migration is highly dependent on the temperature of the river, if delayed on their migration water temperatures down river may rise in the mean time. The elevated temperatures and effort in finding the appropriate way through the dam can leave juvenile salmon less energetic and less suited for live in the ocean (Marchall et al., 2011). Coutant and Whitney (2000) suggest that migrating juvenile salmon generally do not descend to the lower two thirds of the water column and only descend towards turbine intakes as a last resort mainly during night.

At the Dalles Dam the diel distribution of passage through the dam was more variable during summer than spring. Generally during spring and summer passage at the powerhouse turbine intakes peaked at dusk while sluiceway passage was somewhat higher during day than night (Johnson, 2006).

Johnson (2009) observed fish movement behaviour in front of the SFO entrance at the Dalles Dam using a dual-frequency identification sonar (DIDSON) and compared it to a steady state CFD model for a scenario with consistent dam operations. Schooling behaviour was dynamic and prevalent in front of the SFO entrance and the behaviour of individual fish was dependent on distance from the SFO entrance. Passive movement behaviour was only observed 5% of the time making active swimming the most common behavioural response. They also defined fish effort variables which they found to be correlated with water velocity, acceleration and strain.

Haro et al. (1998) compared behaviour and passage rate of smolts of Atlantic salmon and juvenile American shad between a standard sharp-crested weir and modified surface bypass weir, a so called NU-Alden weir. The NU-Alden weir employs uniform flow velocity increase 1 m/s per m in front of the weir. The uniform flow acceleration of the modified weir proved to pass significantly more Atlantic salmon smolts during the first 30 minutes but no differences were in passage rate between the weir types for juvenile American shad. Most individuals that passed the modified weir maintained positive rheotaxis (swimming against the current) and strong swimming through out the length of the weir.

Goodwin et al. (2001) set forth a hypothesis predicting the out-migrating fish behaviour called the Minimal Boundary Effect hypothesis (MBEH). The hypothesis is based on analysis of 3D fish tracks and first principles of fluid dynamics, sensory biology, fluvial geomorphology and evolution. The MBEH relates the response of juvenile salmon to specific features of the flow field and predicts that as juvenile salmon migrate down river they locate them self in the cross section of the river that is approximately equidistant from all boundary effects. There the importance of detecting boundary effects is stated as it is crucial for juvenile fish to travel with minimum delay, injury and the threat of predation.

1.5.2. Development of Downstream Fish Passage Systems

Development of efficient Downstream Migrant Systems (DMS) has been going on since the late 1960s when the U.S. National Marine Fisheries Service and the U.S. Corps of Engineers first developed turbine intake screens to guide juvenile salmon safely from turbine intakes (Helwig et al., 1999). In Washington State's Columbia River and Snake

River systems extensive research on the behaviour of migratory fish close to dams and design of more efficient DMS has been undertaken. This extensive research has generated considerable but often inconclusive results as to factors influencing migrant guidance and passage (Goodwin, 2003). Early bypass systems often achieved only limited and variable success at considerable cost because migrants either could not locate the bypass entrance or simply rejected it once they were within it's hydrodynamic influence (Weber et al., 2006). Poor performance of bypass collectors designs is most commonly the result of the uncertainty about the necessary flow characteristics to attract migrants to the vicinity of the collector and entice them to enter (Goodwin, 2003).

Schilt (2006) defines the routes of fish passage through hydropower dams as turbine passage, juvenile bypass system passage, spillway passage and surface passage.

Passage of migrants through turbines is generally considered the passage most likely to injure or kill fish. Not all fish are injured or killed as they pass through turbines, the mortality rate or injury can vary with time of year, species, age, water temperature, turbine type and other factors. Mechanisms which can injure or kill migrants include pressure changes, shearing between different moving water masses, impact with turbine or dam structures, cavitation, grinding and abrasions. A great deal has gone into making turbines more fish friendly (Schilt, 2006).

Most bypass systems for juvenile salmon at major hydroelectric projects involve screening juveniles from deep turbine intakes (Coutant & Whitney, 2000). The screens located in the turbine intakes of dams, usually rotating conveyor belt like mesh screens, are designed to deflect flow and fish to the upper portion of the turbine intake and upward into a passage called a gatewell slot, a vertical passageway. From the gatewell slot the fish is then passed through an orifice into a juvenile bypass system, were the actual bypass is often a modification of ice and sluiceways (Schilt, 2006).

Passage of migrants through spillways is considered the most benign passage route for juvenile salmon. Disadvantages of spill include elevated dissolved gas downstream which can stress or kill fish as well as reducing swimming performance and resistance to pathogens. Spillway operations also have the drawback of large amount of spill that is foregone power generation (Schilt, 2006).

Surface passage routes or surface flow outlets (SFO) are designed to collect fish near the surface of near-dam forebay and pass the fish into the tailrace. The design is considered cost effective in terms of fish passage and discharge. In the Columbia and Snake river systems too few fish use these routes, relatively small portion of the total downstream migration passes. If the system and design work properly this is thought to be the most benign option of downstream migrant passage system (Schilt, 2006).

Since 1981 the USACE has been collecting juvenile salmon from bypass systems of several dams. The bypass is partially dewatered and rather elaborate system of gates enable the fish to be bypassed to be released directly into the dam's tailrace or diverted and held for separation, examination and tagging and sometimes for transportation by barge or truck downstream past the last dam (Schilt, 2006).

In the 1970s and early 1980s, researchers showed that sluiceways at Bonneville, Ice Harbour and the Dalles Dams passed relatively high proportion of smolts in a relatively low proportion of the flow (Johnson, 2009). These results and observed behavioral patterns of migrating smolts have directed the attention more towards surface bypass structures. In 1995 a major USACE program was initiated to further the development of SFO and SFO prototype structures. In reviews of operations of the new designs concerns were commonly expressed regarding the lack of understanding of the relationship between fish behavior and flow field close to SFO entrances (Johnson, 2009).

Initial SFO designs and operations focused on finding the optimum entrance plume velocity that would entice migrants into the SFO. Water acceleration has in recent years become an attribute of increasing interest though research into its influence is relatively scant (Goodwin, 2003). Haro et al. (1998) studied the response of Atlantic Salmon to accelerating flow fields in vicinity of two weir designs, sharp crested weir and NU-Alden weir. Their results suggest that migrants may be reluctant to enter bypass collectors because of unnatural transition conditions of accelerating water velocity.

SFO designs have a wide variety, Sweeney et al. (2007) define five types of SFO classified by the entrance flow regime. In subcritical flow regime there are low-flow bypasses/sluices, forebay collectors and powerhouse retrofits. Low-flow bypasses/sluices are found at small dams in rivers which have relatively small discharge, they usually have only one entrance measuring about 1 m wide and 1 m deep. Forebay collectors are associated with high head dams where fish is collected in the forebay and conveyed downstream past the dam, entrances of forebay collectors can be large. Powerhouse retrofits are structures built onto the forebay face of powerhouses and have a great variety in size and number. Under critical flow conditions fall high flow sluices and surface spills. High-flow sluices are at dams with relatively high discharges and were originally intended to manage ice and debris but can also be used as fish protection devices. Entrances to high-flow sluices are usually wide (3 to 7 m) and shallow, (1 to 3 m) or deep (5 to 10 m). Surface spills are surface outlets at spillways and vary in design with designs such as notched-spill gates, surface flap gates, removable spillway weirs and bulkheads or stop logs to produce to spill. Usually there is only one wide but relatively shallow entrance, 15 m wide and 4 m deep.

Two hydroelectric power plants in the U.S. have design comparable to the proposed design at Urriðafoss power plant. The two plants are the Wells Dam on the Columbia river and Cowlitz Falls in the Cowlitz river Washington State. Both power plants are a hydrocombine type powerplants. In a hydrocombine design the spillway and SFO are located above the power intake.

Wells Dams started operation in 1967, the power plant is a run of the river plant with mean discharge of 6230 m^3/s and installed power generating capacity of 840 MW. The SFO at Wells Dam was developed in the years 1983 to 1990 and is one of the most successful SFO located on the Columbia river. Research at Wells Dam has showed that up to 89% of juvenile salmon goes into the SFO and their mean survival rate is about 96% (Sweeney et al., 2007).

The Cowlitz Falls powerplant started operation in 1994. It has a mean discharge of 150 m^3/s and installed power generating capacity of 70 MW. The SFO at Cowlitz Falls was built at the same time as the dam and was designed with the successful SFO at Wells Dam in mind. The SFO at Cowlitz Falls has not proved as successful as the SFO at Wells Dam which is considered to be the cause of irregularities in the flow field in front of the SFO entrance. Research has shown that only 48% of juvenile steelhead salmon has entered the SFO at Cowlitz Falls and the success for other species is less. No research is available on the survival rate of juvenile fish at Cowlitz Falls. In recent years considerable effort has been put into making the SFO at Cowlitz Falls more successful (Sweeney et al., 2007).

1.5.3. Numerical Models

The increased capability of computers in resent years has made it possible to tackle more complex numerical problems than before. Numerical modeling in fluid dynamics or Computational Fluid Dynamics (CFD) models have been evolving in the past decades and to date the range of commercially available CFD software is quite extensive. The use of CFD models in design of hydraulic structures is widespread and gives the opportunity to evaluate flow conditions in more detail than is possible in a physical model.

CFD models have been used quite a lot in the U.S. to evaluate downstream fish passage design and flow conditions in and around downstream fish passage structures. CFD models have been made both to evaluate change in forebay hydraulics caused by retrofitted structures or to evaluate new design.

Meselhe and Odgaard (1998) developed a numerical flow model for evaluating different fish bypass systems at the Wanapum Dam on the Columbia River, Washington. Results were compared with 1:16 scale physical model of the powerhouse intake bay. The model was found to reproduce accurately all of the flow conditions important for evaluation of a fish diversion system.

Khan et al. (2008) used a 3D CFD model to model forebay hydraulics of the Dalles Dam Oregon for existing configuration and proposed trashracks. The trashracks were expected to reduce flow velocity near the powerhouse which was thought to be responsible for attracting juvenile salmon into the turbine intake. The model was validated using measurements from location and 1:40 scale physical model. The model confirmed the reduction in flow velocity caused by the proposed structures.

Lee et al. (2008) modelled free surface flow of two conceptual fish passage designs using level-set finite-element method. The two conceptual designs differed in shape at the entrance of the fish passage where one had right-angled entrance from the reservoir to the fish passage chute and the other a curved shaped entrance. The numerical results were compared and validated using a 1:24 scale physical model through comparison of the free surface location and the pressure distribution in the spillway. The results favoured the curved shape concept were flow transition was smooth with small strains whereas the right angled concept yielded a curved free surface at the entrance and pressure distribution in the vicinity of the entrance due to large strains.

CFD models have also been used to predict movement of fish in forebays of dams. Acoustic-tag telemetry and fixed-location multi-beam hydroacoustics of swimming paths of fish have been compared to hydraulic conditions obtained from CFD models to find relations between fish behaviour and different hydraulic conditions. Goodwin et al. (2006) made a model which forecasted 3D fish movement using Eulerian-Langrangian-agent method where hydraulic patterns were calculated using 3-D unsteady, unstructured Reynolds averaged Navier Stokes model U^2RANS. The hydrodynamic pattern from the CFD model was then used to evaluate fish movement behaviour using a numerical fish surrogate that embodied the strain, velocity, pressure hypothesis of fish movement behaviour (Goodwin, 2003). The model was compared and validated to measured behaviour and hydraulic conditions at two hydropower dams.

2. Methods

2.1. Theory

The theory and equations presented in this section are derived from the ANSYS Solver Theory manual (ANSYS, 2011).

2.1.1. Governing Equations

The set of governing equations solved by ANSYS CFX are the Reynolds-averaged Navier-Stokes equations in their conservation form. The continuity equation is expressed as

$$\frac{\partial \rho}{\partial t} + \nabla \cdot (\rho U) = 0 \tag{2.1}$$

where ρ is density and U is velocity magnitude. The momentum equations are defined as

$$\frac{\partial (\rho U)}{\partial t} + \nabla \cdot (\rho U \otimes U) = -\nabla p + \nabla \cdot \tau + S_M \tag{2.2}$$

where p is static pressure, S_M a momentum source and τ the stress tensor which is related to the strain rate by

$$\tau = \mu \left(\nabla U + (\nabla U)^T - \frac{2}{3} \delta \nabla \cdot U \right) \tag{2.3}$$

where μ is dynamic viscosity, T static temperature and δ the Kronecker delta function. The last of the governing equations the total energy equation is expressed as

$$\frac{\partial (\rho h_{tot})}{\partial t} - \frac{\partial p}{\partial t} + \nabla \cdot (\rho U h_{tot}) = \nabla \cdot (\lambda \nabla T) + \nabla \cdot (U \cdot \tau) + U \cdot S_M + S_E \tag{2.4}$$

where λ is thermal conductivity, S_E is an external energy source and h_{tot} is the total enthalpy. The term $\nabla \cdot (U \cdot \tau)$ represents the work due to viscous stresses and is called the viscous work term. The term $U \cdot S_M$ represents work due to external momentum sources and is currently neglected. The total enthalpy h_{tot} is related to the static enthalpy $h(T, p)$ by

$$h_{tot} = h + \frac{1}{2} U^2 \tag{2.5}$$

For further details of ANSYS CFX solver theory see (ANSYS, 2011).

2.1.2. Turbulence Models

Turbulence can be described as fluctuations in a flow field in time and space. The process is very complex and occurs when inertia forces exceed viscous forces in a fluid at high Reynolds numbers. Turbulence length and time scales at realistic Reynolds numbers span a large range, the smallest much smaller than the finest finite volume mesh. Though the Navier-Stokes equations describe both laminar and turbulent flow without additional information, the process of solving the equations directly is impractical and would require computing power of an order of magnitude higher than is available today. Thus great amount of research in numerical modelling has gone into predicting turbulence with the use of turbulence models. The turbulence models have been developed to account for the effects of turbulence without extremely fine mesh and direct numerical simulation and are in most cases statistical models (ANSYS, 2011).

The turbulence model used in this study is the k-ε turbulence model of CFX, for further details see (ANSYS, 2011).

2.1.3. Volume of Fluid Method

ANSYS CFX uses the Volume of Fluid (VOF) method for spatial discretisation of the domain in solution of the free surface flow. The VOF method was first introduced by Hirt and Nichols (1981) and is today widely used in commercial CFD codes such as ANSYS CFX, FLUENT, STAR-CD and Flow-3D.

The VOF method uses a function for each computational cell which describes the volume fraction of phase α in the cell. In each cell the volume fraction for all phases occupying the cell must sum up to unity. Thus if the volume fraction of phase α in a particular cell is equal to unity the cell is full of fluid α and on the contrast if the volume fraction of phase α equals zero the cell is empty.

In ANSYS CFX two sub-models are available for Eulerian-Eulerian multiphase flow, the homogeneous model and the inter-fluid transfer inhomogeneous model. In the case of the inhomogeneous multiphase flow model separate velocity fields and other relevant fields exist for each fluid while the pressure field is shared by all fluids. There the fluids interact via interphase transfer terms. For further details see (ANSYS, 2011).

In the simpler homogeneous multiphase flow model used in this study all relevant fields such as velocity, temperature, pressure, turbulence etc. are shared by all fluids. In the homogeneous model the assumption is made that transported quantities (with the exception of volume fraction) are the same for all phases as follows

$$\varphi_\alpha = \varphi \quad 1 \leq \alpha \leq N_P \tag{2.6}$$

where φ is a general scalar variable, α indicates phase α and N_P is the total number of phases. Because transported quantities are shared the shared fields can be solved using bulk transport equations instead of solving individual phasic transport equations. The bulk transport equations are derived by summing the individual phasic transport equations over all phases into a single transport equation for φ

$$\frac{\partial}{\partial t}(\rho\varphi) + \nabla\cdot(\rho U\varphi - \Gamma\nabla\varphi) = S \tag{2.7}$$

where ρ is density, U velocity, Γ is diffusivity defined and expressed in terms of volume fractions r of phase α as

$$\rho = \sum_{\alpha=1}^{N_P} r_\alpha \rho_\alpha \tag{2.8}$$

$$U = \frac{1}{\rho}\sum_{\alpha=1}^{N_P} r_\alpha \rho_\alpha U_\alpha \tag{2.9}$$

$$\Gamma = \sum_{\alpha=1}^{N_P} r_\alpha \rho_\alpha \Gamma_\alpha \tag{2.10}$$

The momentum equation of the homogeneous model assumes

$$U_\alpha = U \quad 1 \leq \alpha \leq N_P \tag{2.11}$$

The momentum equation becomes

$$\frac{\partial}{\partial}(\rho U) + \nabla\cdot\left(\rho U \otimes U - \mu\left(\nabla U + (\nabla U)^T\right)\right) = S_M - \nabla p \tag{2.12}$$

where μ is dynamic viscosity expressed in terms of volume fraction and phase as

$$\mu = \sum_{\alpha=1}^{N_P} r_\alpha \mu_\alpha \tag{2.13}$$

The continuity equation with volume fractions taken into account becomes

$$\frac{\partial}{\partial t}(r_\alpha \rho_\alpha) + \nabla\cdot(r_\alpha \rho_\alpha U) = S_{MS\alpha} + \sum_{\beta=1}^{N_P} \Gamma_{\alpha\beta} \tag{2.14}$$

where $S_{MS\alpha}$ describes user specified mass sources and $\Gamma_{\alpha\beta}$ the mass flow rate per unit volume from phase β to phase α. This term only occurs if interface mass transfer takes place. The homogeneous volume conservation equation is simply the constrain that the volume fractions sum to unity

$$\sum_{\alpha=1}^{N_P} r_\alpha = 1 \tag{2.15}$$

Combining equation with the continuity equation yields the volume continuity equation solved by the CFX-Solver

$$\sum_\alpha \frac{1}{\rho_\alpha}\left(\frac{\partial}{\partial t}(r_\alpha \rho_\alpha) + \nabla\cdot(r_\alpha \rho_\alpha U)\right) = \sum_\alpha \frac{1}{\rho_\alpha}\left(S_{MS\alpha} + \sum_{\beta=1}^{N_P} \Gamma_{\alpha\beta}\right) \tag{2.16}$$

For further details see (ANSYS, 2011).

2.1.4. Numerical Solver

The coupled solver of ANSYS CFX was used which solves the hydrodynamic equations (for u, v, w, p) as a single system. The coupled solver uses a fully implicit discretization of the equations at any given time step which for steady state problems the time step acts as an acceleration parameter to guide the approximate solutions in a physically based manner to a steady state solution. This approach reduces the number of iterations required for convergence to a steady state (ANSYS, 2011).

2.2. SFO Conceptual Framework

In reviews of SFO development and performances Johnson and Dauble (2006) and Sweeney et al. (2007) use the conceptual framework of SFO to evaluate the effectiveness of SFO design and operation. The conceptual framework defines five zones that correspond to characteristics in hydraulics and fish behavior in the vicinity of hydroelectric projects and SFOs, see Figure 2.1. In the forebay region are three zones; the approach, discovery and decision zones. On the other side of the SFO entrance are the conveyance and outfall zones.

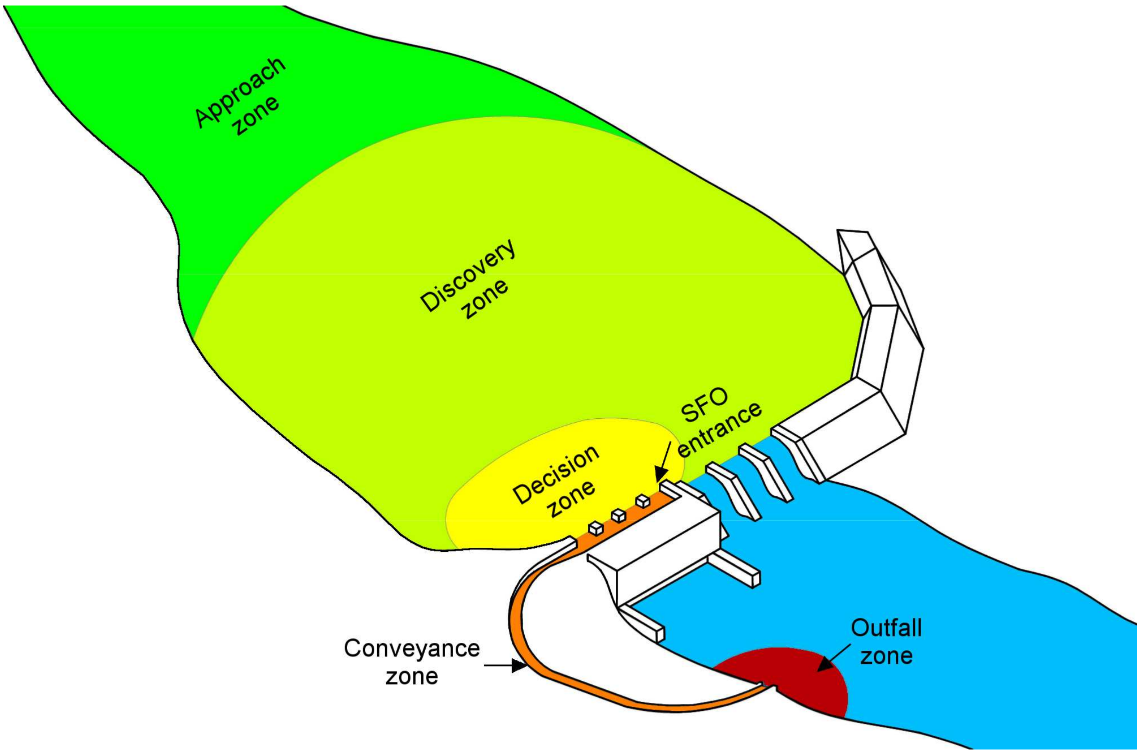

Figure 2.1: Schematic view of zones at an hydroelectric project corresponding to characteristics in hydraulics and fish behaviour.

The **Approach zone** is located at an distance of 100-10000 m from the SFO entrance. In the approach zone juvenile salmon follow the bulk flow as they approach the dam. The distribution of juvenile salmon reflects the distribution upstream in the reservoir, juvenile salmon tends to be surface oriented with densities usually highest in the main channel. At sites were the bulk flow splits in different directions the population of juvenile salmon splits also which can in some cases result in fish not encountering the SFO attraction flow. Swimming in the approach zone consist both of active swimming downstream and passive drift. Principal features of the approach zone are channel depth, channel shape, discharge, shoreline features and current pattern.

The **Discovery zone** is located at a distance of 10-100 m from the SFO entrance. This is where the juvenile salmon first encounter the SFO attraction flow in the forebay. The attraction flow of the SFO is characterised by gradual acceleration of water velocity towards the SFO entrance. The location at which the effects of the SFO attraction flow start to emerge is highly dependent on the hydraulic characteristics of the forebay and flow into the SFO. The distribution of juvenile salmon in the discovery zone is variable, juvenile salmon is mainly surface oriented as before but horizontal distribution is influenced by approach path and dam operations. As in the approach zone juvenile salmon mainly follows the main current but may meander or mill as it comes closer to the dam showing less direct behavioural pattern than upstream. Turbine operations can create strong downward flow component in the discovery zone. Juvenile salmon can pass a dam through turbines with out ever discovering the SFO attraction flow. The main features of the discovery zones are forebay bathymetry, structures, velocity gradients (from spill and turbine loading), sound and light. Juvenile salmon discover the SFO attraction flow because migration is active, vertical distribution is surface oriented, horizontal distribution is concentrated in front of the SFO, SFO attraction flow is distinct from other project flow and juvenile salmon prefer shallow over deep passage at dams.

The **Decision zone** is the zone immediately upstream of the SFO entrance, 1-10 m from the entrance. In the decision zone juvenile salmon decide to enter or reject the SFO entrance. The flow starts to accelerate more rapidly towards the SFO entrance. Fish response to the SFO entrance depends on principal features such as velocity, acceleration, strain, turbulence, structures, sound, light and other fish. For a successful design SFO entrance conditions must not cause an avoidance response before the fish is entrained into the SFO.

The **Conveyance and outfall zones** are where the fish is conveyed through the dam and to the tailwater downstream of the dam.

2.3. SFO Design Guidelines and Criteria

Design guidelines and criteria used to evaluate the SFO design at Urriðafoss dam are based on standards from published articles and regulations from the National Oceanographic and Atmospheric Administration (NOAA) in the US.

2.3.1. Design criteria upstream of SFO entrance

Johnson (2009) suggests the total discharge through the SFO is at least 7% of the total project discharge that includes discharge to turbines, discharge of SFO, mandatory release and spill. In general the importance of smooth flow conditions, no rapid change in flow, upstream of SFO is expressed. Gradual acceleration towards the SFO of 1 m/s per meter just upstream of the SFO entrance. No irregularities should exist in the approach flow such as stagnant zones with deceleration, local areas were flow abruptly accelerates or sharp shear zones which can lead to juvenile salmon rejecting the SFO entrance. In order to make the juvenile salmon discover the SFO attraction flow as soon as possible the SFO attraction flow should expand as far upstream as possible.

Johnson (2009) suggest flow velocity at an SFO entrance should be not less than 3 m/s to capture the juvenile salmon but Johnson and Dauble (2006) suggest mean flow velocity at SFO entrance not less than 2 m/s. The depth of flow over the SFO crest should not go under 0.3 m were discharge is more than 0.7 m^3/s (NOAA, 2008).

2.3.2. Design criteria in SFO and conveyance channel

Sweeney et al. (2007) state in their review of SFO design and function that design of conveyance channels for SFOs in the States are usually designed by regulations and standards of NOAA. The following criteria is based on NOAA regulations (NOAA, 2008).

The travel time inside the conveyance system should be minimized by limiting the length of the conveyance system and ensuring sufficient flow velocity of 2 - 4 m/s for all flow conditions. All changes of flow conditions, direction or transitions should be smooth. The walls and invert of conveyance system should be smooth with no sharp corners or edges which fish can collide with and be injured. Sharp corners and edges inside the conveyance system can also produce vortices were debris and sediment can accumulate which can be harmful for fish. To minimize sediment accumulation velocities should be maintained above 0.6 m/s. Local acceleration inside the conveyance channel should not exceed 0.3 m/s per meter and no areas of deceleration should exist. If the conveyance system has a circular cross section, depth of water in the cross section should never be less than 40%

of the diameter of the circular cross section. A hydraulic jump should never occur inside the conveyance channel, the flow should in all cases be free surface flow and fish should never endure free fall inside the channel. Pressure inside the system should never be less than atmospheric pressure.

In the NOAA regulations the aforementioned criteria is to be considered for bypass structures with discharges up to 28 m^3/s. For larger discharges the design should be done with direct engineering involvement of the National Marine Fisheries Service (NMFS) (NOAA, 2008).

(Bell, 1990) and (NRCS, 2007) list principal features for a successful fish bypass design. In general the listed features are in accordance with those presented in the NOAA regulations and include smooth surfaces and flow transitions with no hydraulic jumps forming inside the channel.

2.3.3. Design criteria at outfall

The outfall of the SFO conveyance channel should be located at a location downriver were the velocity in the river is more than 1.2 m/s, where no vortices or reverse flow exist. The outfall should be located were sufficient depth is in the river to prevent injury of fish due to collision with riverbed. Maximum velocity at outfall, including both vertical and horizontal components of velocity, should not exceed 7.6 m/s (NOAA, 2008).

2.3.4. Summary of design criteria

The following is a summary of design values and criteria presented in sections 2.3.1 to 2.3.3 used to evaluate the effectiveness of the Urriðafoss HEP layout and design.

- Upstream of SFO
  - Flow to SFO at least 7% of total flow in the system
  - Smooth flow and acceleration
  - Smooth acceleration, about 1 m/s per meter just upstream of SFO entrance
  - No null zones or deceleration
  - Flow velocity at SFO entrance > 2-3 m/s
  - Depth at SFO crest > 0.3 m if discharge is more than 0.7 m^3/s
- In SFO conveyance channel for design discharge up to 28 m^3/s
  - Minimize travel time in conveyance channel
  - Free surface flow
  - Ensure 2-4 m/s flow velocity for all discharges

  - Conveyance channel should be as smooth as possible, no intrusions, sharp corners or rough walls
  - Ensure sediment or debris can not accumulate in channel
  - No deceleration or local acceleration more than 0.3 m/s per meter
  - No hydraulic jump inside channel
  - Pressure larger than or equal to atmospheric pressure

- Outfall
  - Locate were flow velocity in river is more than 1.2 m/s
  - No vortices or reverse flow
  - Sufficient depth eliminating potential collision of juvenile salmon with riverbed
  - Maximum velocity of 7.6 m/s

2.4. Numerical Model

2.4.1. Geometry

The geometry of the intake and SFO structure, the spillway and the approach channel are designed by Verkís engineering consultants. Planar and detail drawings from the designers are used to construct a three dimensional model of the topography and structures using Autodesks Autocad 2012 and Inventor Professional 2012.

The topography and structures were modelled separately in the beginning but in final stages combined in Inventor. The topography was made using contour lines with 1 m elevation interval. Most of the land that the future intake pond will cover is today under the Þjórsá River. No bathymetry measurements exist of the river from Heiðartangi point to Ferjutangi point, the area covered by the numerical domain. During an ice formation study for Þjórsá River (Hrafnsdottir & Freysteinsson, 2009) cross sections were estimated for use in a HEC-RAS model used in the study. The estimated cross sections from the ice study were used in construction of the reservoir topography. The topography of the reservoir was constructed using Autocad Civil 3D, elevation lines were used to construct a surface of the topography. To be able to connect the topography to the structures and approach channel made in Inventor, the topography surface had to be converted to a solid body. The surface topography consisted of triangular elements, in order to convert the surface to a solid body type the surface elements were detached and all the element were extruded in towards the same plane. Finally the extruded parts were all united into a single solid body.

The intake and spillway structures were modelled in Inventor using planar and cross section detail drawings of the structures. Because of the complexity of the structures a great effort was put into making them in as simple manner as possible. Topography, approach channel and structures were combined into a single solid using Inventor, as shown in Figures 2.2 and 2.3.

The final stage in preparation for meshing is to extract the fluid volume from the geometry. A second solid is made which covers the whole domain and the topography solid subtracted from the second solid, see Figures 2.4 and 2.5.

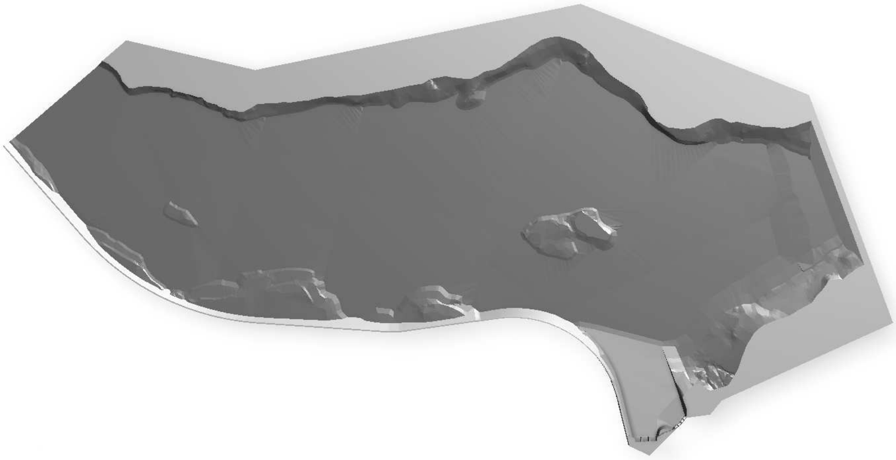

Figure 2.2: Overview of 3D model of Heiðarlón reservoir and structures used in numerical model computation.

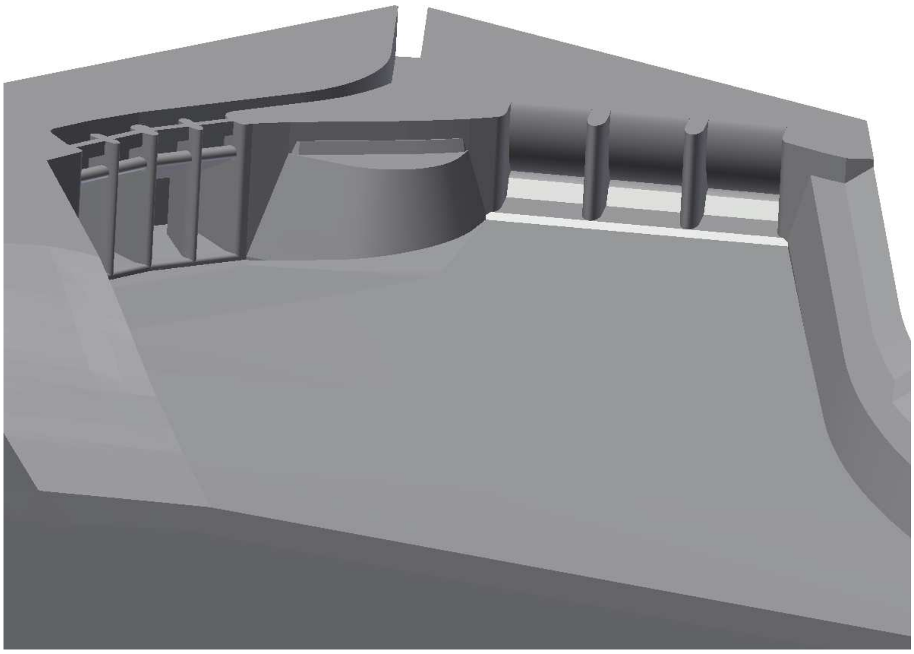

Figure 2.3: Overview of approach channel and structures.

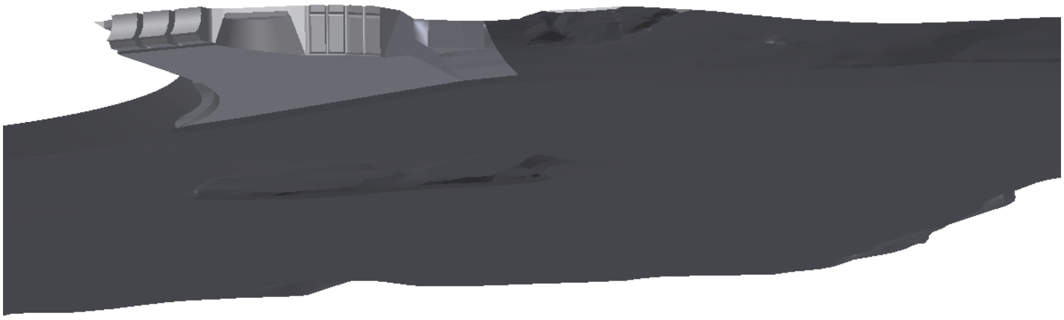

Figure 2.4: Volume of fluid subtracted from geometry of reservoir used as input for meshing process.

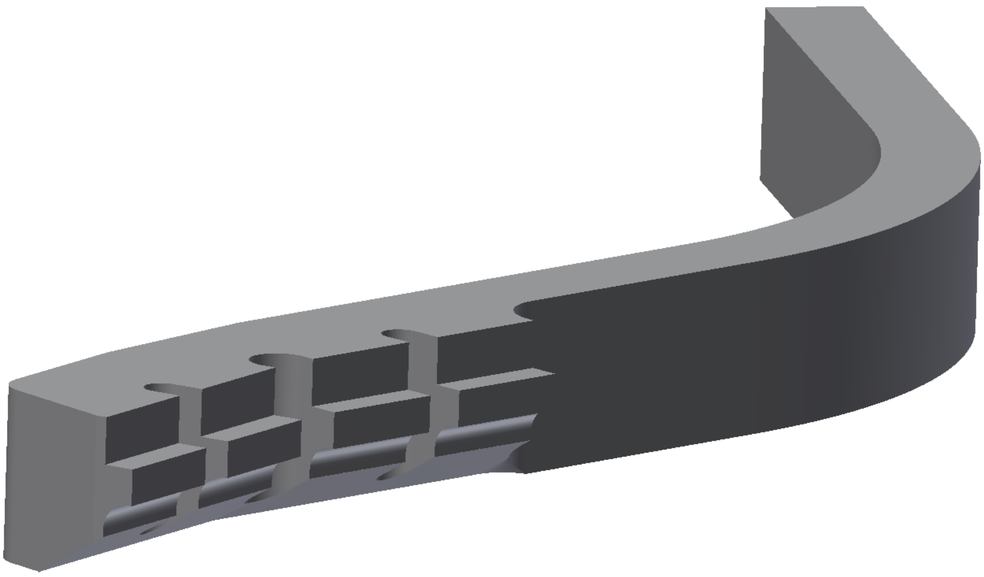

Figure 2.5: Volume of fluid subtracted from SFO model geometry used as input for meshing process.

2.4.2. Mesh

ANSYS ICEM CFD was used for the mesh process. ICEM CFD has a variety of tools for hex mesh generation and manipulation. The use of a hexahedral mesh makes it possible to limit the number of elements to a great extent making the grid denser around areas of interest such as the free surface boundary. Because of the complex nature of the topography an O-grid type mesh was used closest to the surface boundaries in the reservoir model. The modification of a single block to an O-grid block consists of dividing a single block down to five smaller blocks, seven in 3D, as shown in Figure 2.6. The grid lines are arranged into an "O" shape to reduce skew where a block corner lies on a continuous curve or surface. The reservoir mesh was made coarse at the inlet boundary and in the reservoir but was gradually refined in the approach flow channel towards the SFO entrances as shown in Figure 2.7. The vertical distribution of mesh was also refined at the air - water interface over the whole domain of both the reservoir model and the SFO model as shown in Figures 2.8 and 2.9. The reservoir mesh consisted of 1.866.768 hexahedron elements and 1.930.440 computational nodes while the SFO model consisted of 963.380 hexahedron elements and 1.010.460 computational nodes. Overview of the SFO mesh is shown in Figure 2.10

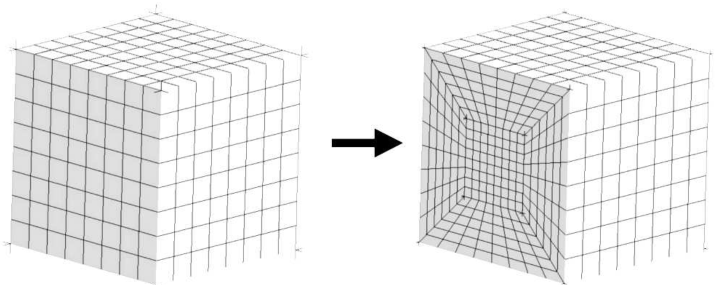

Figure 2.6: Transformation of a single block to O-grid block.

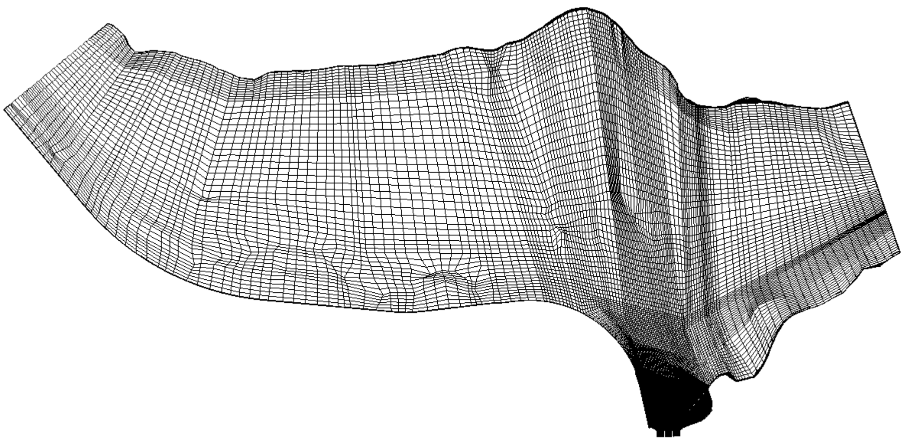

Figure 2.7: Top view of reservoir mesh.

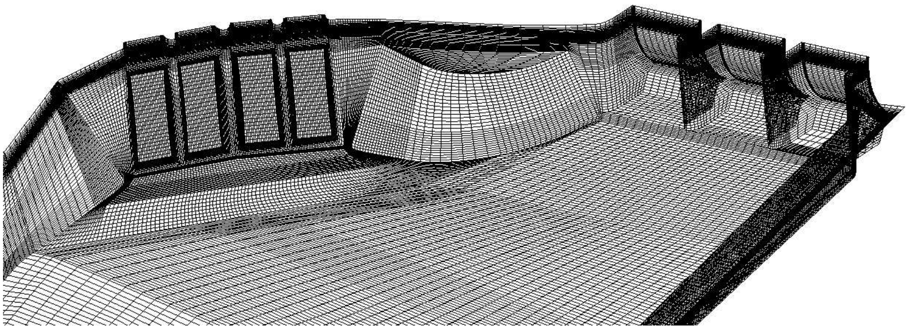

Figure 2.8: Overview of approach flow channel mesh.

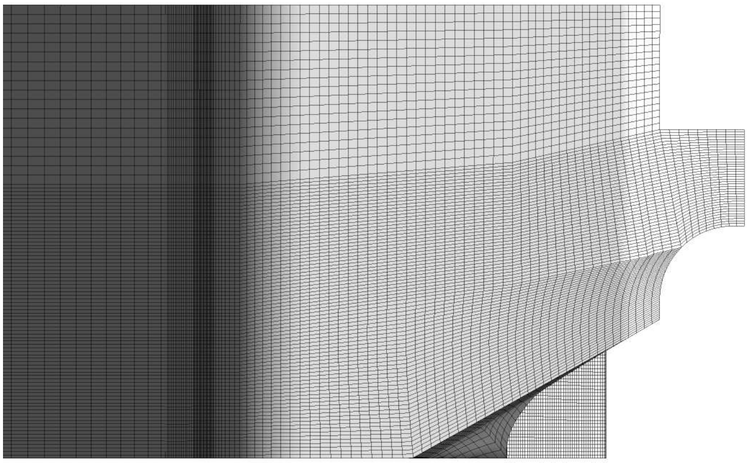

Figure 2.9: Side view of SFO mesh.

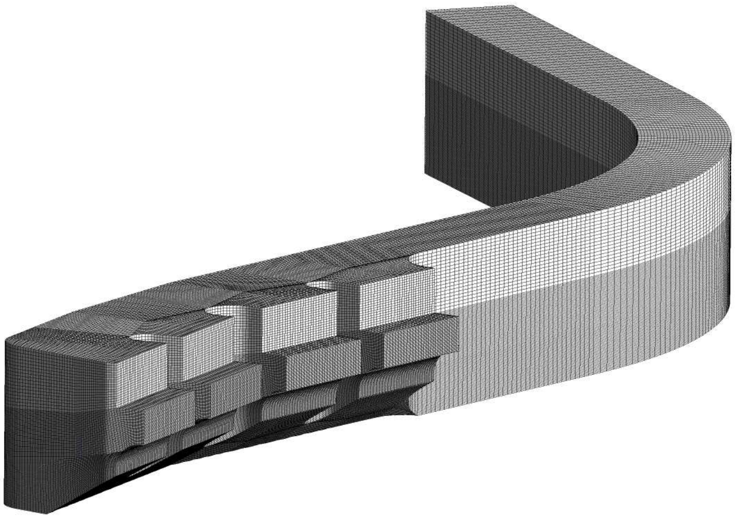

Figure 2.10: Overview of SFO mesh.

2.4.3. Solver set up

CFX PRE is the preprocessing part of CFX where all physical properties, boundary conditions, initial conditions, solver set up etc. are defined. The first step in the set up is to define expressions using the CFX Expression Language (CEL), CEL expressions are used to define the water elevation at inlet and outlet boundaries. The water elevation is defined as a static pressure boundary with the static pressure as a function of volume fraction of water. The predefined *step* function is used to determine the volume fraction in each cell as

$$\alpha_{air} = step((y_i - H)/1\,[m]) \tag{2.17}$$

where α_{air} is the volume fraction of air, y_i is the elevation at location i and H is the predefined water elevation. The *step* function takes a value of 0 for negative values, 0.5 for a value of 0 and 1 for positive values. For all values under H the volume fraction of air is 0 and at the boundary where $y_i = H$ the volume fraction of air is 0.5 etc. The volume fraction of water α_{water} is defined as

$$\alpha_{water} = 1 - \alpha_{air} \tag{2.18}$$

The physical properties of the numerical domain are then defined, the two fluids air and water are predefined with normal properties, for the water phase a buoyancy model is activated and a κ–ε turbulence model selected. The two models in this study the reservoir and the SFO models have similar boundary conditions. The reservoir model has extra outlet boundaries for the power intakes and the spillway gates. The inlet boundaries are defined as a velocity inlets, with normal speed divided uniformly over the boundary. For the inlet boundary the volume fractions of both fluids are also defined and the turbulence option set as zero gradient. For the SFO outlets a static pressure boundary is defined (critical depth). The outlets for the power intakes and spillways are defined as mass flow outlets where the total mass flow to the turbines is divided evenly between the four outlets. The top of the numerical domain is defined as an opening boundary where the volume fraction of air is always one but water always zero. The topography and walls of the structures are defined as no–slip walls, smooth with no roughness.

When the boundary conditions have been defined initial conditions and the solver set up is defined. As an initial condition a pressure condition is defined corresponding to NRWL in all the numerical domain. Initial flow velocities were defined as automatic.

For the solver control a first order advection scheme was used for both models. For Cases B and C of the reservoir model a specified blend factor was specified for the advection scheme, a low value 0.1 was used for increased robustness. For Case A of the reservoir model and all cases of the SFO model a high resolution advection scheme was used. A local timescale factor for timescale control was used for Cases B and C of the reservoir model while a physical time scale factor was used for Case A of the reservoir model and for all cases of the SFO model. The local timescale factor option enables the use of different time scales at different regions in the computational domain. The local time scale factor which is entered is a multiplier of a local element based time scale where smaller time scales are applied to regions of fast flow and larger time scales at slower flow regions. A local timescale factor of 0.3 was used. With the physical timescale, a fixed time scale is used for the entire computational domain. The physical timescale was used to provide sufficient relaxation of the equation nonlinearities to obtain a steady state solution. A physical timescale of 0.3 s was used for Case A in the reservoir model while a physical timescale of 0.1 s was used for the SFO model (ANSYS, 2011). To reduce the simulation time of Case B in the reservoir model, the results of Case C were used as initial conditions for the Case B simulation.

2.4.4. Execution

The numerical models were calculated with double precision, the models were iterated until a specific convergence criteria had been reached which differed between the reservoir and SFO models.

The reservoir model was iterated until the residuals for the root mean square for the governing equations had reached a value of $1 \cdot 10^{-4}$. The stability of velocity inside the approach flow channel was also used as a convergence indicator. For the SFO model the convergence criterion was specified as 1% global mass imbalance for the water phase and steady massflow of water at the outlet boundary.

The size and complexity of the reservoir model topography resulted in much longer computational time of the numerical simulation. In Table 2.1 the total iterations and accumulated time of simulation are shown. The simulation times are quite variable for the reservoir cases, Case A took almost two days longer to simulate than Case C because of the different advection scheme and timescale control where a more robust approach was used for Cases B and C. For reservoir Case B, Case C results were used as initial conditions for the simulation which reduced the simulation time down to approximately 2 days. For the SFO cases small difference in simulation time is observed which is due to different computers used in the calculations. The SFO cases labelled Q20 to Q50 refer to the discharge series tested, that is Q20 refers to the case where the SFO discharge is 20 m^3/s, Q30 to a discharge of 30 m^3/s and so forth. Cases Q20 and Q30 were computed using a laptop equipped with a 2.8 GHz Intel i7 processor while Cases Q40 and Q50 where computed using a desktop equipped with 3.4 GHz Intel i7 processor. The laptop had problems with cpu cooling which reduced the performance of the processor while the desktop cpu maintained steady performance because of better cooling. All reservoir simulations where conducted using the aforementioned desktop.

Table 2.1: Computational time of of the numerical model cases.

Model	Iterations	CPU Time	Accumulated Time		
		[Seconds]	[Days]	[Hours]	[Minutes]
Reservoir Case A	7903	3289000	9	12	24
Reservoir Case B	2082	676600	1	22	59
Reservoir Case C	7994	2641000	7	15	24
SFO Q20	1578	330900	0	22	59
SFO Q30	1500	312000	0	21	40
SFO Q40	1516	265800	0	18	27
SFO Q50	1500	264500	0	18	22
Total			**22**	**12**	**16**

2.5. Physical Model

The physical model study was conducted at the hydraulic laboratory of the Icelandic Maritime Administration during a 3 month period. The intake, SFO and spillway structures were made of industrial plastics sculpted with a cnc milling machine. The intake and SFO structure is shown in Figure 2.11. The SFO channel has a plywood invert with plexiglas sidewalls. The topography of the model was made out of fiber reinforced mortar. An overview of the physical model is shown in Figure 2.12

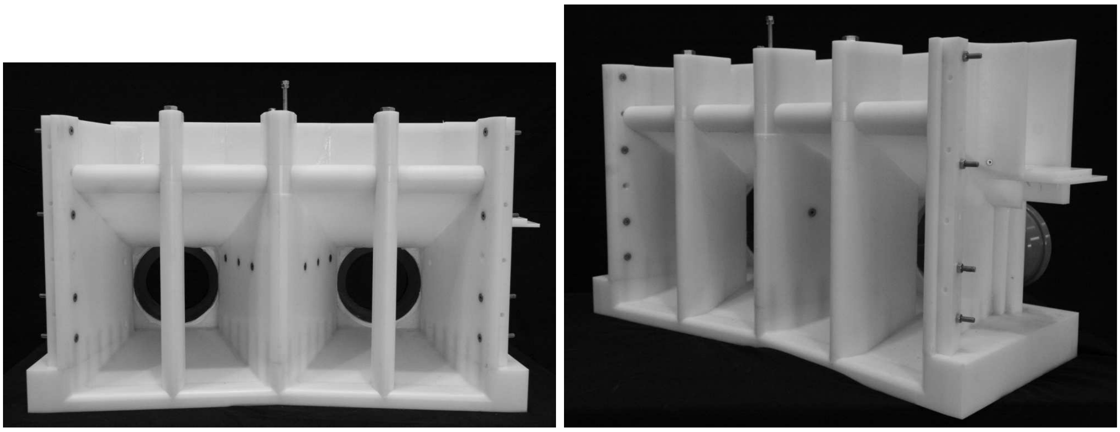

Figure 2.11: The intake and SFO structure of the physical model.

Discharge in the model was regulated with two pumps with frequency inverters. Two reservoir tanks, one downstream and one upstream, collected the water which was circulated in a closed loop as shown in Figure 2.13. High accuracy ultrasonic sensors measured the discharge in the system and manual gauges measured pond water elevations and monitored stability. A flow straightness structure was located at the outlet of the upstream reservoir tank. The flow straightness structure was used to direct the flow entering the approach flow channel more along the right approach bank which was in accordance with preliminary results from the numerical model.

Measurement methods used to describe and quantify the behaviour of the system consisted of particle tests, dye tests, velocity measurements and visual observations documented with photographs and videos.

The physical model study and measurements techniques are described in more detail in (Tomasson et al., 2013).

Figure 2.12: Overview of physical model.

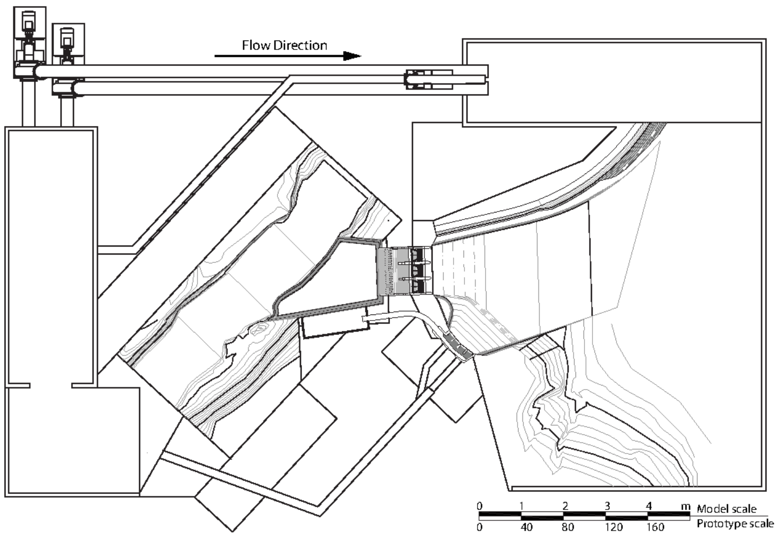

Figure 2.13: Schematic layout of physical model.

2.5.1. Velocity Measurements

Velocity measurements were conducted using a Sontek ADV which measures the three velocity components. Each measurement lasted for 60 seconds, collecting 300 data points. The ADV, which is downward looking, has a blind zone of 50 mm from the sensors probe (Sontek, 1997). Because of the blind zone measurements were limited to a depth exceeding 2 m (prototype depth) from the surface. ADV measurements were made at a depth of 2.6 m at points divided on a 10 m x 10 m rectangular grid closest to the SFO entrance and 20 m x 20 m grid further away from the SFO, a total of 51 points. ADV data processing and filtering was done with USBR's WinADV32 software (Bureau of Reclamation & Group, 2011).

2.5.2. Particle Test

Plastic particles, 1 cm diameter by 1 cm long cylinders shown in Figure 2.14, were scattered upstream in the model, for a given case, and the movements of the particles in the approach flow channel were documented by a video. The paths of the particles were computed from the videos by image processing program written in Matlab. The image processing program takes each frame of the video subtracts it from the previous frame, filters out noise and locates movement in the video. A single image showing particle tracks was obtained from the image processing, the images and videos were then used to derive schematic drawings of the approach flow characteristics. The aim was to identify irregularities and stagnant velocity zones in the approach flow and focus on general flow characteristics in the system. The scattering of particles took place immediately downstream of the flow straightness structures in the model.

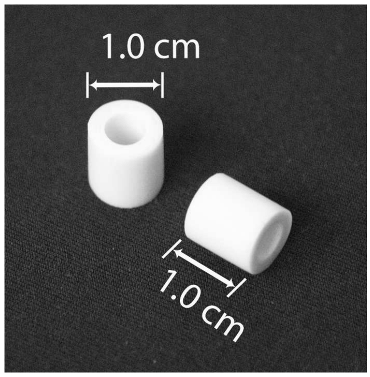

Figure 2.14: Particles used in particle tests.

2.5.3. Dye Test

A dye was released through a pitot tube at depths ranging from 0.5 m to 3 m immediately upstream of the SFO crest. The dye was a solution of potassium permanganate dissolved in water which has approximately the same buoyancy as water. The dye was used to assess the streamline separation immediately upstream of the SFO crest and quantify the surface layer transported by the SFO. The streamline separation was documented by a video. The depths at which water was completely transported by the SFO, equally transported by the intake and SFO and where water was completely transported by the intake were determined.

2.5.4. Visual Observations

All cases were documented in an appropriate manner. Documentation includes: videos, pictures and noted observations. All observed abnormalities were carefully documented and supported with the suitable method of measurement, e.g. velocity or streamline tracking.

2.5.5. Scale Effects

The physical model was built according to Froude similarity scale ratio. In free surface flow gravity forces are dominant, the use of Froude similitude ensures the ratio between inertia and gravity forces to be the same. Scale effects in free surface flow models are defined as distortions introduced by effects, viscosity and surface tension, which are other than the dominant effect of gravity. Scale effects take place when one or more dimensionless parameters differ between model and prototype. If the same fluid is used in both prototype and model scale it is impossible to keep both the Froude and Reynolds numbers in model and full scale. In physical models of open channel flow the model flow must be fully turbulent that is the Reynolds number of the model must be higher than 5000 to minimize viscous effects (*The Hydraulics of Open Channel Flow: An Introduction*, 2004). Results from physical model studies showed that Weber numbers greater or equal to 12 would produce results without significant scale effects (Pfister & Chanson, 2011). In Table 2.2 the calculated Reynolds and Weber numbers for the SFO inlet are shown. The Reynolds and Weber numbers are calculated for values, depth and velocity, on the SFO crest where the flow is critical. As the calculations show the Reynolds and Weber numbers for the model are above those limits thus keeping potential scale effects to minimum.

Table 2.2: Calculated Reynolds and Weber numbers for the SFO inlet in prototype and model scale.

	Prototype	Model
Reynolds number, Re	4.8.E+06	1.9E+04
Weber number, We	4.8.E+04	30

2.6. Post Processing

In the post processing phase the data was handled, manipulated and set forth in a presentable manner. As the measurements and numerical results are large data sets, great work had to be done to make the data presentable.

The ADV measurements from the physical model were processed and filtered using USBR's WinADV32 software. The ADV data was further processed and sorted using Matlab routines before being plotted and evaluated.

For the numerical data the post processing part of the ANSYS software package CFD-Post was used. The numerical results were directly imported into CFD-Post which is equipped with multiple tools to create contours, vectors and streamlines from the data. Physical model results were imported into CFD-Post as comma separated files and contour plots were made.

All graphs were made in Matlab. Numerical results were exported from CFD-Post as comma separated files. To created for example a water elevation plot the first step in CFD-Post was to create a slice plane with contour levels of volume fractions at the slice plane shown. A poly line was traced along the contour line where the volume fraction of water was equal to 0.5. The poly line was plotted onto a chart in CFD-Post where it was exported as comma separated file. Because of air entrainment in the model downstream of the SFO crest contour lines of water volume fraction equal to 0.5 were in some cases observed below the water surface. In order to create a water surface plot such features were removed using Matlab routines.

The water surface is always presented at water volume fraction of 0.5 and velocities are always presented as the velocity magnitude at a particular location.

3. Results and Discussion

3.1. Design Development

3.1.1. Preliminary Design

A preliminary design of the SFO and the approach flow channel was released in 2010. In the design a funnel shaped approach flow channel approximately 130 m wide 200 m upstream of the spillway gradually narrowed down to 45 m width in front of the spillway. The approach channel towards the spillway was at constant elevation of 39 m a.s.l. From the left side of the spillway approach channel another separate channel leads towards the intake and the SFO structure. The intake approach channel sloped gradually from the spillway approach invert to an elevation of 31.5 m a.s.l. in front of the intake. Another distinct feature of the 2010 design was a large sheltered off shallow water area in front of the fuse plug. The layout of the preliminary design from 2010 is shown in Figure 3.1.

The modelling group in cooperation with the designers at Verkís reviewed the design from 2010 in January 2012 prior to the construction of the physical model of Urriðafoss HEP. Following the review both the approach channel and SFO structure were changed in order to make the design more effective in terms of fish passage. The power intake and the SFO structure was rotated so the SFO entrance would take the main current head on to provide a more direct path for the juvenile salmon towards the SFO. The approach channel was widened to smooth the approach to the SFO. The curb between the spillway and power intake in the 2010 design was reduced and lowered to an elevation of 48 m a.s.l. to open a path for juvenile salmon which might get lost in front of the spillway. The large shallow area in front of the fuse plug was considered likely to become a stagnant velocity zone where the juvenile salmon might get lost. To prevent this the fuse plug was moved closer to the approach channel. The layout of the reviewed design is shown in Figure 3.4.

The sharp crest of the SFO entrance was changed to a rounded nose to make the entrance flow transition more smooth as shown in Figure 3.5. Inside the SFO the different invert elevations and structural blocks in the 2010 design where thought to lead to abrasion or other injury of juvenile salmon and possible accumulation of debris and trash which might also be harmful for the fish. Because of this the structural blocks where removed and the SFO channel invert was changed to a single elevation of 45 m a.s.l. As to further improve the design all corners where made rounded and more streamlined as shown in Figure 3.6.

Figure 3.1: Overview of the Urriðafoss HEP original design layout (Landsvirkjun, 2010).

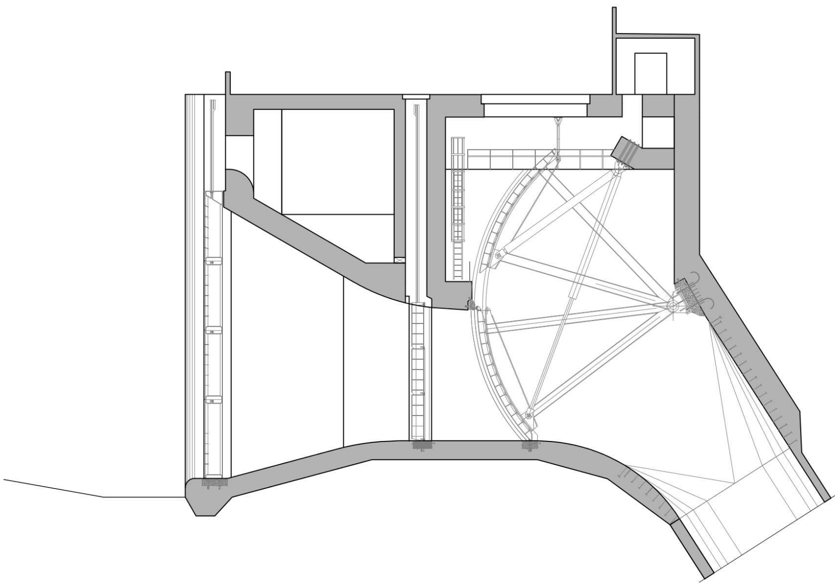

Figure 3.2: A longitudinal view of the original SFO design (Landsvirkjun, 2010).

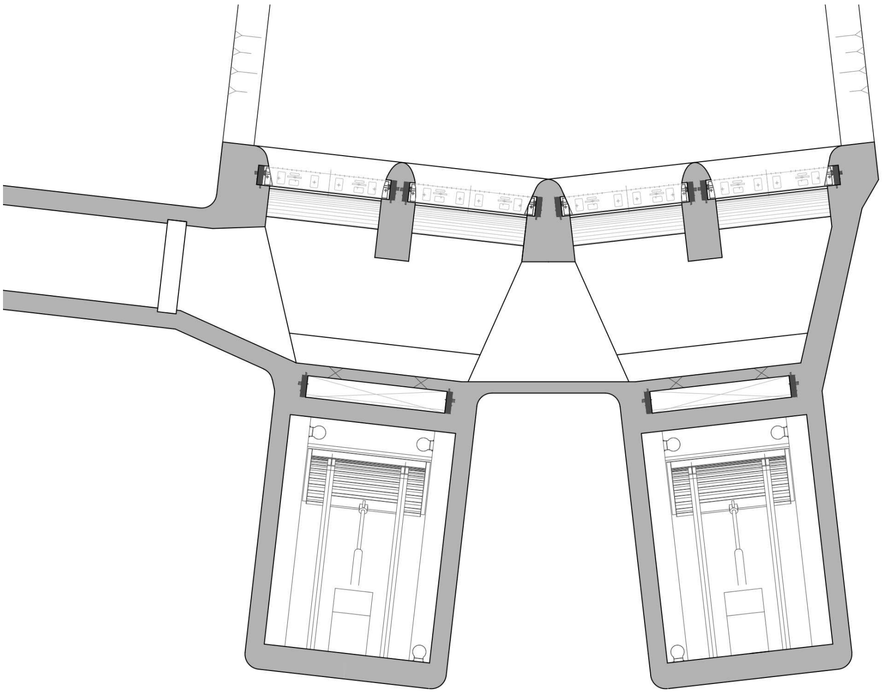

Figure 3.3: A plan view of the original SFO design (Landsvirkjun, 2010).

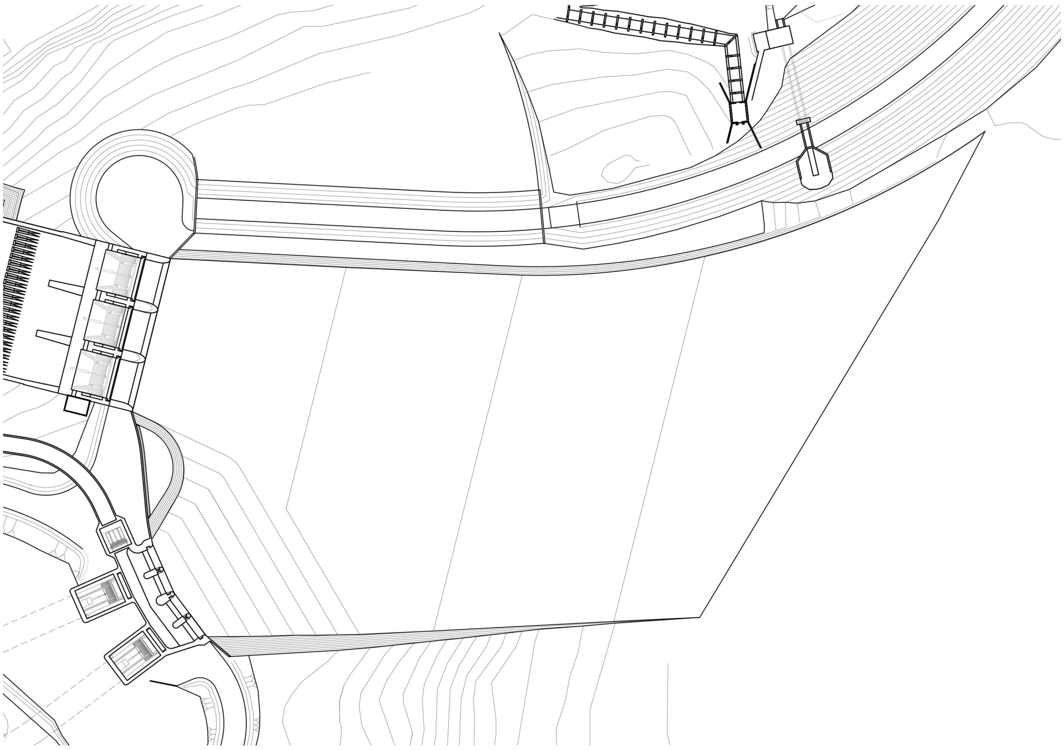

Figure 3.4: Revised layout of the approach channel with modifications from February 2012 (Landsvirkjun, 2010).

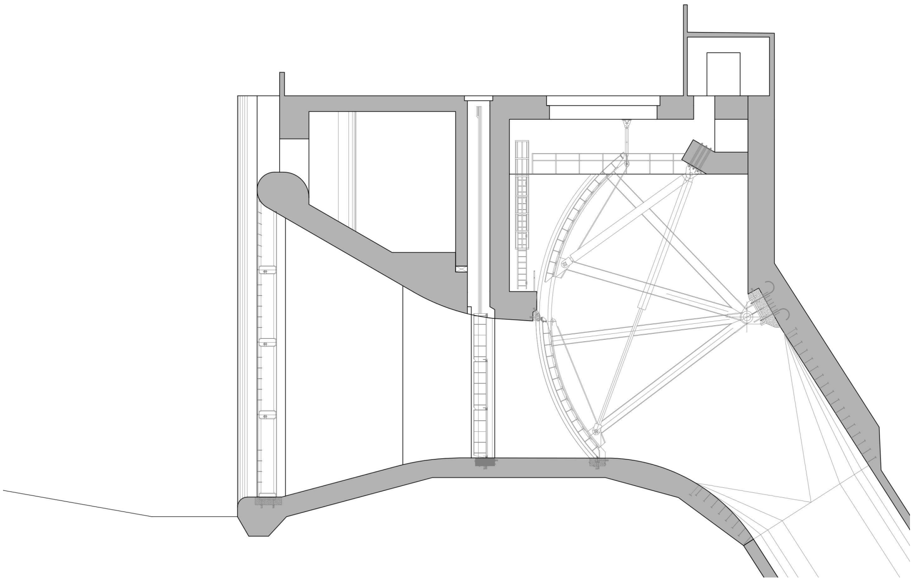

Figure 3.5: A longitudinal view of the revised SFO design (Landsvirkjun, 2010).

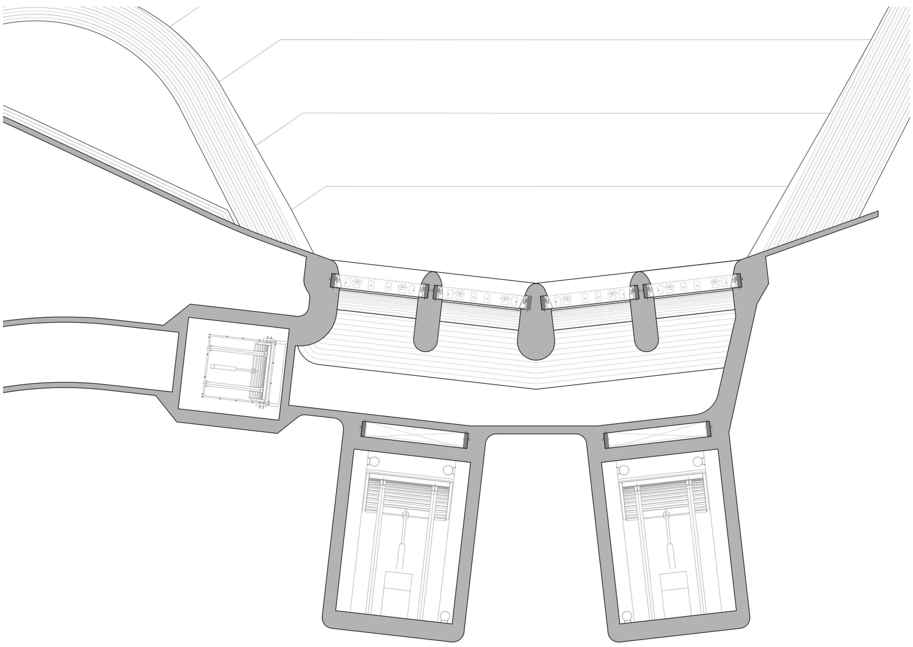

Figure 3.6: A plan view of the revised SFO design (Landsvirkjun, 2010).

The physical model of Urriðafoss HEP and the numerical model were built according to the revised design. Preliminary tests in the physical model and preliminary results from the numerical model showed irregularities forming at the left approach bank (looking downstream). At the left approach bank the topography sways upstream causing the discharge coming over the bank to flow in near opposite direction to the incoming main current in the approach flow channel. Because of the upstream sway of the topography irregularities form around the left approach bank and the main current is diverted from the bank into the center of the approach flow channel. A velocity contour plot from the preliminary numerical model is shown in Figure 3.8. The diversion of flow from the left approach bank is shown in Figure 3.7 taken during preliminary tests in the physical model.

Figure 3.7: Photograph of a dye test from preliminary tests in the physical model showing diversion of flow away from left approach bank.

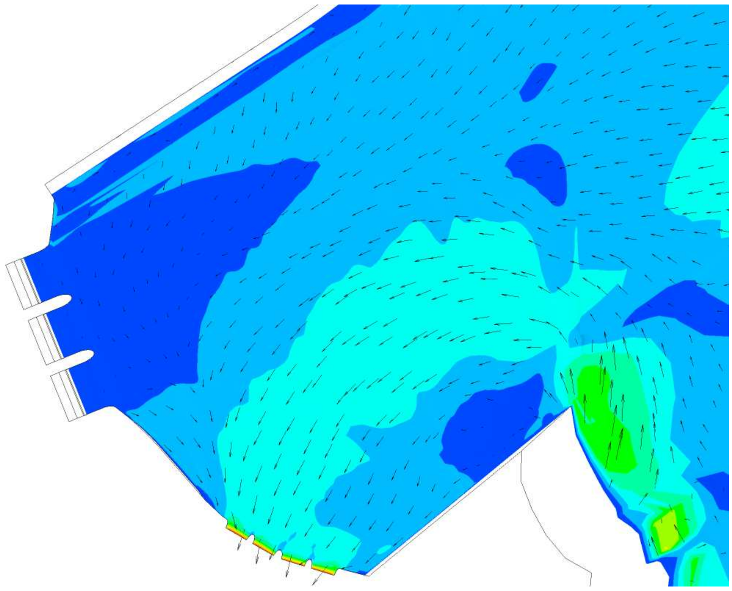

Figure 3.8: Contour and vector plot from the preliminary numerical model showing flow diversion from left approach bank.

In light of the irregularities forming at the left approach bank modifications were made in attempt to get the flow more along the left approach bank limiting the formation of vortices and stagnant velocity zones along the left approach bank. The modifications consisted of changing the left approach bank in order to get the water flowing from the left approach bank to enter the approach channel parallel to the main current. The angle of the left abutment of the power intake was also increased to limit the potential of a stagnant velocity zone forming at the left abutment.

3.1.2. Final Design

The final design layout for Urriðafoss HEP and the intake and SFO structure is shown in Figures 3.9 and 3.10 as an overview of the project with the relevant elements to the project and longitudinal sections of the intake and spillway respectively.

The Heiðarlón Reservoir is formed by a dam crossing the river at Heiðartangi Point and dykes along the west banks of the river. The spillway and the intake structures are located at Heiðartangi Point. In general, the overall layout of the approach flow channel, the intake to the powerhouse and the SFO type juvenile bypass structure were investigated. The elements investigated and relevant to this study are as follows (numbers refer to Figure 3.9):

- (1) the original river bed of Þjórsá River upstream of the dam

- (2) an excavated Approach Flow Channel (AFC) for the spillway and intake. The AFC invert slopes towards the spillway from an elevation of 41 m a.s.l. to 37 m a.s.l. in front of the spillway. It is approximately 120 m wide, excavated in an arch shape, starting at the original riverbank approximately 200 m upstream of the spillway crest. The sides of the channel have a steep 4:1 (vertical:horizontal) slope. At the right side of the channel (looking downstream) the side walls reach an elevation of 49 m a.s.l. From 49 m a.s.l. the fuse plug and dykes start to rise above the right approach bank and continue to elevations of 51.8 m a.s.l. and 53.5 m a.s.l. respectively.

- (3) an excavated AFC for the intake and SFO structure. The AFC slopes downward to the left of the main AFC towards the intake and SFO structure to an elevation of 31.5 m a.s.l. in front of the intake. On the right side of the channel, a curb, reaching an elevation 48 m a.s.l. separates the intake and spillway. The side walls of the channel are steep with 4:1 slopes.

- (4) a power intake and SFO structure shown in detail in Figure 3.10. The intake is a conventional structure with a SFO type juvenile bypass system incorporated at the top of the structure. The intake has four 5.95 m wide entrances, uniting in pairs, into two separate draft tubes. The design discharge for the intake is 370 m^3/s. The SFO has four 5.95 m wide entrances, each with a smooth rounded crest at an elevation of 49.1 m a.s.l., providing an estimated discharge of 40 m^3/s at Normal Reservoir Water Level (NRWL) 50 m a.s.l. From the crest the water from the four entrances is united in a single sideway channel and routed through a 4.5 m wide concrete channel to the original riverbed downstream of the dam.

- (5) a gated spillway with three radial gates for reservoir regulation and flood passing. The spillway has three 12 by 10 m radial gates (width x height), the spillway crest is at an elevation of 41 m a.s.l.

- (6) a fuse plug with crest elevation at 51.8 m a.s.l. to pass larger floods than Q_{1000}.
- (7) an upstream fishway to aid the migration of salmon up river.
- (8) a mandatory release structure which provides constant discharge of 10 m^3/s to the riverbed downstream of the dam.
- (9) Urriðafoss dam forming Heiðarlón Reservoir.

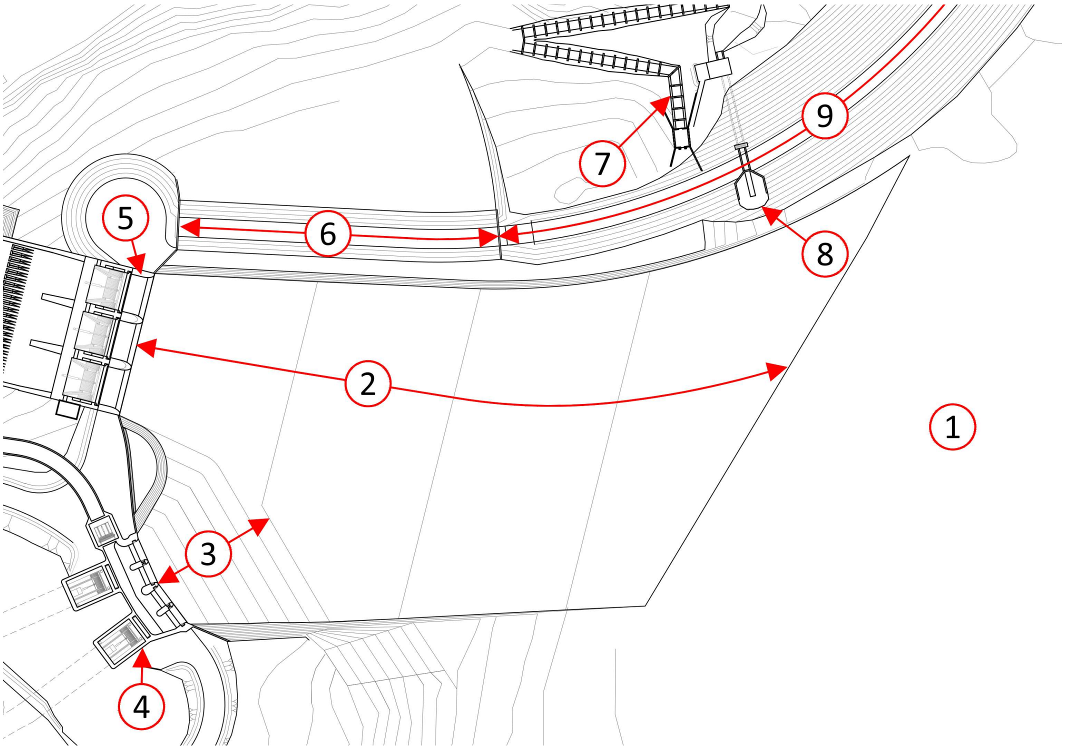

Figure 3.9: Overview of the Urriðafoss HEP final design: (1) the original riverbed, (2) spillway approach flow channel, (3) intake and SFO approach flow channel, (4) intake to the power house and SFO structure, (5) the spillway structure, (6) the fuse plug, (7) the upstream fishway, (8) the mandatory release structure, (9) Urriðafoss Dam (Landsvirkjun, 2010)

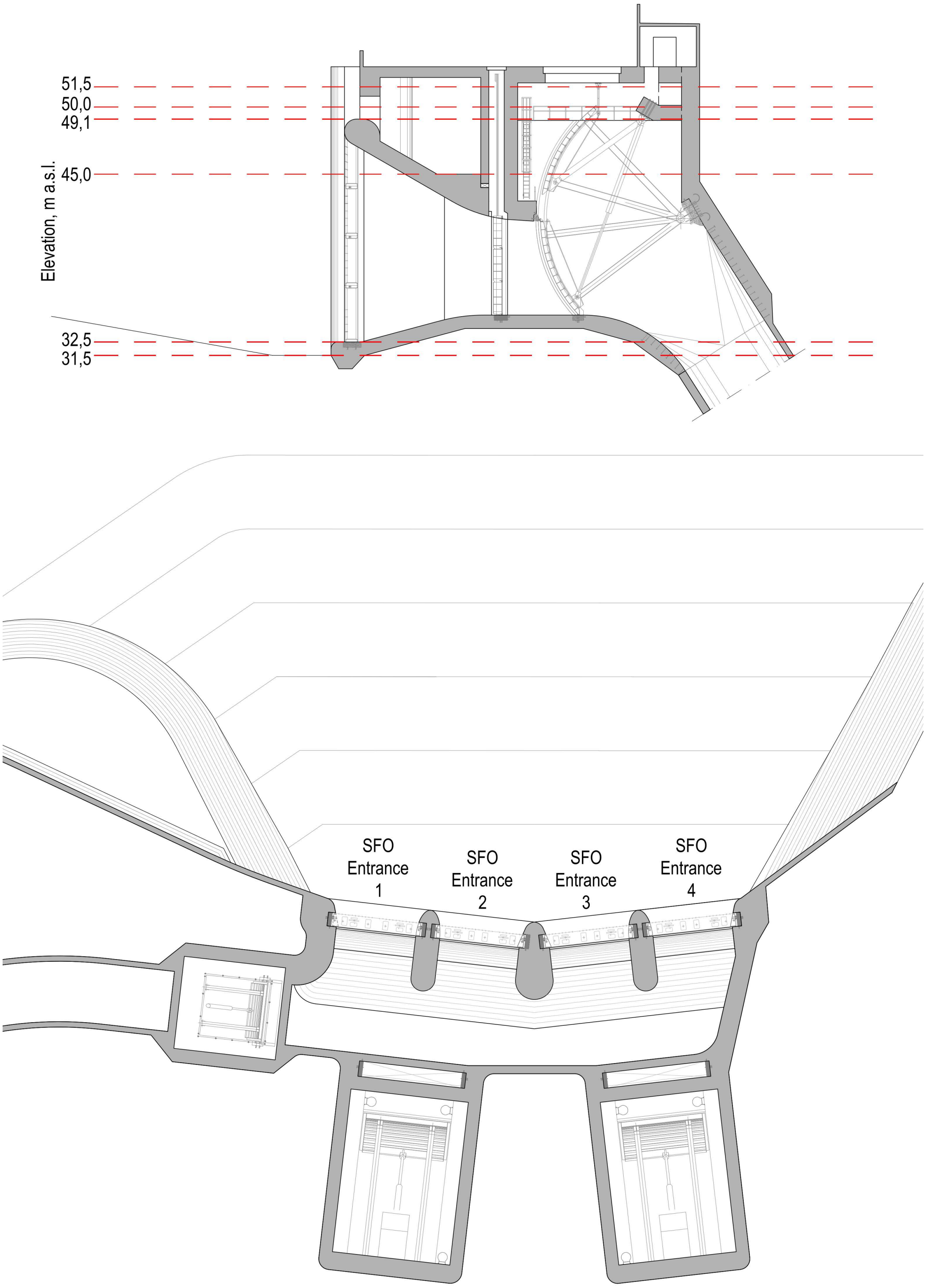

Figure 3.10: Top view and longitudinal section of the intake and SFO structure (Landsvirkjun, 2010)

3.2. Reservoir

The reservoir model was tested with respect to three operational scenarios, Cases A, B and C corresponding to Cases 1.2, 1.3 and 1.4 set forth by Karadottir and Gudjonsson (2012b). The cases represent normal operational conditions expected at the time of migration of juvenile salmon. Measurements showed the SFO discharge capacity being about 30% lower than the calculated design discharge at NRWL, 50 m a.s.l. Scale effects are only considered to account for small amount of the reduction in discharge capacity as discussed in Section 2.5.5. Some unconventional features of the SFO, such as the geometric layout of the crest probably accounts for most of the difference in measured and calculated discharge capacity as discussed by (Tomasson et al., 2013). To ensure similar conditions in the numerical model a reservoir elevation of 50.2 m a.s.l. was used. Discharges for each case and the percentage of time of equal or more discharge are presented in Table 3.1. In Figure 3.11 the flow duration curve derived from a discharge series spanning 55 years, 1950 to 2005, is shown. The flow duration curve is derived for the time period which the downstream migration of juvenile salmon occurs in the Lower Þjórsá River, which is annually from the 15th of May to the 15th of June. As shown in the figure 41% of the time the discharge is equal or more than the discharge going to the power intake (370 m^3/s), the SFO (40 m^3/s) and the environmental flow (10 m^3/s) combined. This means that 59% of the time discharge to the power plant has to be reduced in order to maintain a flow of 40 m^3/s through the SFO. According to the flow duration curve no discharge is routed through the spillway in 59% of the time. Karadottir and Gudjonsson (2012a) found out that 88% of the juvenile salmon entering the reservoir would be attracted towards the SFO and 12% would be attracted towards the spillway. They assumed the juvenile salmon run would divide between the structures in direct relation to the discharge routed through each structure. They also assumed the magnitude of the salmon run each day to be directly related to the discharge, that is more juveniles migrating in more flow. When they assumed the juvenile salmon to migrate evenly over the migration period 91% of the fish would enter the SFO and 9% would be attracted towards the spillway. It should be noted that there is a small discrepancy in the topography between the physical and numerical models in the approach flow channel. The effect of this topographic difference is discussed.

Table 3.1: Overview of the cases tested in the physical and the numerical models.

Case	RWL [m a.s.l.]	Q_{Intake} [m^3/s]	$Q_{Spillway}$ [m^3/s]	Q_{SFO} [m^3/s]	Q_{Total} [m^3/s]	Percentage of time of equal or more discharge*
A	50.2	370	0	$\simeq 40$	410	41 %
B	50.2	370	70	$\simeq 40$	480	25 %
C	50.2	370	235	$\simeq 40$	645	5%

* (Káradóttir & Guðjónsson, 2012a).

Velocity measurements were conducted in the physical model at cross sections spaced 20 m apart in the approach flow channel, closer to the intake and the SFO the spacing was refined down to 10 m. This resulted in fifty measurement points in total for each case. The velocity measurements were compared to the numerical model results at six section lines labelled Section 10, 20, 40, 60, 80 and 100 as shown in Figure 3.12.

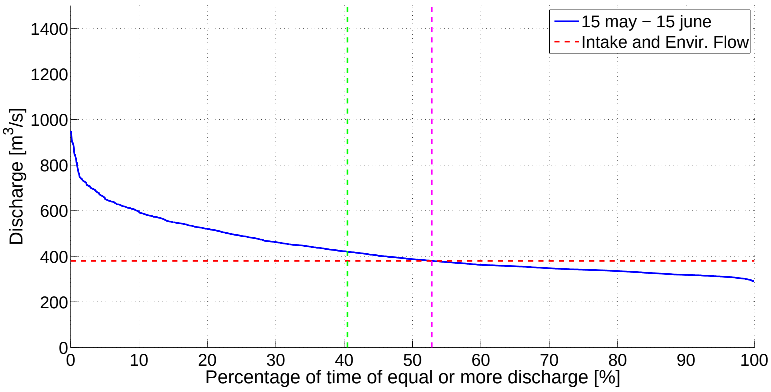

Figure 3.11: Flow duration curve for time period where annual downstream migration occurs, 15th of May to 15th of June. The purple line shows percentage of time when the discharge is equal or more than the intake and environmental flow combined while the green line shows the time when the discharge is greater than the intake, the SFO and environmental flow combined.

Figure 3.12: Section lines of measurements in physical model used in validation of numerical model.

3.2.1. Case A

In Figure 3.13 velocities from ADV measurements in the physical model (dots) and results from the numerical model (solid line) taken at 2.6 m depth, are compared at Section lines 10, 20, 40, 60, 80 and 100 for Case A; RWL = 50.2 m a.s.l., Q_{Intake} = 370 m^3/s and Q_{SFO} $\simeq$ 40 m^3/s. The ADV measurement points are shown with one standard deviation error band to indicate the magnitude of the flow fluctuations.

At Section 10, shown in Figure 3.13, a slow moving water is observed in front of the spillway entrances with gradually increasing velocity from Station 70 to a maximum velocity in front of the intake. The physical and numerical data differ most between Stations 80 and 90 where two peaks are observed in the numerical model right in front of the curb between the spillway and intake but are otherwise in good agreement.

As at Section 10, low velocities are observed in front of the spillway at Section 20 as seen in Figure 3.13. The velocity at Section 20 gradually increases from Station 50 towards the intake structure reaching a maximum for the physical model at Stations 110 and 120 from where the velocity decreases again at Station 130. For the numerical model the velocity takes an absolute maximum value at Station 130 opposite to the decrease in velocity observed in the physical model.

At Section 40, the ADV measurements from the physical model show that the velocity gradually increases from Station 30 to Station 90 where maximum value is reached. From Station 90 to 110 the velocity is similar but from Station 110 a gradual decrease is observed in the physical model. The character in the numerical model at Section 40 is in good agreement with the physical model results from Station 30 to Station 110 where the results start to differ. Note the higher standard deviation of the ADV measurements at Stations 110 to 130 which is due to irregularities forming at the left approach bank (looking downstream) affecting the measurements. The irregularities formed where discharge flowing over the left approach bank enters the approach flow channel perpendicular to the main current in the approach flow channel. Small topographic features upstream of the left approach bank also contribute to the formation of irregularities.

For the ADV measurements from the physical model at Section 60 the velocity gradually increases from Station 30 to Station 90 where a maximum value is reached. From Station 90 the velocity gradually decreases again to 0.28 m/s at Station 130. The numerical model has a rather different character at Section 60. Instead of a U-shape distribution, the velocity gradually increases to an absolute maximum at Station 122 which is somewhat higher than observed in the physical model. The standard deviation of the ADV measurements is higher for the values at Stations 110 to 130 as in Section 40 due to the same artefact as discussed for Section 40.

At Section 80, the difference between ADV measurements and numerical model results increase further. ADV measurements from the physical model are distributed in a somewhat U-shape manner with a minimum value at the right approach bank and maximum value in the center of the approach flow channel at Station 70. Meanwhile, the velocity distribution in the numerical model at Section 80 increases almost linearly from the right approach bank to the left approach bank where a maximum value is reached. A noticeable higher value of standard deviation for the ADV measurements is seen at Station 130 due to the same artefact as discussed before.

At Section 100, the ADV measurement values are somewhat lower than values from the numerical model. In both models the velocity distribution is almost uniform over the section with a maximum value observed at Station 130. At Station 130 high standard deviation of the ADV measurements is observed which is caused by the same artefact as discussed before.

In Figure 3.13 the characteristic difference between the experiments and numerical model increases as observations are made further upstream from the spillway and intake structures. The models are in good agreement especially for Sections 10 to 40. At Section 40 a high value of standard deviation is observed at Station 120, for Sections 60 to 100 high standard deviation values are observed at Station 130 which are caused by irregularities forming at the left approach bank. Some of the difference may also be caused by effect of the upstream boundary conditions in the physical model.

Figures 3.14 and 3.15 show velocity magnitude contours and vectors for the physical and numerical models, respectively, at 2.6 m depth. In both models the extent of the stagnant velocity zone in front of the spillway is evident. Here the difference in character observed in Figure 3.13 is clear. In the physical model the flow entering the approach channel around the left approach bank cuts the approach flow at a steep angle diverting the main current away from the left approach bank and creating a low velocity zone close to the left approach bank. In the numerical model the flow takes a path along the left approach bank with velocities reaching a maximum at the point where the two currents intersect. The difference is caused by small discrepancy in the topography between the physical and numerical models at the left approach bank where modifications were made during the physical model study in order to amend the approach flow conditions. The modifications were made to both the physical and the numerical model but a small topographic feature in the physical model is the source of the irregularities in the flow and is responsible for diverting the flow away from the land into the approach flow channel. The aforementioned irregularities in the flow at the left approach bank do not significantly affect the approach flow conditions which are in general good. In the figures, the extensive attraction flow and gradual increase in velocity towards the intake and the SFO is clear which should be ideal for attracting juvenile salmon towards the SFO.

Plastic particles were scattered in the approach flow channel of the physical model and their movement documented in order to get a better understanding of the approach flow characteristics and the relationship between spillway and intake discharge. Figures 3.16

and 3.17 show general flow behaviour and streamlines in the approach flow channel for the physical and numerical model, respectively. The plot on left in Figure 3.17 shows bulk flow streamlines (three dimensional streamlines changing both laterally and vertically) while the plot on the right shows surface streamlines. The bulk flow and surface streamlines represent consistent flow behaviour over the depth of the numerical model. The models are in good agreement, in both figures the extent of the attraction flow is great as most of the approach channel flow is drawn towards the intake and the SFO. Two zones of irregularities are observed in the physical model, labelled stagnant zone and vortex zone in Figure 3.16. The stagnant zone located immediately upstream of spillway is occupied by a slow moving water body. Particles entering the zone may linger for some time until finally drawn towards the intake and the SFO. In the vortex zone located by the left approach bank irregularities form where different currents intersect with steady formation of small shallow vortices.

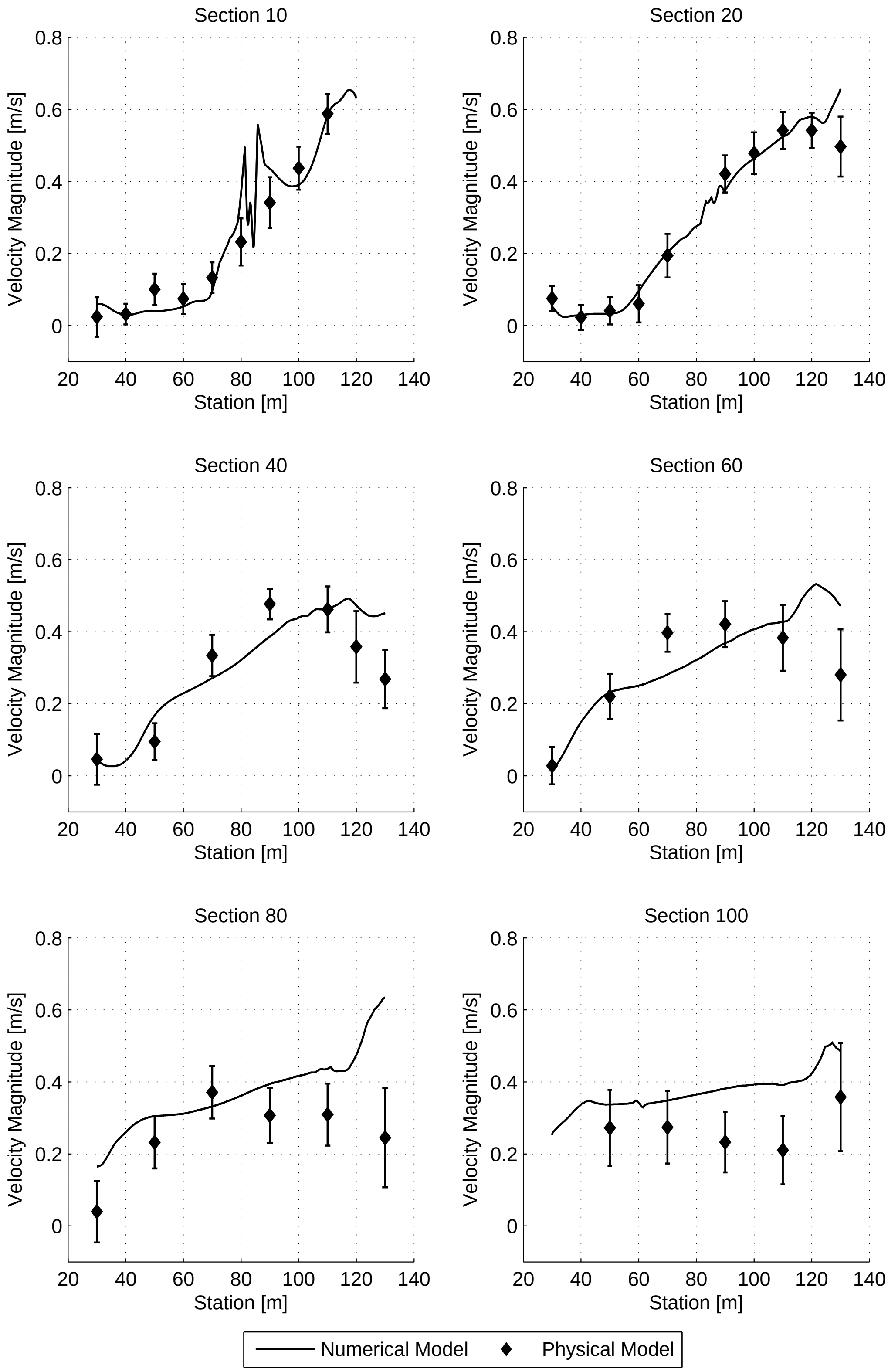

Figure 3.13: Velocity comparison between physical and numerical models taken at 2.6 m depth at Section Lines 10, 20, 40, 60, 80 and 100 for Case A: RWL = 50.2 m a.s.l., Q_{Intake} = 370 m^3/s and $Q_{SFO} \simeq 40$ m^3/s.

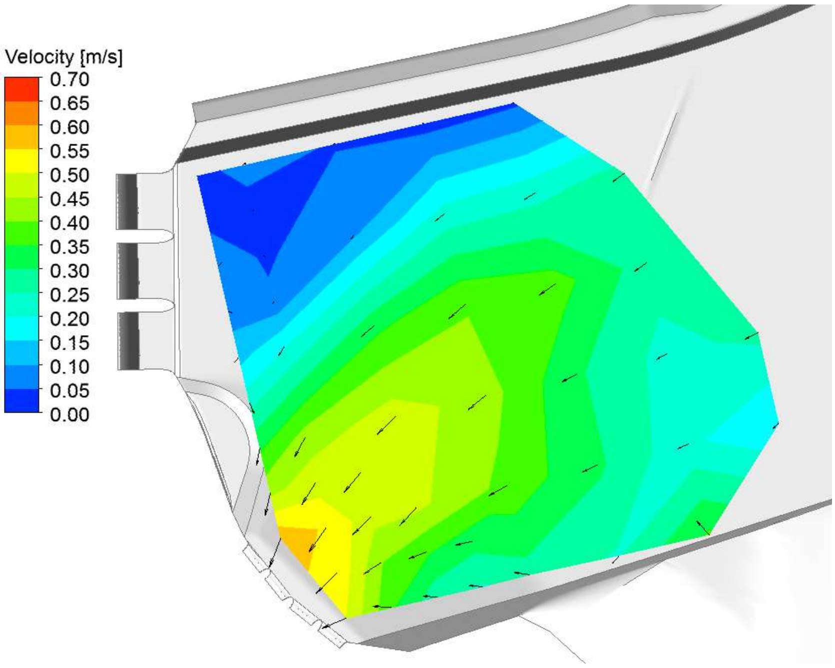

Figure 3.14: Velocity contours and vectors at 2.6 m depth from the physical model for Case A: RWL = 50.2 m a.s.l., Q_{Intake} = 370 m^3/s and $Q_{SFO} \simeq$ 40 m^3/s.

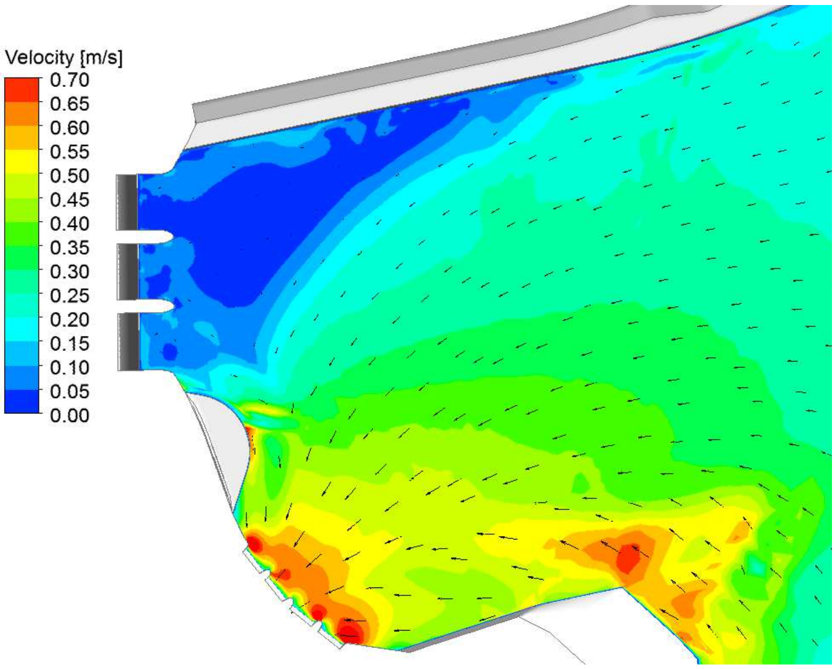

Figure 3.15: Velocity contours and vectors at 2.6 m depth from the numerical model for Case A: RWL = 50.2 m a.s.l., Q_{Intake} = 370 m^3/s and $Q_{SFO} \simeq$ 40 m^3/s.

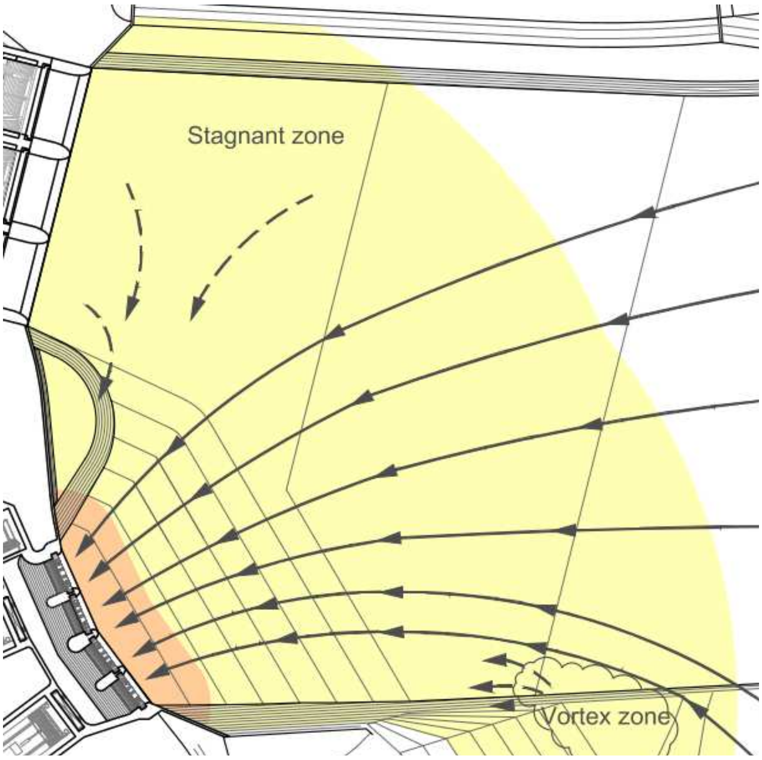

Figure 3.16: Results from particle test for Case A, Q_{Intake} = 370 m^3/s, Q_{SFO} = 40 m^3/s and $Q_{Spillway}$ = 0 m^3/s. Lines with arrows represent general flow characteristics. Colours refer to zones described in section 2.2, the decision zone is shown in orange and the discovery zone in yellow.

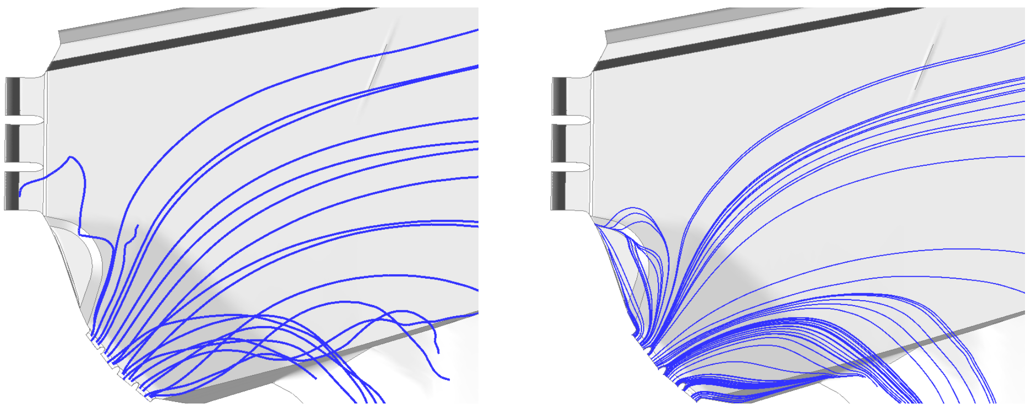

Figure 3.17: Streamlines in approach flow channel from the numerical model, Case A. On left: Bulk flow streamlines. On right: Surface streamlines.

In Figure 3.18 velocity magnitude contours and vectors are shown at an elevation of 49.5 m a.s.l., 0.7 m depth, in the numerical model. As the physical and numerical model are in good agreement for Case A, as seen in Figures 3.14 and 3.15 for water depth 2.6 m, it can be assumed that the numerical model represents accurately the conditions at this shallower depth, 0.7 m, a depth where the juvenile salmon is likely to inhabit. As seen in Figure 3.18 the conditions at 0.7 m depth are very similar to the conditions at 2.6 m depth in Figure 3.15, the extent of the attraction flow is extensive with gradual increase in velocity towards the intake and the SFO. The only difference observed is the stagnant velocity in front of the spillway extends somewhat further upstream than observed at 2.6 m depth.

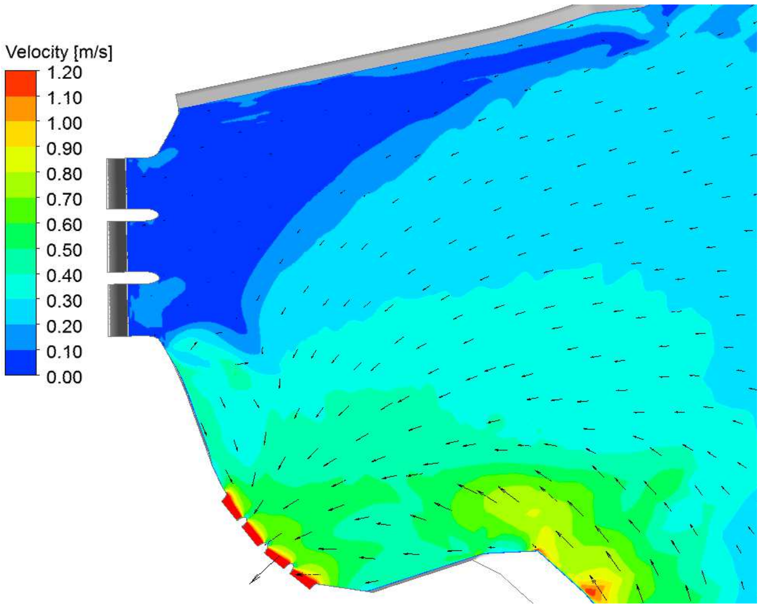

Figure 3.18: Velocity contours and vectors at 0.7 m depth from the numerical model for Case A: RWL = 50.2 m a.s.l., Q_{Intake} = 370 m^3/s and $Q_{SFO} \simeq 40$ m^3/s.

3.2.2. Case B

In Figure 3.19 velocities from ADV measurements in the physical model (dots) and results from the numerical model (solid line) taken at 2.6 m depth, are compared at Section Lines 10, 20, 40, 60, 80 and 100 for Case B: RWL = 50.2 m a.s.l., Q_{Intake} = 370 m^3/s, Q_{SFO} $\simeq$ 40 m^3/s and $Q_{Spillway}$ = 70 m^3/s. The ADV measurement points are shown with one standard deviation error band to indicate the magnitude of the flow fluctuations.

At Section 10 shown in Figure 3.19, a slow moving water is observed in front of the spillway entrances with gradually increasing velocity from station 70 to a maximum velocity in front of the intake. The physical and numerical data differ most between Stations 80 and 90 where two peaks are observed in the numerical model right in front of the curb between the spillway and intake but are otherwise in good agreement.

At Section 20, the velocity distribution is almost uniform, increasing gradually from the right approach bank towards the intake and the SFO. The ADV measurements and numerical model results are in good agreement and differ only slightly at Stations 120 and 130 where the ADV measurement values decrease in magnitude instead of increasing as observed in the numerical model.

At Section 40, the velocity distribution in both models take a U-shape with minimum values at the right approach bank and maximum values observed at Station 110. The models are in good agreement as numerical values are all within one standard deviation of the physical model results with the exception of Station 120. At station 120 the ADV measurements take a much lower value with very high standard deviation, the fluctuation presented as standard deviation is caused by irregularities forming at the left approach bank as were described in Case A.

At Section 60 a similar U-shape velocity distribution is observed in both models as at Section 40. A minimum value is observed at the right approach bank from where the velocity increases gradually towards the center of the approach flow channel. In the center of the approach flow channel the velocity distribution is relatively flat, at the left approach bank, Station 130, the velocity decreases again and a high standard deviation in the ADV measurements is observed. The models show similar character, ADV measurement values are lower than numerical values in all stations and differ most at Stations 50 and 70.

At Section 80, the models have similar character, a minimum value at Station 30 and a uniform distribution from Station 50 to Station 130. The ADV measurement values are all lower than the numerical values with the exception of Station 130 where the models have almost the same value. The models differ most at Station 30. As before the highest standard deviation is observed at the left approach bank where aforementioned irregularities form.

At Section 100, the maximum values of the numerical model are reached at Station 50, for the physical model a maximum value is reached at Station 130. At these two stations the models differ most. All numerical values are within one standard deviation of the ADV measurements with the exception of Station 50. The models are thus in good agreement at Section 100. The most fluctuation is observed at Station 130 as before as the standard deviation shows.

In Figure 3.19 the characteristic flow behaviour is similar at all section lines and the models are in good agreement especially for Sections 10 and 20. For Sections 40 to 100 the character is similar with somewhat lower velocities observed in the physical model. At Section 40 a high value of standard deviation is observed at Station 120, for Sections 60 to 100 high standard deviation values are observed at Station 130 which are caused by irregularities forming at the left approach bank.

Figures 3.20 and 3.21 show velocity contours and vectors for the physical and numerical models, respectively, at 2.6 m depth. The models show similar characteristic flow behaviour, the stagnant velocity zone in front of the spillway has reduced considerably in both models from Case A. The stagnant zone extends upstream along the right approach bank. Maximum values are observed in front of the intake and the SFO in both models. In the numerical model high velocities are observed at right approach bank where water falls over the bank. The main current is located in the center of the approach flow channel, the current reaches further downstream than in Case A as is expected with the added spillway discharge. The main current is headed towards the intake and the SFO as in Case A. Irregularities are observed at the left approach bank as in Case A, the same characteristic difference between models is also observed as in Case A. Although visually the physical and the numerical model are in a better agreement for Case B than Case A. The figures show extensive attraction flow towards the SFO and the intake with gradual increase in velocity towards the structures. In both models the extent of the stagnant velocity zone in front of the spillway has decreased considerably from Case A due to of the spillway discharge. In the figures, the extensive attraction flow and gradual increase in velocity towards the intake and the SFO is clear which should be ideal for attracting juvenile salmon towards the SFO.

The vertical extent of the stagnant velocity zone is shown in Figure 3.22 where velocity contour lines and velocity vectors are shown at a longitudinal section perpendicular to spillway gate 2. As the figure shows the stagnant zone extends to depths of approximately 4 m immediately upstream of the spillway crest and the extent laterally is also considerable. Fish attracted towards the spillway may loose meander for some time in front of the spillway gates as they generally dive through deep passages as last resort. The distance from the stagnant zone to the point where the surface flow starts to accelerate towards the SFO is not great. Assuming that juvenile salmon is active in search of appropriate route through the system they should be able to find the SFO attraction flow.

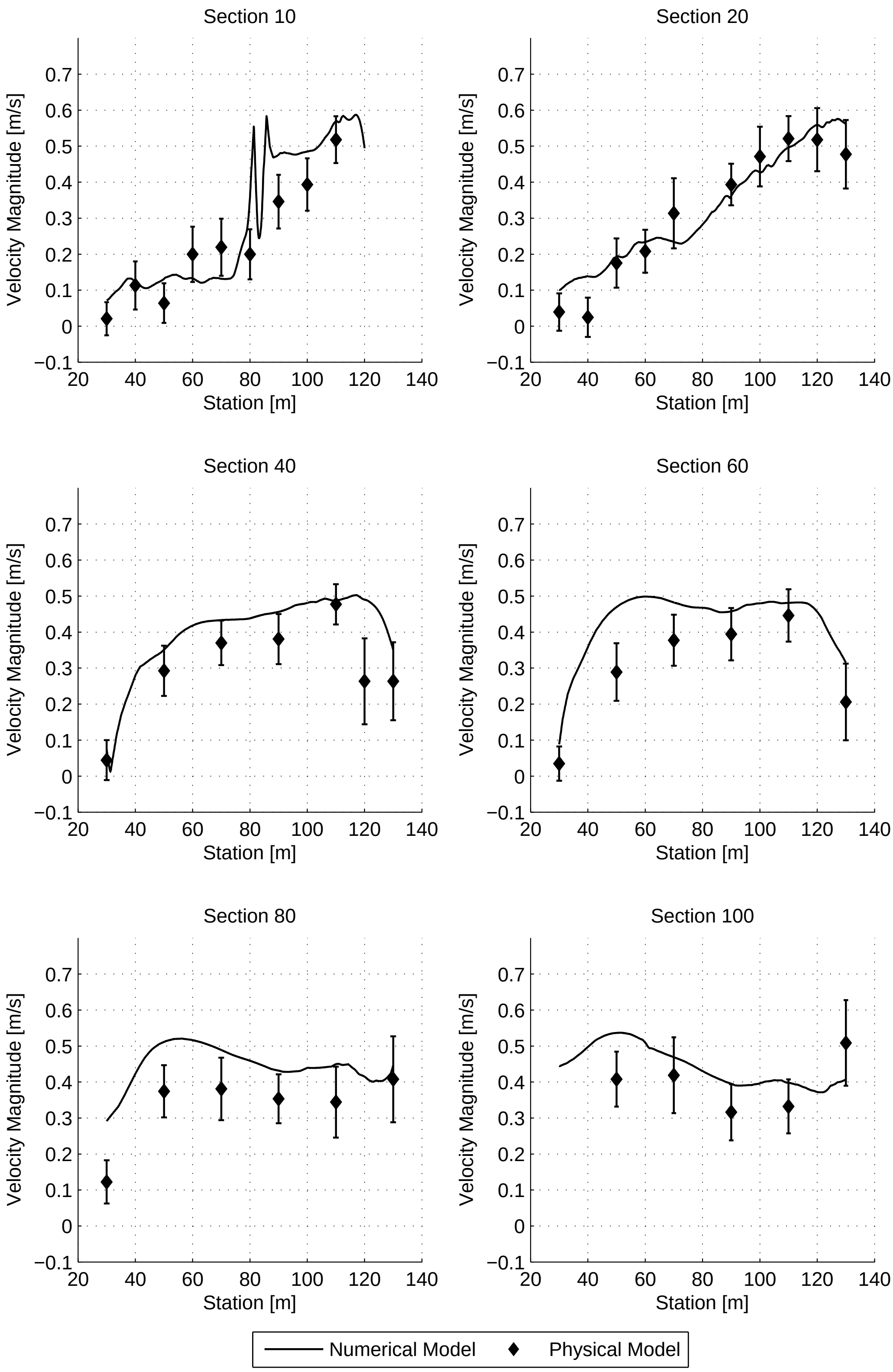

Figure 3.19: Velocity comparison between physical and numerical models taken at 2.6 m depth at Section Lines 10, 20, 40, 60, 80 and 100 for Case B: RWL = 50.2 m a.s.l., Q_{Intake} = 370 m^3/s, $Q_{SFO} \simeq 40$ m^3/s and $Q_{Spillway}$ = 70 m^3/s.

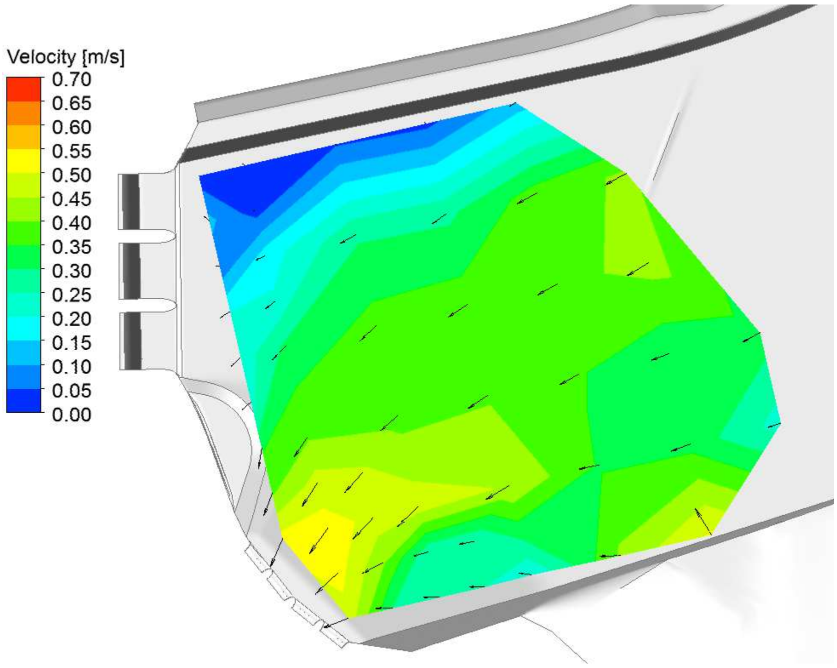

Figure 3.20: Velocity contours and vectors at 2.6 m depth from the physical model for Case B: RWL = 50.2 m a.s.l., Q_{Intake} = 370 m^3/s, $Q_{SFO} \simeq$ 40 m^3/s and $Q_{Spillway}$ = 70 m^3/s.

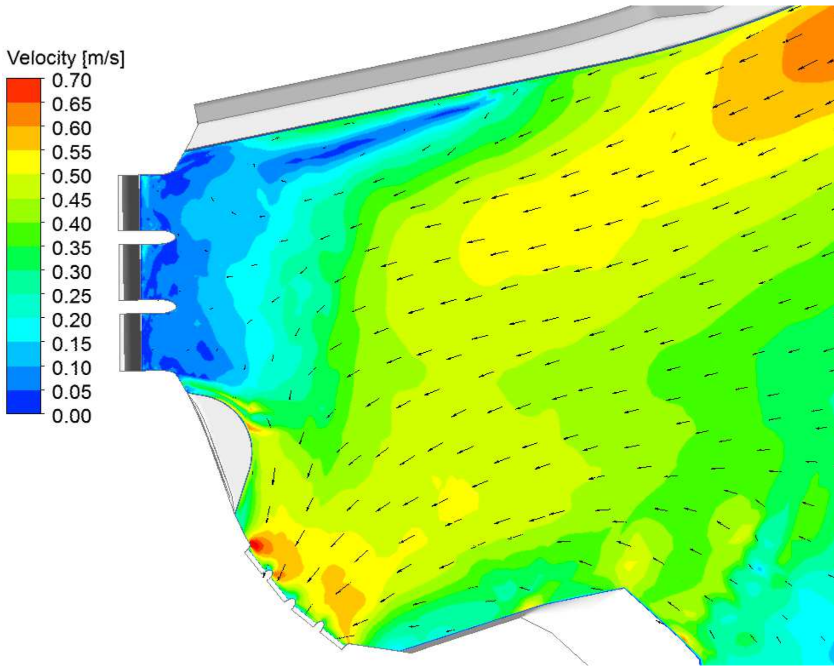

Figure 3.21: Velocity contours and vectors at 2.6 m depth from the numerical model for Case B: RWL = 50.2 m a.s.l., Q_{Intake} = 370 m^3/s, $Q_{SFO} \simeq$ 40 m^3/s and $Q_{Spillway}$ = 70 m^3/s.

In Figure 3.23 velocity contours and vectors are shown for the approach flow channel at an elevation of 49.5 m a.s.l. (0.7 m depth) in the numerical model. As the physical and numerical model are in good agreement for Case B, for water depth 2.6 m, the assumption can be made that the numerical model represents accurately the conditions at this shallower depth , 0.7 m, a depth the juvenile salmon is likely to inhabit. As seen in Figure 3.23 the conditions at 0.7 m depth are very similar to the conditions at 2.6 m depth in Figure 3.21, the attraction flow is extensive with gradual increase in velocity towards the intake and the SFO. The stagnant velocity in front of the spillway extends somewhat further upstream than observed at 2.6 m depth.

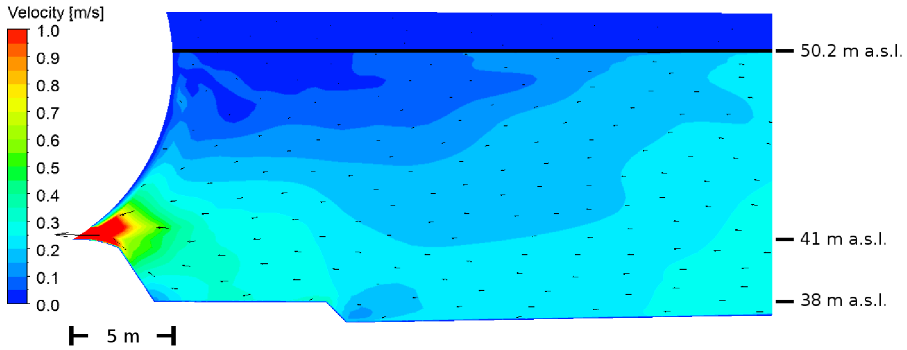

Figure 3.22: Velocity contours and vectors at an longitudinal section perpendicular to spillway gate 2, Case B. The solid black line shows the water surface.

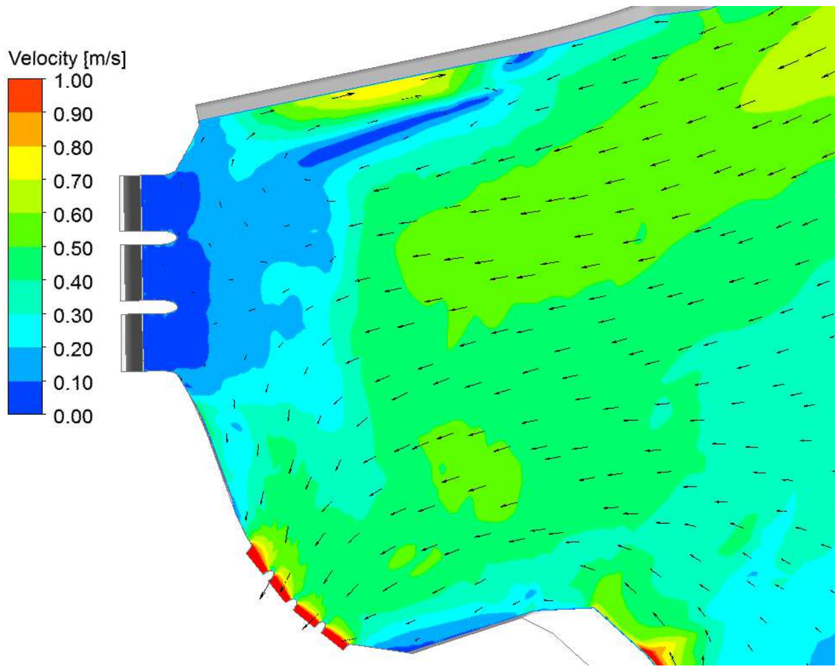

Figure 3.23: Velocity contours and vectors at 0.7 m depth from the numerical model for Case B: RWL = 50.2 m a.s.l., Q_{Intake} = 370 m^3/s, $Q_{SFO} \simeq$ 40 m^3/s and $Q_{Spillway}$ = 70 m^3/s.

Figures 3.24 and 3.25 show general flow behaviour and streamlines in the approach flow channel for the physical and numerical models respectively, for Case B. In Figure 3.25 bulk flow stream lines are shown on the left while surface streamlines are shown on the right. The models are in good agreement as the separation of streamlines heading towards the spillway is very similar between models, especially the particle tracks from the physical model and the bulk flow streamlines. A circular movement is observed close to the right approach bank in Figure 3.25. Although the movement is not presented in Figure 3.24, weak circular movement was documented during the particle test in the physical model just upstream from the location where the circular movement is observed in the numerical model. From Figures 3.24 and 3.25 the separation of streamlines is clear indicating the intake and the SFO as dominating features influencing the overall approach flow character.

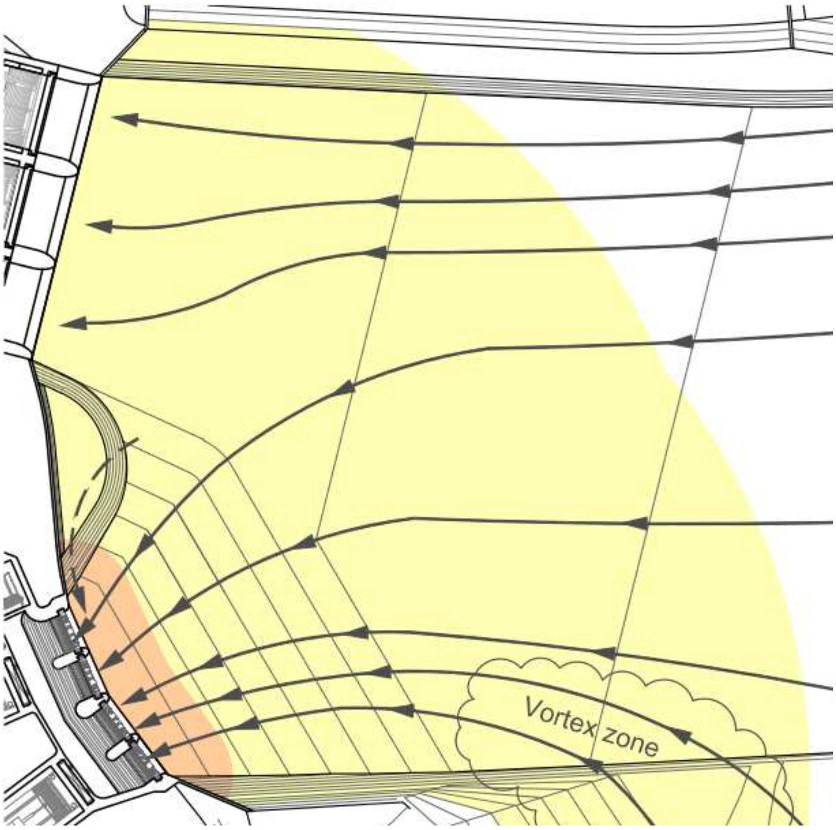

Figure 3.24: Results from particle test for Case B., Q_{Intake} = 370 m^3/s, Q_{SFO} = 40 m^3/s and $Q_{Spillway}$ = 70 m^3/s. Lines with arrows represent general flow characteristics, the decision zone is shown orange and the discovery zone yellow.

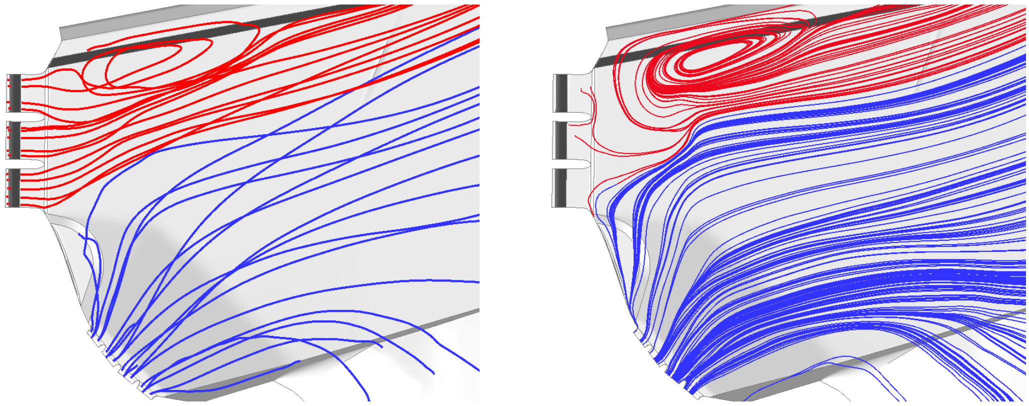

Figure 3.25: Streamlines in approach flow channel from the numerical model, Case B. On left: Bulk flow streamlines. On right: Surface streamlines.

3.2.3. Case C

In Figure 3.26 velocities from ADV measurements in the physical model (dots) and results from the numerical model (solid line) taken at 2.6 m depth are compared at Section Lines 10, 20, 40, 60, 80 and 100 for Case C: RWL = 50.2 m a.s.l., Q_{Intake} = 370 m^3/s, Q_{SFO} $\simeq$ 40 m^3/s and $Q_{Spillway}$ = 235 m^3/s. The ADV measurement points are shown with one standard deviation error band to indicate the magnitude of the flow fluctuations.

At Section 10 shown in Figure 3.26 the velocity distribution in the physical model is consistent with the numerical model results. A relatively even distribution is seen between Stations 30 to 70 with the exception of Station 30 in the physical model where a considerably lower value is observed. At Station 80 the velocity decreases in both models but from thereon increase to a maximum value at Station 110.

At Section 20 the velocity distribution is similar to the distribution at Section 10, the velocity from Station 30 to 80 has increased a bit for the numerical model. The models are in good agreement for Stations 50 to 120. At Stations 30, 40 and 130 the physical model show considerably lower values than the numerical results though the numerical values at Station 130 are within one standard deviation of the physical model value. Maximum value is reached for both models at Station 120.

At Section 40 the velocity distribution differs between models with lower values in most cases observed in the physical model. The physical model velocity distribution is in a U-shape manner whereas the numerical velocity distribution takes minimum values at each side of the approach flow channel and has a flat top from Station 40 to Station 120. Numerical values are only within one standard deviation of the physical model values at Station 70 and Station 110.

At Section 60 a U-shape velocity distribution is observed in both models with the numerical model having a flatter top. The models differ in values at Stations 30, 110 and 130 where the physical model takes considerably lower values. At other locations numerical results are within one standard deviation of the physical model results.

At Section 80 the models are in good agreement with the exception of the physical model value at Station 30 being considerably lower. The lower value at Station 30 has high standard deviation indicating fluctuations caused by turbulence in the model. The velocity distribution is relatively flat over the whole section with values ranging between 0.4 m/s and 0.6 m/s.

At Section 100 the models are consistent at Stations 50 and 70, at Stations 90 and 110 the velocity is considerably lower in the physical model. At Station 130 the ADV measurements take a maximum value of 0.8 m/s which is higher than the numerical model value at same location. The overall behaviour at Section 100 is consistent between the models if the outlier at Station 130 is ignored.

In Figure 3.26 the character between the models is very similar for Sections 10, 20 and 80. For Sections 40 and 60 the character differs more between the models with physical model velocity distribution in a somewhat U-shape manner while the numerical represents a more even velocity distribution. At Section 100 at noticeable outlier is observed at Station 130 at the left approach bank.

Figures 3.27 and 3.28 show velocity contours and vectors in the approach flow channel in the physical and numerical model respectively at 2.6 m depth. A similar behaviour is observed in the approach flow channel in both models, the stagnant velocity zone in front of the spillway has almost vanished and the approach flow spreads over the width of the approach flow channel. The approach flow channel is split into two parts, one is occupied by the current heading towards the intake and the SFO, the other heading towards the spillway. The main difference between the models is as in Cases A and B a strong current represented by a large velocity component at the left approach bank in the physical model perpendicular to the main current in the approach flow channel. Small stagnant velocity zones are observed inside the spillway bays in the numerical model as the water is pulled down under the spillway gates. In the figures the extensive attraction flow and gradual increase in velocity towards the intake and the SFO is clear. In both models the extent of the stagnant velocity zone in front of the spillway has reduced and almost disappeared because of the increased spillway discharge. The whole approach flow channel is now occupied by the main approach flow current.

The vertical extent of the stagnant velocity zone is shown in Figure 3.29 where velocity contour lines and velocity vectors are shown at a longitudinal section perpendicular to spillway gate 2. As the figure shows the stagnant zone extends to depths of approximately 2 m immediately upstream of the spillway crest, the lateral extent of the stagnant zone has decreased from Case B and occupies almost exclusively the area within the spillway bays. Fish attracted towards the spillway may loose meander for some time in front of the spillway gates as they generally dive through deep passages as last resort. The distance from the stagnant zone to the point where the surface flow starts to accelerate towards the SFO is not great (about 85 m). Assuming the juvenile salmon is active in search of appropriate route through the system they should be able to find the SFO attraction flow.

In Figure 3.30 velocity contours and vectors are shown for the approach flow channel at an elevation of 49.5 m a.s.l., 0.7 m depth, in the numerical model. As the physical and numerical model are in good agreement for Case C as shown in Figures 3.27 and 3.28 the assumption can be made that the numerical model represents similar conditions as the physical model at a shallower depth, 0.7 m, a depth the juvenile salmon is likely to inhabit. As seen in Figure 3.30 the conditions at 0.7 m depth are almost identical to the conditions at 2.6 m depth in Figure 3.28, the extent of the attraction flow is extensive with gradual increase in velocity towards the intake and the SFO. The stagnant velocity in front of the spillway has expanded somewhat further upstream than observed at 2.6 m depth. The main current occupies almost the whole approach flow channel, the separation of flow between the spillway and the intake is clear and the attraction flow is extensive with gradual increase in velocity towards the intake and the SFO. The stagnant velocity in front of the spillway extends somewhat further upstream than observed at 2.6 m depth, a small stagnant zone is observed at the left abutment of the intake and the SFO. Velocity distribution in the approach flow channel is more even than at 2.6 m water depth.

Figures 3.31 and 3.32 show general flow behaviour and streamlines in the approach flow channel for the physical and numerical model respectively for Case C. In Figure 3.32 bulk flow streamlines are shown on left while surface streamlines are shown on right. The models are in good agreement as the separation of streamlines heading towards the spillway is very similar between the physical model particle tracks and the numerical bulk flow streamlines. From Figures 3.31 and 3.32 the separation of streamlines is clear indicating the spillway and intake have near equal influence on the approach flow conditions.

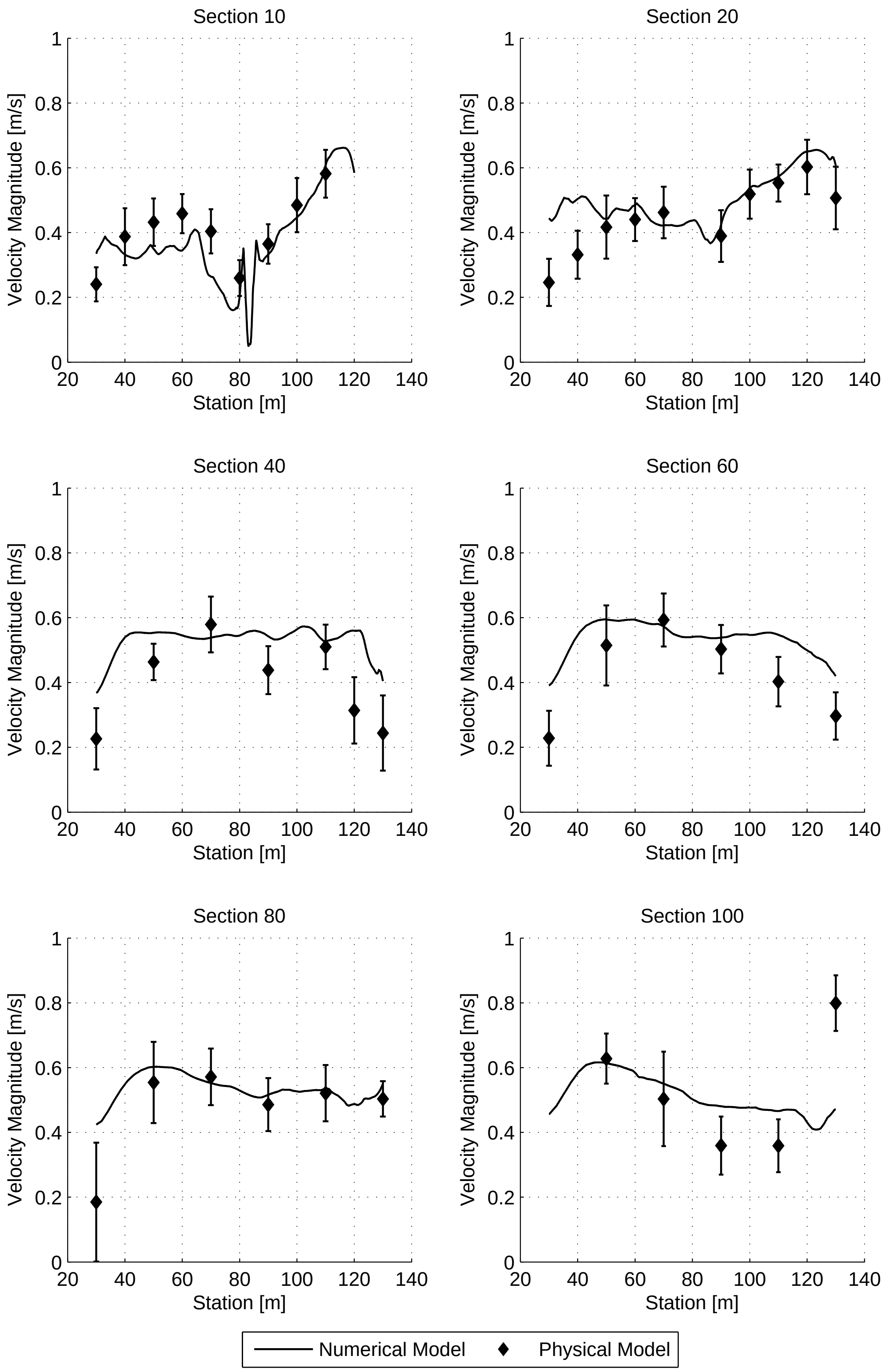

Figure 3.26: Velocity comparison between physical and numerical models at Section Lines 10, 20, 40, 60, 80 and 100 for Case C: RWL = 50.2 m a.s.l., Q_{Intake} = 370 m^3/s, $Q_{SFO} \simeq$ 40 m^3/s and $Q_{Spillway}$ = 235 m^3/s.

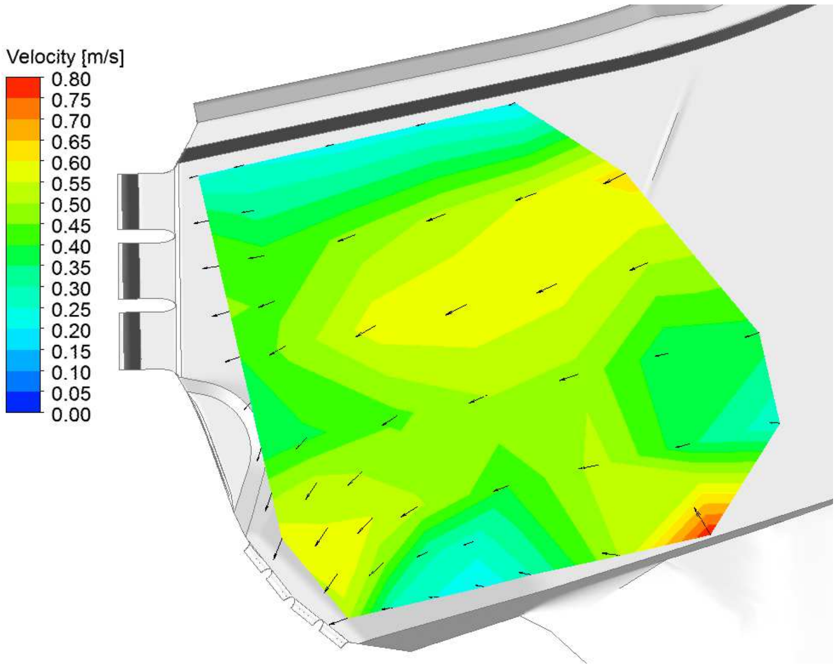

Figure 3.27: Velocity contours and vectors at 2.6 m depth from the physical model for Case C: RWL = 50.2 m a.s.l., Q_{Intake} = 370 m^3/s, $Q_{SFO} \simeq 40$ m^3/s and $Q_{Spillway}$ = 235 m^3/s.

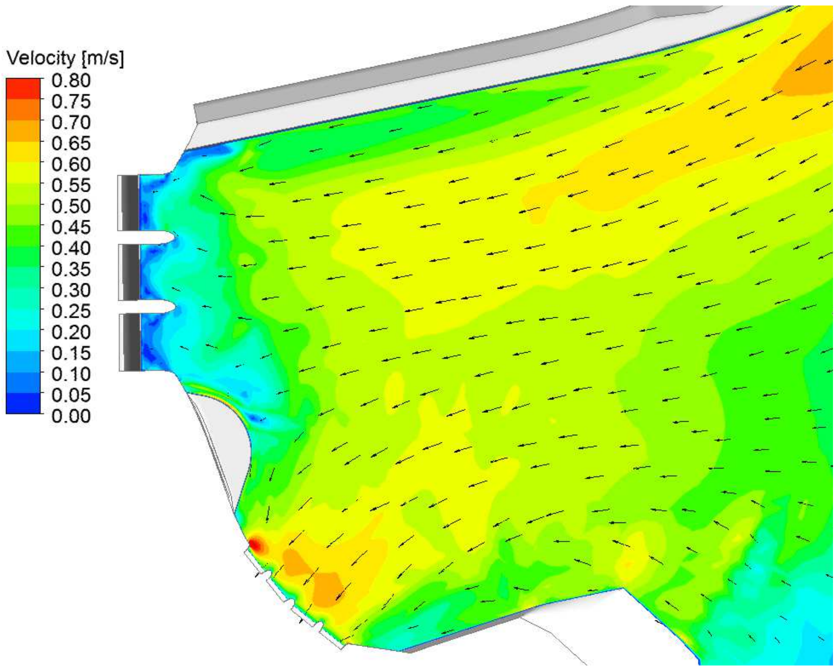

Figure 3.28: Velocity contours and vectors at 2.6 m depth from the numerical model for Case C: RWL = 50.2 m a.s.l., Q_{Intake} = 370 m^3/s, $Q_{SFO} \simeq 40$ m^3/s and $Q_{Spillway}$ = 235 m^3/s.

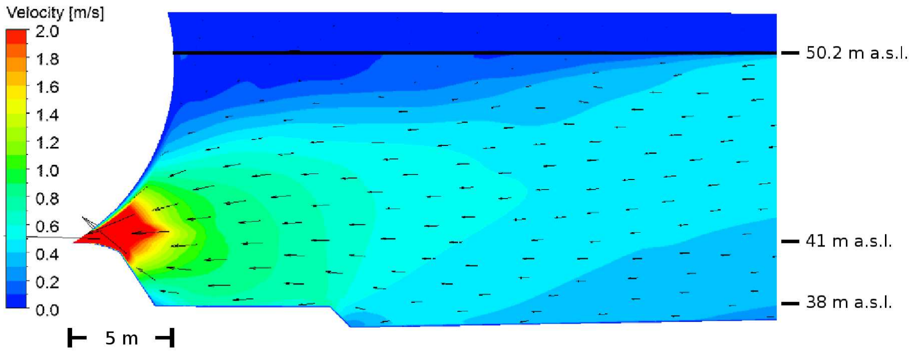

Figure 3.29: Velocity contours and vectors at an longitudinal section perpendicular to spillway gate 2, Case C. The solid black line shows the water surface.

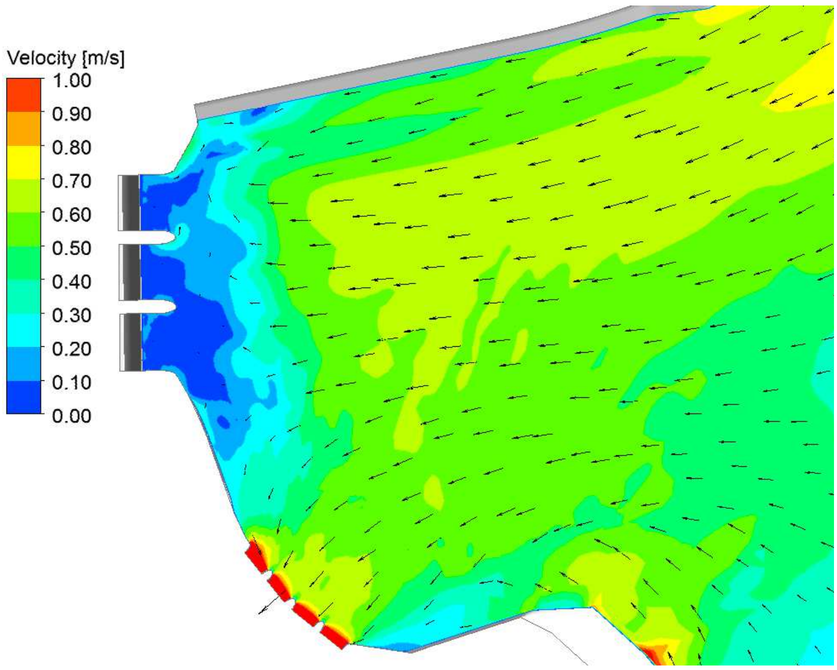

Figure 3.30: Velocity contours and vectors at 0.7 m depth from the numerical model for Case C: RWL = 50.2 m a.s.l., Q_{Intake} = 370 m^3/s, $Q_{SFO} \simeq$ 40 m^3/s and $Q_{Spillway}$ = 235 m^3/s.

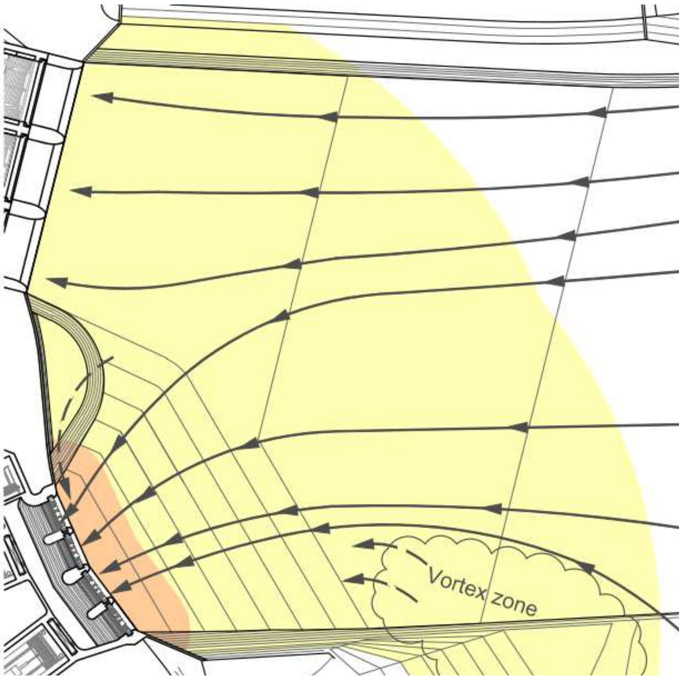

Figure 3.31: Results from particle test for Case C, Q_{Intake} = 370 m^3/s, Q_{SFO} = 40 m^3/s and $Q_{Spillway}$ = 235 m^3/s. Lines with arrows represent general flow characteristics, the decision zone is shown orange and the discovery zone yellow.

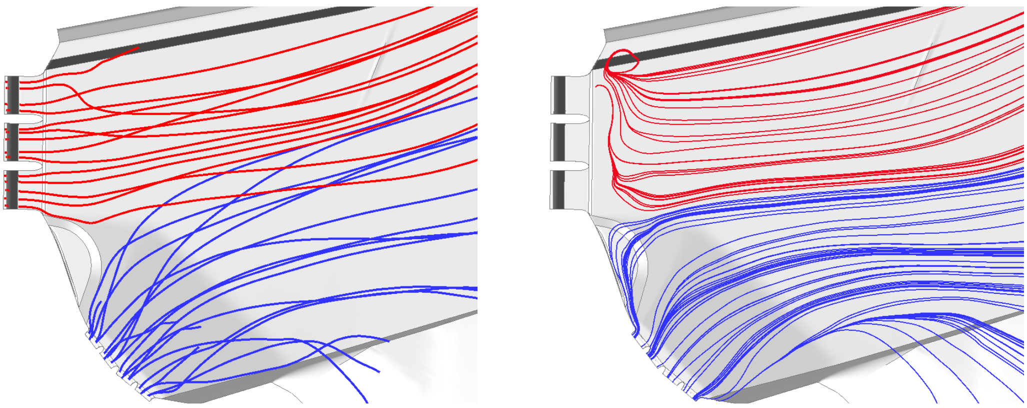

Figure 3.32: Streamlines in approach flow channel from the numerical model, Case C. On left: Bulk flow streamlines. On right: Surface streamlines.

3.2.4. Vertical Streamline Separation between the SFO and the Intake

In Table 3.2 results of the dye tests conducted during the physical model test are shown. The result show the depth of water which the SFO transports ranges between 1 m and 1.5 m for cases A, B and C. The depth at which half of the water is transported by the SFO and half by the intake ranges between 1.5 m and 2 m. The depth at which the intake starts solely to draw water is below 2 m depth.

Table 3.2: Results from dye tests showing Reservoir Water Level (RWL), depth where water flows only to the SFO (Only SFO), depth where water is divided evenly between the intake and the SFO (Intake/SFO; 50/50) and the depth where water flows only to intake (Only Intake). The dye is released 10 m upstream of the intake.

Case	RWL [m a.s.l.]	Only SFO [m] depth	Intake/SFO; 50/50 [m] depth	Only Intake [m] depth
A	50.2	1-1.5	1.5-2	>2
B	50.2	1-1.5	1.5-2	>2
C	50.2	<1	1.5	>2

During the dye test a distinct behaviour was observed immediately upstream of the SFO crest where a dye released perpendicular to SFO Entrances 1 and 4 was drawn toward the center entrances, Entrances 2 and 3. The observed behaviour shown in Figure 3.33 is be caused by lateral flow as can be seen from Figure 3.32.

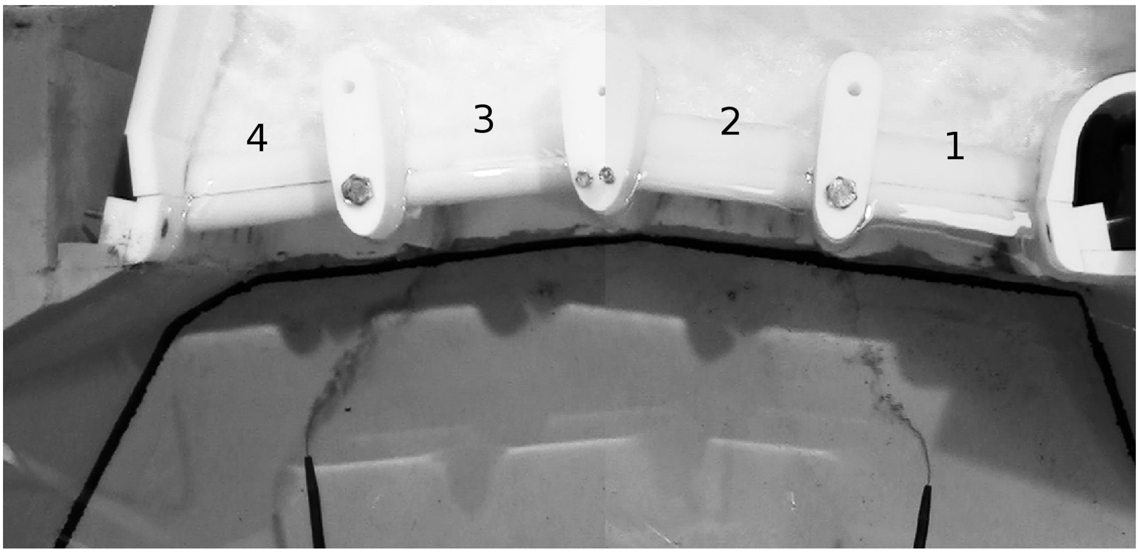

Figure 3.33: Streamlines drawn towards SFO Entrances 2 and 3 during a dye test.

In Figure 3.34 streamline separation in front of the intake and the SFO is shown. In the figure two plots are shown, on left a plot extending the whole depth in front of the intake and the SFO and reaching 25 m upstream, on right a close up of the streamline separation in front of the SFO crest is shown. On the plot on the right side the streamline separation is clear at 47.5 m a.s.l. or 2.7 m depth.

If the streamline separation results from the physical and numerical models are compared the numerical model indicates water transported from greater depth by the SFO than physical model results indicate. During the dye test in the physical model estimating the depth of water transported by the SFO proved not trivial as turbulence in front of the intake would mix the dye vertically. Because of this, the dye did in some cases enter both the SFO and the intake. Hence, the numerical model is a valuable tool in estimating the water depth the SFO can transport and confirms that the criteria of 1 m water depth transport is fulfilled. There is a good agreement between the results of the numerical model (Figure 3.34) and the physical model (Table 3.2).

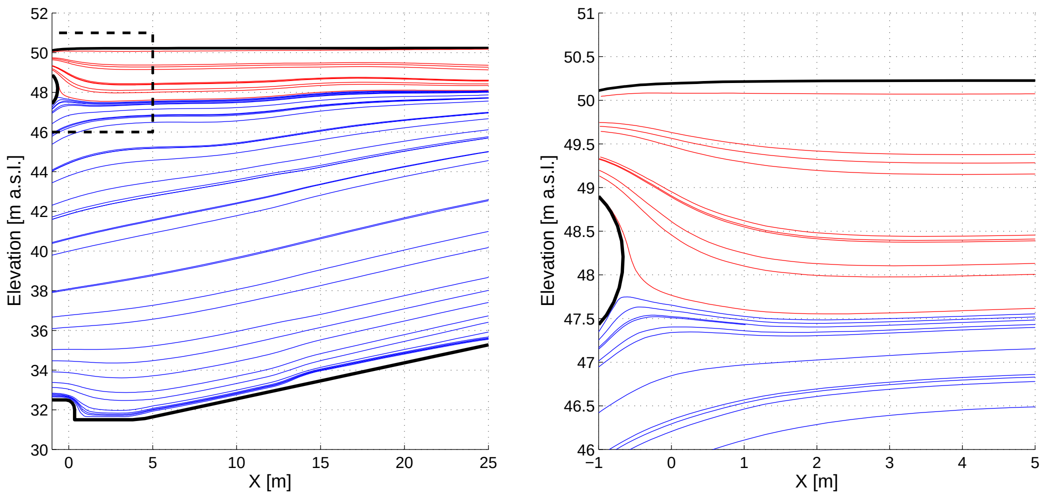

Figure 3.34: Streamline separation between the intake and the SFO in the numerical model for Case A. The blue streamlines head to the intake and the red streamlines to the SFO. On the left, the streamline separation over the whole depth in front of the intake is shown and on the right a more detailed view of the streamline separation at the SFO nose is shown. The detailed area is shown on the left as a box with dashed lines.

3.2.5. Velocities in the Decision Zone

In Figure 3.35 water velocities at 0.5 m water depth are shown at lines perpendicular to the SFO entrances for Case A in the numerical model. The figure shows that the velocity distribution is similar upstream of all the SFO entrances. The velocity increases gradually from 0.5 m/s 10 m upstream of the SFO entrances to approximately 1 m/s 2 m upstream of the SFO entrances. From thereon the flow accelerates to almost 3 m/s at the SFO crest. The acceleration is smooth with the acceleration almost 1 m/s per meter over the last 2 m towards the SFO entrances. Thus the SFO fulfils the design criteria set forth in Section

2.3, smooth acceleration about 1 m/s per meter just upstream of the SFO entrance and flow velocities at the SFO entrance > 2-3 m/s.

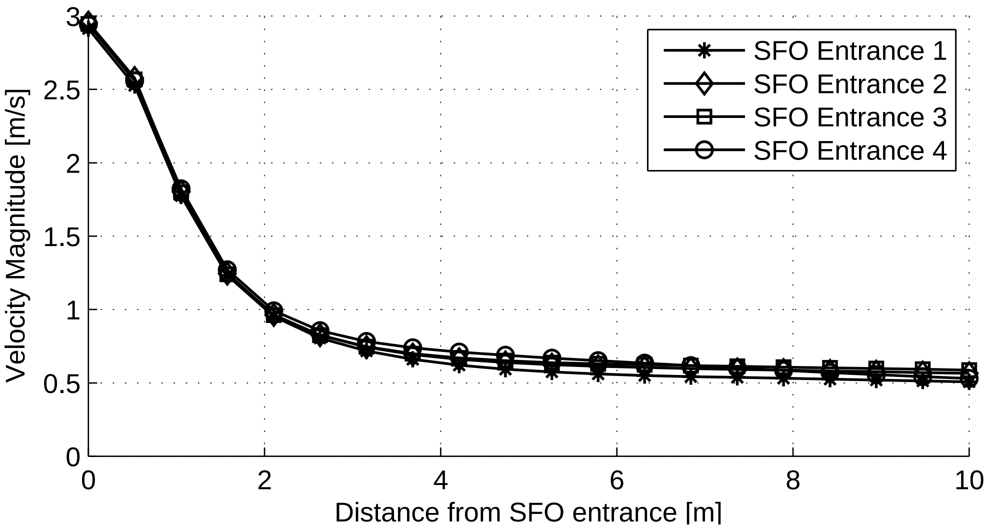

Figure 3.35: Velocity magnitudes in the Decision zone at lines perpendicular to the SFO entrances for Case A.

3.2.6. Summary

The models represent a prediction of conditions in the discovery and decision zones which can be used to evaluate the effectiveness of the approach and the SFO layout. In general, the approach flow conditions for all cases are satisfactory for juvenile fish passage and the models are in good agreement regarding the general flow behaviour. The approach flow conditions inside the approach flow channel are influenced by project operations, when spillway discharge is zero the intake and the SFO are the main factors influencing the approach flow conditions. This good performance of the SFO can be expected in 59 % of the time as shown in Table 3.1. With increasing spillway discharge the spillway influence increases. It can therefore be concluded that the approach flow conditions are directly related to the ratio between the spillway and the intake discharge. In the stagnant velocity zone in front of the spillway juvenile salmon might get delayed, losing track of the main current towards the SFO. Likewise during spillway operation fish attracted towards the spillway may enter the stagnant zone in front of the spillway and loose track of the SFO attraction flow. However, this is in most cases a small portion of the flow and events of significant amount of spillway discharge as in Case C can only be expected over 5 % of time as shown in Table 3.1.

The physical and numerical models are consistent with regards to streamline separation in the approach flow channel. The bulk flow streamlines from the physical model represent behaviour more consistent with the physical particle tracks. As the separation of flow between spillway and intake in the approach flow channel is distinct there is the possibility of a large portion of the juvenile salmon swimming towards the spillway during events with large discharge to the spillway. Johnson and Dauble (2006) and Sweeney et al. (2007) discuss the population of fish splitting up where the bulk flow splits. With regard to the vertical flow distribution Coutant and Whitney (2000) suggest migrating juvenile salmon generally not descending to the lower two thirds of the water column and fish drawn towards the spillway may not want to dive under the spillway gates and therefore get delayed on their migration route. However, events of spillway discharge are expected over less than 41 % of the time as shown in Table 3.1. During the migration period 91% of the juvenile salmon are expected to enter the SFO (Karadottir & Gudjonsson, 2012a).

Irregularities observed at the left approach bank are not consistent between the models. With increasing discharge in the physical model the irregularities increase which may be the cause of increasing amount of water in the physical model travelling by the boundary of the model and finally coming with increased momentum over the left approach bank. The increased amount of water travelling by the boundary of the physical model with increased discharge can also account for considerably less velocities observed in the approach flow channel for cases B and C in the physical model compared to the numerical model. Irregularities affecting attraction flow in such manner that the attraction flow becomes less distinct may have negative effect on the juvenile salmon (Johnson & Dauble, 2006). The irregularities do not seem to affect the attraction flow considerably and therefore the negative effect should be minimal.

The results from the dye test and numerical model indicate the SFO transporting water from depths ranging from 1 m to 2.7 m depending on project operation. The numerical model showed more distinct separation of streamlines at greater depth than the physical model where distinguishing the separation depth proved not trivial due to vortices scattering the dye vertically.

The SFO layout fulfils the design criteria set forth in Section 2.3 (upstream of SFO). During Case A, total discharge in the system is 410 m^3/s, 9.7 % of the total discharge flows to the SFO. With increased spillway discharge the percentage of flow to the SFO reduces. However, events where significant amount of spillway discharge is observed occur in low percentage of time. The attraction flow towards the SFO is smooth with gradual acceleration towards the SFO entrances. Acceleration of almost 1 m/s per meter at the SFO entrances are observed with the velocity taking a maximum value of almost 3 m/s on the SFO crest. No significant abnormalities are observed within the attraction flow with null zones or deceleration zones observed on the boundaries of the attraction flow without affecting it significantly.

The result show the extensive attraction flow created by the intake and the SFO should effectively attract the juvenile salmon and guide it towards the SFO entrance.

3.3. Surface Flow Outlet

The Surface Flow Outlet (SFO) model was tested for four different discharges 20 m^3/s, 30 m^3/s, 40 m^3/s and 50 m^3/s. The model is intended to shed a light on the flow conditions inside the SFO channel with regards to the design criteria set forth in Section 2.3. Measurements inside the SFO conveyance channel were not carried out due to the small scale of the channel which made it hard to carry out measurements inside the SFO conveyance channel. As of that numerical results could not be compared or validated using the physical model. That said the numerical model of the SFO channel is only used as an indication of flow conditions inside the channel. Figure 3.36 shows location of cross section and naming convention for the SFO channel. The downstream end of the model is a control with a critical depth, 60 m downstream of the gate house.

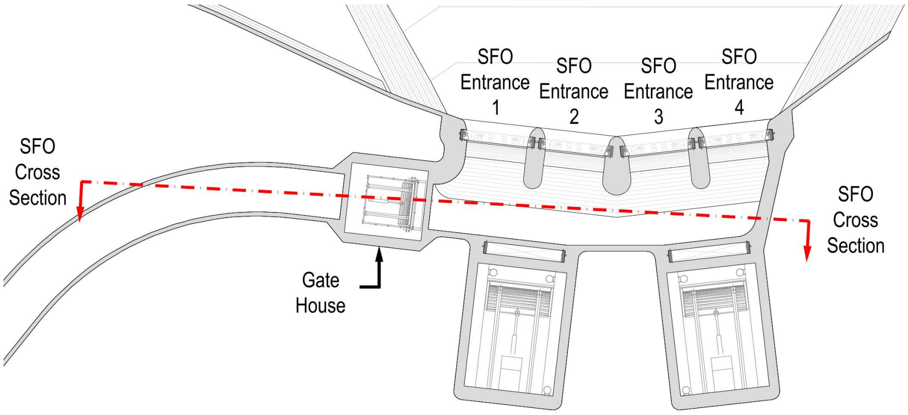

Figure 3.36: SFO channel naming convention and cross section location.

3.3.1. Water Elevations and Velocity

Figure 3.37 shows water elevations at a cross section shown in Figure 3.36 located at the center of the SFO channel for discharges 20 m^3/s, 30 m^3/s, 40 m^3/s and 50 m^3/s. The water elevations are derived from contour plots of volume fractions of water, from the contour plots poly lines are extracted at a desired contour level which represents the water surface as was described in detail in Section 2.6. Similar contour plots as used to derive the water elevations are shown in Figure 3.42. Figure 3.37 shows the water levels downstream of the SFO crest. Water surface elevations at Stations 30 to 60 are considerably higher than water surface elevations downstream in the conveyance channel at Stations 0 to 25. The difference becomes more distinct at higher discharges. Water depths inside the channel range from 2 m up to 4.4 m. The figure shows a draw down at Station 25 during discharges of 40 m^3/s and 50 m^3/s. Figure 3.38 shows the wave at 50 m^3/s in a perspective view. The draw down is caused by the transition where the SFO channel contracts. At the contraction the unit discharge increases but the specific energy stays constant, because the flow regime is subcritical a draw down occurs.

In Figure 3.39 velocity contours at the cross section in Figure 3.36 are shown for the discharge series. The figure shows velocities downstream of the SFO entrances range from 1 m/s to 4.7 m/s with the velocities after the contraction downstream of Entrance 1 above 2 m/s. Maximum values of velocity are observed at the contraction where the aforementioned draw down occurs.

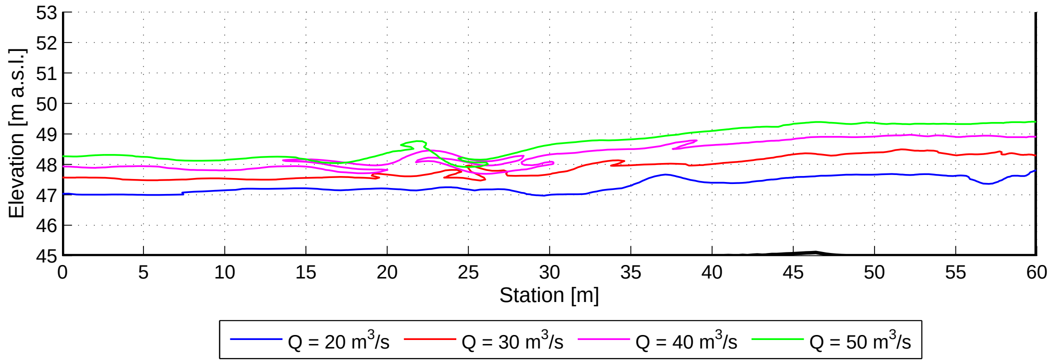

Figure 3.37: Water levels inside the SFO channel at a cross section shown in Figure 3.36.

In Figure 3.40 water levels inside the SFO at longitudinal sections perpendicular to each SFO entrance are shown. The water levels range from 47.2 m a.s.l. to 49.4 m a.s.l., which corresponds to 2.2 m to 4.4 m water depths, respectively. The water levels downstream of the SFO crest rise above the SFO crest elevation, 49.1 m a.s.l., for discharges, 40 m^3/s and 50 m^3/s at Entrances 3 and 4. At 50 m^3/s discharge water levels downstream of entrance 2 rise also above the SFO crest elevation. Though the water elevations rise high during 40 to 50 m^3/s discharge the downstream water elevation only starts to affect the SFO discharge capacity downstream of Entrance 4 at 50 m^3/s discharge as calculations in Table 3.3 show. Spillway discharge capacity is

$$Q = CL_{eff}H_0^{3/2} \tag{3.1}$$

where Q is total discharge, L_{eff} is the effective length of the spillway crest and H_0 is the total head on the spillway crest. The constant C is the dimensionless coefficient of discharge derived as a multiplication of many factors, including a factor k_2 which accounts for downstream submergence. As shown in Table 3.3 all cases except for case shown gray in the table, Entrance 4 at 50 m^3/s, the k_2 factor is equal to one and in that case it is 0.9 yielding some effect on the SFO Entrance 4 discharge capacity.

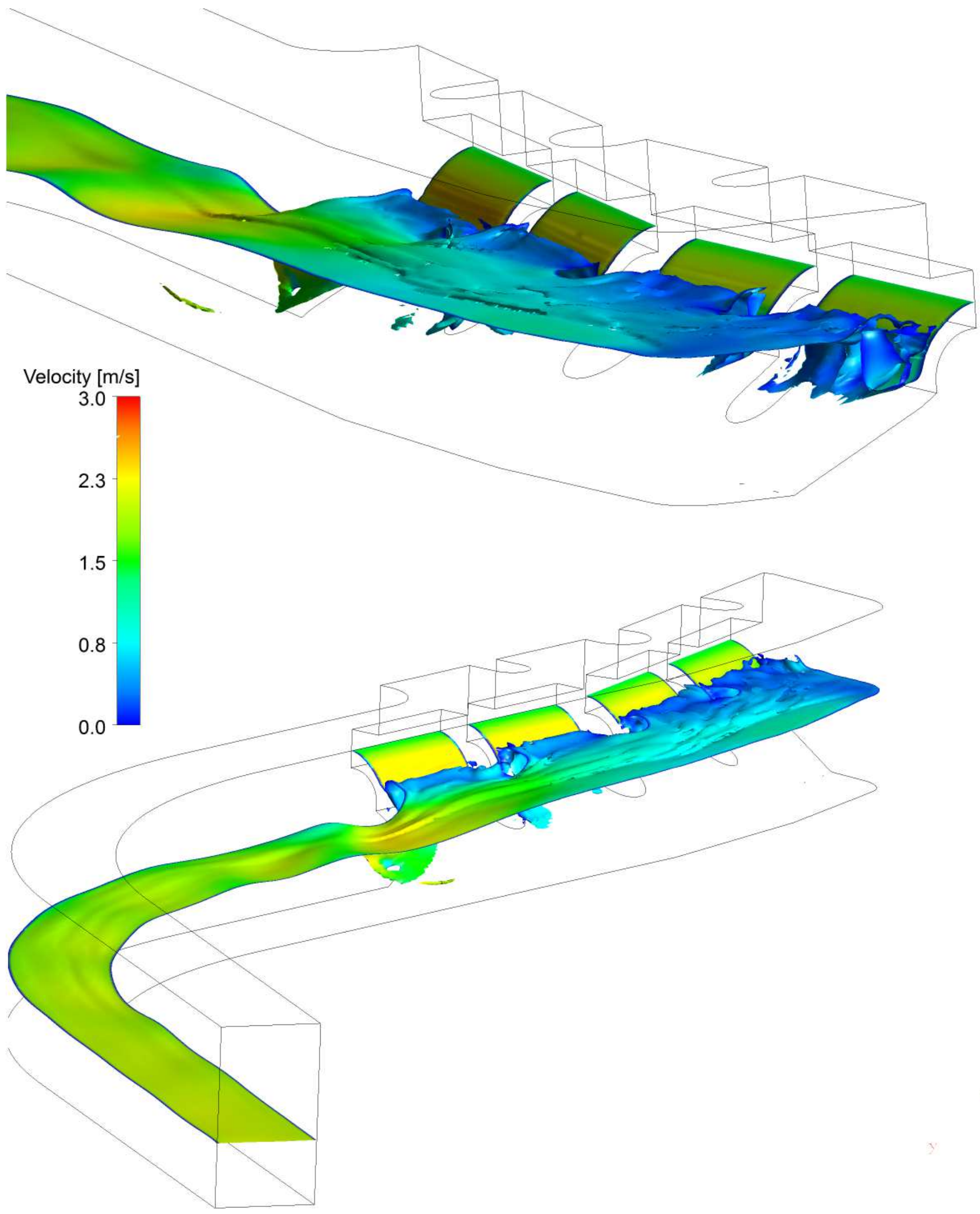

Figure 3.38: Perspective views of the velocity magnitude at the water surface in the SFO channel at discharge 50 m^3/s.

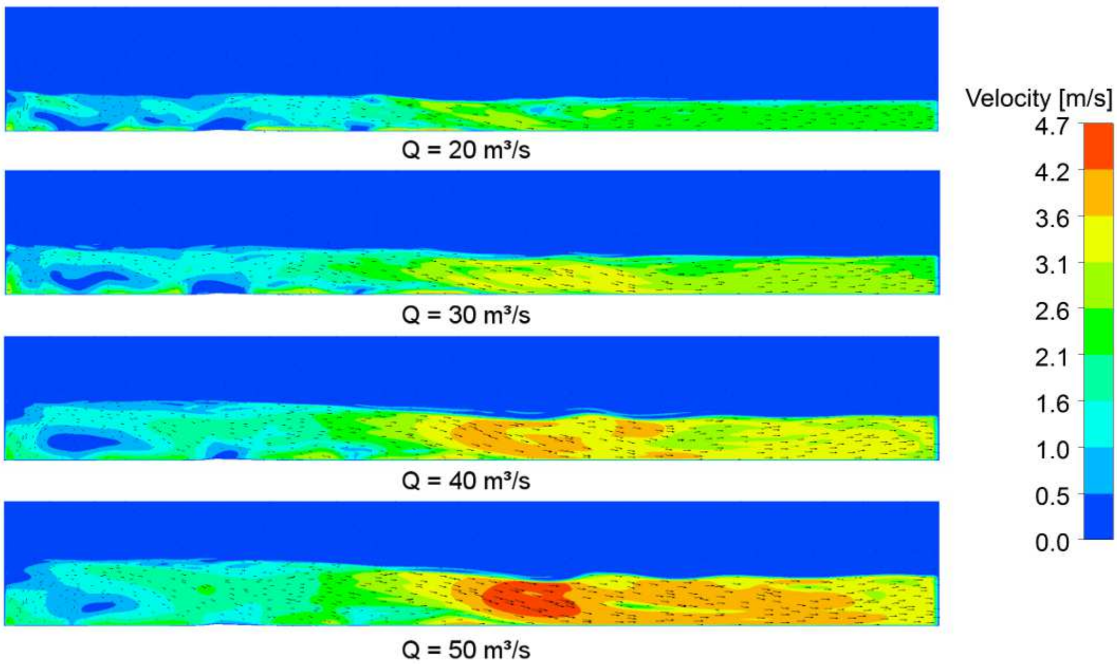

Figure 3.39: Water velocity magnitudes at cross section shown in Figure 3.36 inside the SFO for discharges 20 m^3/s, 30 m^3/s, 40 m^3/s and 50 m^3/s.

Table 3.3: Calculations of the downstream water elevation on the SFO discharge capacity. H_d/H_a is the ratio between the difference of critical water elevation on the SFO crest and the water elevation downstream of the SFO crest (H_d) and the water depth on the SFO crest (H)

	Discharge [m^3/s]	Critical water elevation on the SFO crest [m a.s.l.]	Water elevation inside downstream of crest [m a.s.l.]	H_d/H_a	k_2
Entrance 1	20	49.77	47.36	3.6	1
	30	49.98	48.23	2.0	1
	40	50.16	48.49	1.6	1
	50	50.34	48.79	1.2	1
Entrance 2	20	49.77	47.51	3.4	1
	30	49.98	48.37	1.8	1
	40	50.16	48.95	1.1	1
	50	50.34	49.18	0.9	1
Entrance 3	20	49.77	48.09	2.5	1
	30	49.98	48.45	1.7	1
	40	50.16	48.87	1.2	1
	50	50.34	49.36	0.8	1
Entrance 4	20	49.77	48.10	2.5	1
	30	49.98	48.69	1.5	1
	40	50.16	48.77	1.3	1
	50	50.34	49.56	0.6	0.9

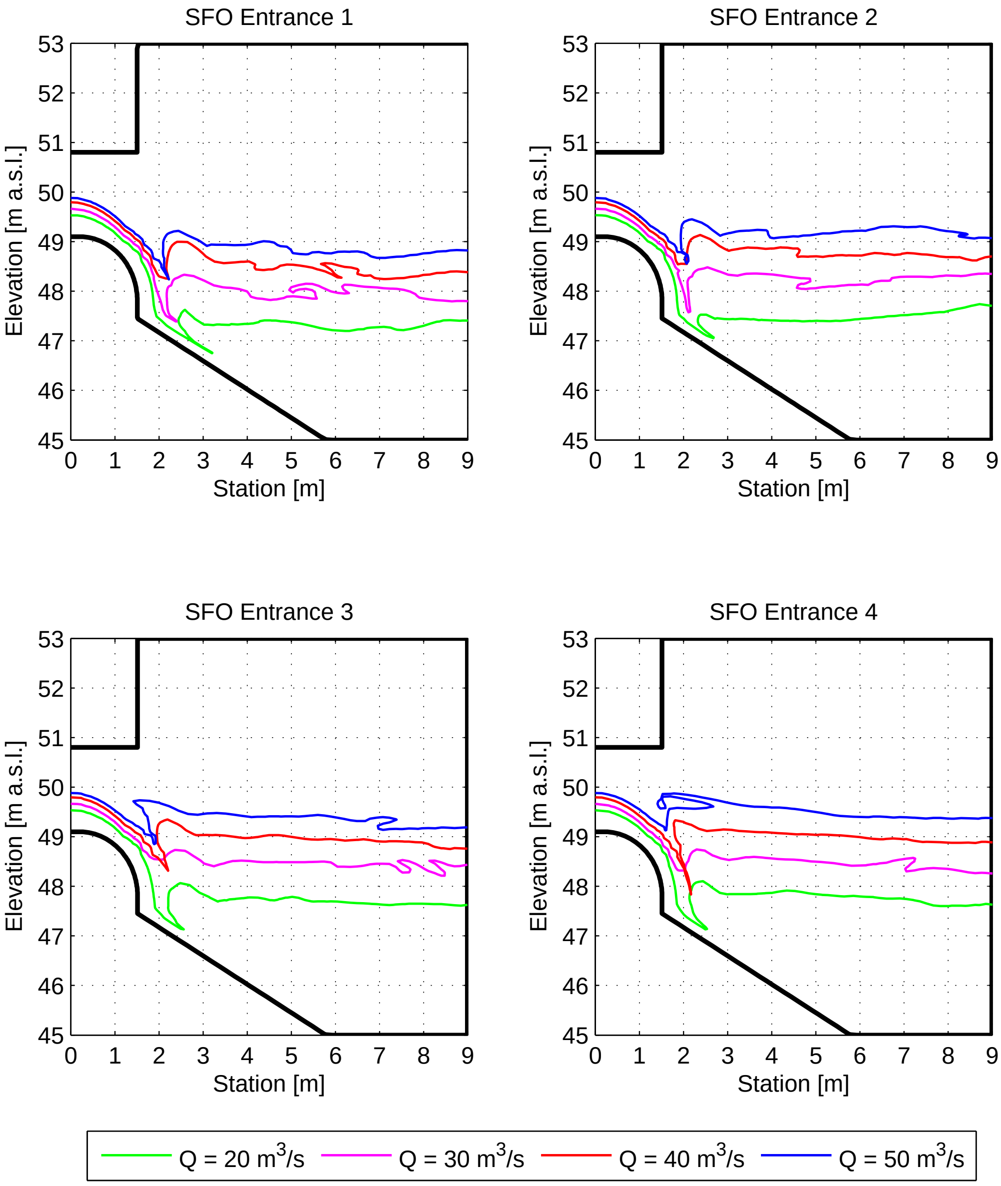

Figure 3.40: Water levels inside the SFO channel at longitudinal sections perpendicular to the middle of each SFO entrance.

3.3.2. SFO Flow Character

In the SFO, the water flows over the SFO crest down into a side way channel, turns 90 degrees and continues downstream. In Figure 3.41 streamlines in the SFO channel are shown at 50 m^3/s discharge. The figure shows the streamlines flowing down from the SFO crest into the side way channel along the bottom, taking a halfway roll and continue downstream. The same behaviour is observed at smaller discharges.

In Figure 3.42 water elevations and velocity vectors at longitudinal sections perpendicular to the middle of Entrances 1, 2, 3 and 4 at the design discharge 40 m^3/s are shown. The figure shows clearly the rolling motion as the water takes the 90 degree turn downstream. A turbulence mixture of water and air downstream of the SFO entrance is observed.

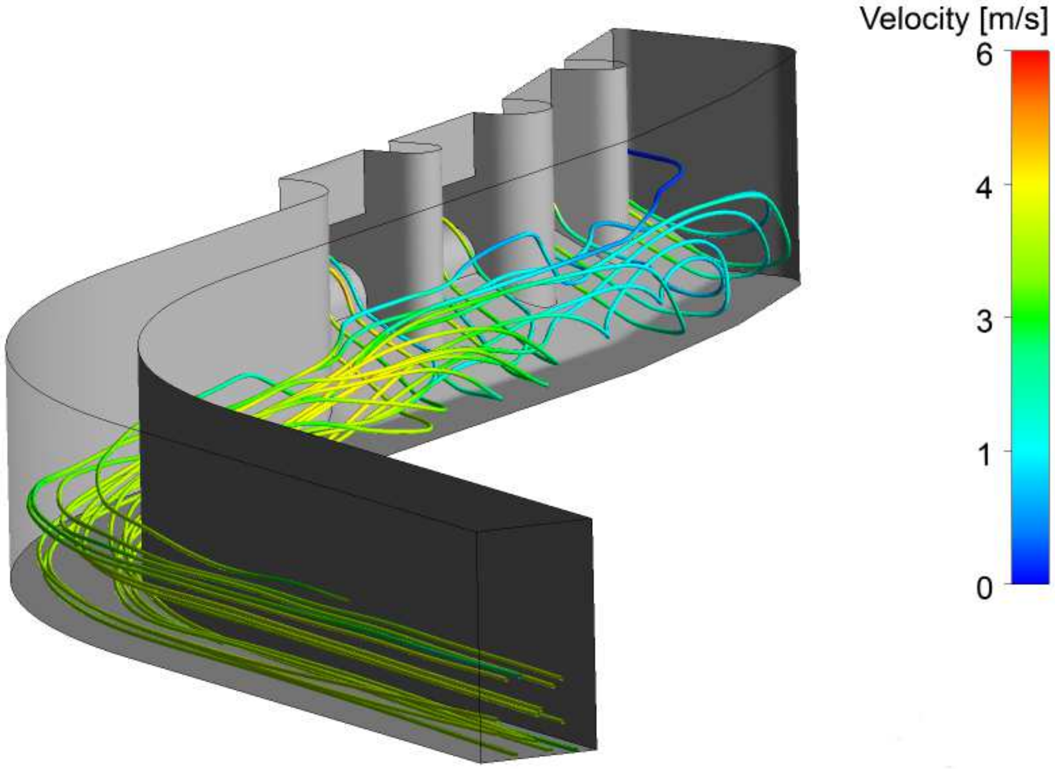

Figure 3.41: Streamlines inside the SFO channel at discharge of 50 m^3/s.

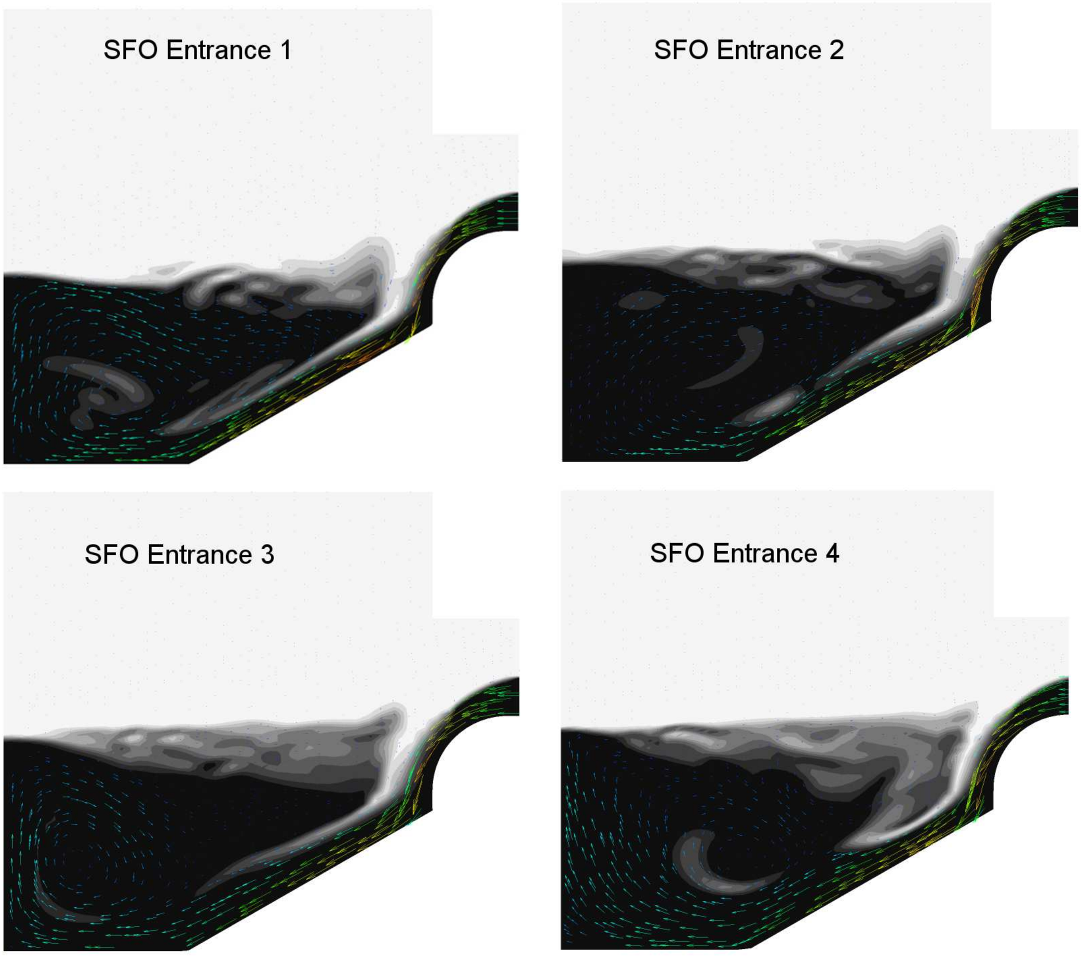

Figure 3.42: Water levels and velocity vectors at longitudinal sections in the SFO at discharge 40 m^3/s.

3.3.3. SFO Summary

The flow characteristics inside the SFO conveyance channel are in general satisfactory for the discharges tested. In general the SFO layout fulfils the design criteria set forth in Section 2.3. The flow enters the side way channel, takes a swift 90 degree turn and carries on without delay downstream in the channel. Flow velocities range from 1.5 to 4.7 m/s in the conveyance channel where local abrupt changes in acceleration are only observed downstream of the SFO entrances and at Station 25 where a drop in water elevation is observed because of channel contraction. The SFO channel is smooth with no intrusions, sharp corners, rough walls or locations where sediment or debris is likely to accumulate.

When water flows over a spillway crest the water can get aerated with bubbles forming in the water. If bubbles are carried deep into a stilling basin or a downstream pool the water can get supersaturated with dissolved gases, oxygen and nitrogen, when the gases inside the bubbles are dissolved into the water by pressure (Pickett et al., 2004). Supersaturation of dissolved gases in water can cause gas bubble trauma in fish which can severely traumatise the fish or even lead it to death (Fidler & Miller, 1994). The probability of supersaturation of dissolved gases because of air entrainment in the SFO is low, although air may get entrained into the water, the depth inside the channel and pressures are not large enough to dissolve the gases into the water phase.

In general, the SFO should be able to carry the juvenile salmon safely and with out delay downstream to the tailwater of the dam.

3.4. Verification

Solutions of numerical models can be dependent on the quality and size of the computational grid or mesh. To evaluate whether the mesh had been refined to the point where no significant changes where observed in the character of the flow behaviour in the numerical model additional models with different mesh sizes were computed for the SFO and reservoir models. The reservoir models were computed for conditions representing Case A while the SFO models were computed for a discharge of 40 m^3/s. In Table 3.4 relevant parameters of the meshes tested are shown.

Table 3.4: Parameters of computational meshes used for verification of main mesh. The parameters for the meshes used in the main test cases highlighted in gray.

Model	Number of nodes	Number of elements	Percentage of final mesh size
Reservoir	1930440	1866768	100
Reservoir	1715580	1657713	89
Reservoir	1582932	1528549	82
SFO	1206225	1153540	119
SFO	1010460	963380	100
SFO	587955	555264	58
SFO	332253	310141	33

Figure 3.43 shows velocity distribution at Section 20 in the reservoir model (location of sections shown in Figure 3.12). As seen in the figure the velocity distribution is very similar with only slight difference between smaller two meshes and the largest at Stations 40 and from Station 120 to Station 130. It can therefore be concluded that the mesh used, M1930, is sufficient for evaluation of the approach flow characteristics.

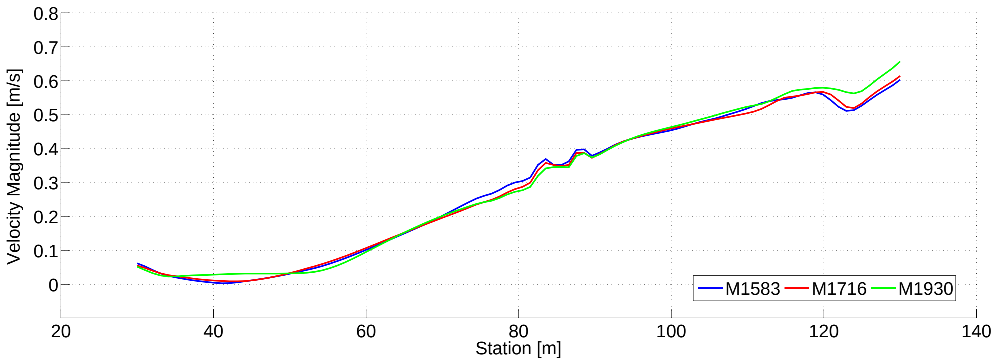

Figure 3.43: Velocity distribution at Section 20 for different reservoir mesh sizes. M1583 = 1528549 nodes, M1716= 1715580 nodes and M1930 = 1930440 nodes.

Figure 3.44 shows water elevations at a cross section in the SFO model shown in Figure 3.36. The figure shows the water elevations are very similar for all mesh sizes especially for meshes M588, M1010 and M1206. A small difference is observed at Station 20 for Mesh M332. It can therefore be concluded that the mesh used for the evaluation, M1010, is sufficient to show the character of the SFO conveyance channel.

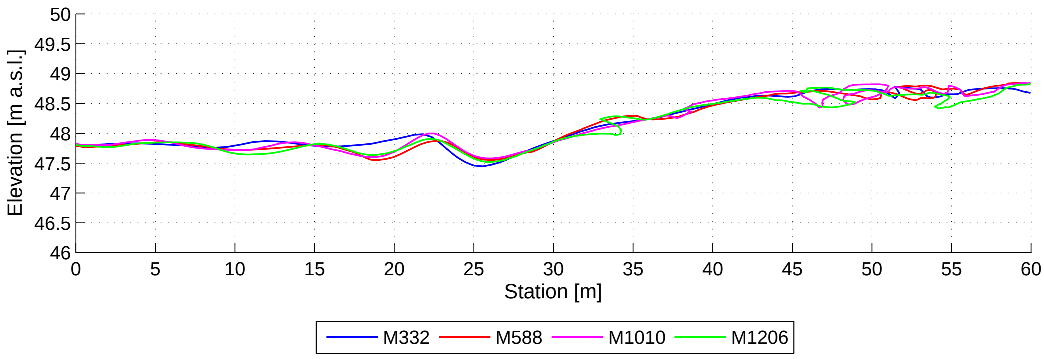

Figure 3.44: Water elevations for different SFO mesh sizes at a cross section. M332 = 332253 nodes, M588 = 587955 nodes, M1010 = 1010460 nodes and M1206 = 1206225 nodes.

4. Conclusion

In this report, results from a physical model and a numerical model of Heiðarlón Reservoir are compared upstream of the proposed Surface Flow Outlet (SFO) structure. The models are tested with regard to parameters related to fish passage in order to evaluate the effectiveness of the SFO structure. The study also includes an investigation of the SFO conveyance channel with a separate numerical model. The SFO conveyance channel model is tested and evaluated with respect to flow conditions and other features which may prove hazardous to the juvenile salmon as it is transported downstream to the tail waters.

In general the overall flow characteristic of the reservoir models are in good agreement and can be used to evaluate the effectiveness of the approach flow channel and the SFO layout. A stagnant velocity zone forms immediately upstream of the spillway, the extent of the stagnant zone is directly related to spillway discharge, reducing with increased spillway discharge. Juvenile salmon entering the stagnant velocity zone immediately upstream of the spillway may loose track of the attraction flow causing delay on their way to the ocean. The models differ most at the left approach bank where a current coming over the bank intersects the main current in the approach flow channel at an steep angle forming irregularities in the flow. The irregularities are not likely to affect the juvenile salmon as the irregularities do not affect the attraction flow significantly. To prevent negative impact during the operation of the power plant aforementioned abnormalities in the approach flow should be considered.

The attraction flow towards the SFO is extensive reaching far upstream and should guide the juvenile salmon in an safe and timely manner through the structures. Separation of flow between the spillway and intake and SFO is consistent between the physical and the numerical models. Results from a dye test conducted in the physical model and numerical model results indicate the SFO transporting water from depths ranging from 1 m to 2.7 m depending on project operation. The numerical model showed more distinct separation of streamlines at greater depth than the physical model where distinguishing the separation depth proved not trivial due to vortices scattering the dye vertically. The numerical model result show a smooth acceleration towards the SFO, the flow accelerates 1 m/s per meter over the last 2 m in front of the SFO. Maximum values in velocity magnitude of almost 3 m/s are observed at the SFO crests which should suffice to capture the juvenile salmon. During the migration period 91% of the juvenile salmon are expected to enter the SFO (Karadottir & Gudjonsson, 2012a).

The SFO model presents an estimation of the flow conditions inside the SFO conveyance channel. Water elevations are at maximum downstream of the upstream most entrances, Entrances 3 and 4, with water elevations higher than SFO crest elevation at discharges 40 m^3/s and 50 m^3/s. A distinct draw down is observed downstream of Entrance 1 where the width of the channel decreases. Because the flow regime is subcritical the contraction in the channel causes a draw down in water level. The flow conditions inside the conveyance channel are satisfactory and show the SFO design providing means of safe and timely passage of the juvenile salmon through the project.

The combination of numerical and physical models proves to be a valuable tool in the evaluation of a hydraulic design. The models strengthen each other and with good comparison between the models comes the opportunity to look into features in the numerical model which are hard or impossible to measure in the physical model. The good comparison also provides a calibrated tool that can be used after the physical model is no longer available.

References

ANSYS, I. (2011). Ansys cfx release 14.0 - theory guide [Computer software manual].

Antonsson, T., & Gudjonsson, S. (2002). Variability in timing and characteristics of atlantic salmon smolt in Icelandic rivers. *Transactions of the American Fisheries Society*, *131*, 643-655.

Bell, M. C. (1990). *Fisheries handbook of engineering requirements and biological criteria* (3rd ed.). U.S. Army Corps of Engineers, North Pacific Division.

Bureau of Reclamation, H. I., & Group, L. S. (2011). *Winadv - version 2.028.*

Coutant, C. C., & Whitney, R. R. (2000). Fish behavior in relation to passage through hydropower turbines: A review. *Transactions of the American Fisheries Society*, *129*(Iss.2), 351-380.

Fidler, L. E., & Miller, S. B. (1994, September). *British Columbia water quality guidelines for dissolved gas supersaturation.*

Goodwin, R. A. (2003). *Hydrodynamics and juvenile salmon movement behavior at Lower Grandite dam: Decoding the relationship using 3-d space-time (Cel Agent Ibm) Simulation*. Unpublished doctoral dissertation, Cornell University.

Goodwin, R. A., Nestler, J. M., Anderson, J. J., Weber, L. J., & Loucks, D. P. (2006). Forecasting 3-d fish movement behavior using a Eulerian-Lagrangian-Agne Method (ELAM). *Ecological modeling*, *192*, 197-223.

Goodwin, R. A., Nestler, J. M., Weber, L., Lai, Y. G., & Loucks, D. P. (2001). Ecologically sensitive hydraulic design for rivers: Lessons learned in coupled modeling for improved fish passage. In *Wetlands engineering and river restoration proceedings of wetlands engineering and river restoration conference 2001.*

Gudjonsson, S., & Johannesson, H. (2009). *Laxaseiði og hverflar Í virkjunum Í Neðri Þjórsá.* Landsvirkjun, Veiðimálastofnun.

Gudmundsson, A. (2013). *Model investigations of a juvenile fish bypass system at Urriðafoss hep, M.Sc. thesis, Faculty of Civil and Environmental Engineering, University of Iceland*.

Gudmundsson, A., Gardarsson, S. M., Tomasson, G. G., Gunnarsson, A., & Johannesson, H. (2012). Model investigation of a juvenile bypass system at Urridafoss hydroelectric project in Iceland. In *Hydro 2012,innovative approaches to global challenges, Bilbao, Spain.* The international journal on hydropower and dams.

Gunnarsson, A., Gardarsson, S. M., Tomasson, G. G., & Johannesson, H. (2012). Stilling basin length optimization for Hvammur hydro electric project. In *Proceedings from IAHR 2nd Europe Congress, Munich.*

Gunnarsson, A. (2012). *Physical model investigation on the Hvammur HEP spillway, M.Sc. thesis, Faculty of Environmental and Civil Engineering, University of Iceland.*

Haro, A., Odeh, M., Noreika, J., & Castro-Santos, T. (1998). Effect of water acceleration on downstream migratory behavior and passage of atlantic salmon smolts and juvenile american shad at surface bypasses. *Transactlons of the American Fisheries Society*, *127*(1), 118-127.

Helwig, L., Katzenberger, G., & Stensby, D. (1999). A new juvenile fish bypass system at bonneville dam. In *Waterpower '99 - hydro's future: Technology, markets, and policy proceedings of waterpower conference 1999.* ASCE.

Hirt, C. W., & Nichols, B. D. (1981). Volume of fluid (VOF) method for the dynamics of free boundaries. *Journal of Computational Physics*, *39*, 201-215.

Hrafnsdottir, H., & Freysteinsson, S. (2009). *Þjórsá River - South Iceland, Hvammur and Urriðafoss hydroelectric projects, ice jam evaluation. LV-2009/127.* Landsvirkjun.

The hydraulics of open channel flow: An introduction. (2004). Elsevier.

Johannsson, M., Jonsson, B., Ornolfsdottir, E. B., Gudjonsson, S., & Magnusdottir, R. (2002, September). *Rannsóknir á lífríki Þjórsár og þveráa hennar vegna virkjana neðan Búrfells.* Veiðimálastofnun. (Unnið fyrir Landsvirkjun)

Johnson, G. E. (2006). *Hydroacoustic evaluation of juvenile salmonid passage at the dalles dam sluiceway, 2005* (Tech. Rep.). Pacific Northwest National Laboratory.

Johnson, G. E. (2009). *Smolt responses to hydrodynamic conditions in forebay flow nets of surface flow outlets, 2007* (Tech. Rep.). Pacific Northwest National Laboratory.

Johnson, G. E., & Dauble, D. D. (2006). Surface flow outlets to protect juvenile salmonids. *Reviews in Fisheries Science*, *14*, 213-244.

Karadottir, O. R., & Gudjonsson, S. (2009). *Nth-60 Neðri Þjórsá minnisblað, málefni: Fiskvegir við Urriðafossvirkjun.* Landsvirkjun, Verkís, Veiðimálastofnun. (VERKNÚMER: 2007.0306)

Karadottir, O. R., & Gudjonsson, S. (2012a). *Nth-60 Neðri Þjórsá minnisblað, málefni: Seiðafleyta - stýring flóðgátta á göngutíma seiða.* Landsvirkjun, Verkís, Veiðimálastofnun. (VERKNÚMER: 11036-001)

Karadottir, O. R., & Gudjonsson, S. (2012b). *Nth-60 Neðri Þjórsá minnisblað, málefni: Seiðafleyta Urriðafossvirkjun - líkanprófanir.* Landsvirkjun, Verkís, Veiðimálastofnun. (VERKNÚMER: 11036-001)

Khan, L. A., Wicklein, E. A., Rashid, M., Ebner, L. L., & Richards, N. A. (2008). Case study of and application of a computational fluid dynamics model to the forebay of the dalles dam, oregon. *Journal of Hydraulic Engineering*, *134*(5), 509-519.

Landsvirkjun. (2010-2012). *Engineering drawings issued by the designers during the design phase of the project. (Drawings might be altered from original).* Supplied by Mannvit and Verkís Engineering.

Lee, H., Lin, C.-L., & Weber, L. J. (2008, July 1). Application of a nonhydrostatic model to flow in a free surface fish passage facility. *Journal of Hydraulic Engineering*, *134*(7).

Marchall, E., Mather, M., Parrish, D., Allison, G., & McMenemy, J. (2011). Migration delays caused by anthropogenic barriers: Modelling dams, temperature, and success of migrating salmon smolts. *Ecological Applications*.

Meselhe, E. A., & Odgaard, A. J. (1998). 3D numerical flow model for fish diversion studies at Wanapum Dam. *Journal of Hydraulic Engineering*, *124*(12), 1203-1214.

NOAA. (2008, February). *Anadromous salmonid passage facility design* (Tech. Rep.). Retrieved from `www.nwr.noaa.gov`

NRCS. (2007, August). *Technical supplement 14n, fish passage and screening design, part 654 of the National Engineering Handbook.*

Pfister, M., & Chanson, H. (2011). Scale effects in physical hydraulic engineering models. *Journal of Hydraulic Research*, *49*(3), 293-306.

Pickett, P. J., Rueda, H., & Herold, M. (2004, June). *Total maximum daily load for total dissolved gas in the Mid-Columbia river and Lake Roosevelt* (Tech. Rep.). Washington State Department of Ecology, U.S. Environmental Agency, Washington State Department of Ecology. (Submittal Report)

Schilt, C. R. (2006). Review: Developing fish passage and protection at hydropower dams. *Applied Animal Behaviour Science*.

Seear, P. J., Carmichael, S. N., Talbot, R., Taggart, J. B., Bron, J. E., & Sweeney, G. E. (2010). Differential gene expression during smoltification of atlantic salmon (salmo salar l.): A first large-scale microarray study. *Mar Biotechnol*, *12*, 126-140.

Sontek. (1997). *Acoustic Doppler Velocimeter technical documentation v.4.0.* San Diego, USA.

Sweeney, C. E., Hall, R., Giorgi, A. E., Miller, M., & Johnson, G. E. (2007, December). *Surface bypass program comprehensive review report* (Tech. Rep.). ENSR Corporation. (Prepared for U.S. Army Corps of Engineers, Portland District)

Tomasson, G. G., Gardarsson, S. M., & Gunnarsson, A. (2012). *Hvammur HEP Lower Þjórsá: Physical model investigation on the spillway and juvenile fish passage. Final report*. Landsvirkjun, LV-2012-111.

Tomasson, G. G., Gardarsson, S. M., Gunnarsson, A., Petursson, G. S., & Gudmundsson, A. (2013). *Urriðafoss HEP Lower Þjórsá: Physical model investigation on the spillway and juvenile fish passage. Final report*. Landsvirkjun, LV-2013-016.

Weber, L. J., Goodwin, R. A., Li, S., Nestler, J. M., & Anderson, J. J. (2006). Application of an eulerian lagrangian agent method(elam) to rank alternative designs of a juvenile fish passage facility. *Journal of Hydroinformatics*, *08.4*.

A. Memos from the Designers

NTH-60 URRIÐAFOSSVIRKJUN

MINNISBLAÐ

VERKNÚMER:	11036-001	DAGS.:	2012-08-29
VERKÞÁTTUR:	308 - Seiðafleyta	NR.:	
HÖFUNDUR:	Ólöf Rós Káradóttir Verkís og Sigurður Guðjónsson Veiðimálastofnun		
DREIFING:	Helgi Jóhannesson Landsvirkjun, KMS Verkís		

Málefni: Seiðafleyta – stýring flóðgátta á göngutíma seiða

Hér eru teknar saman forsendur um rekstur flóðvirkja við Heiðarlón sem byggja á niðurstöðum líkanprófana og virkni seiðafleytu við mismunandi rennslisaðstæður.

Skilgreindur göngutími laxaseiða er frá 15. maí til 15. júní og gert er ráð fyrir að á þeim tíma sé fleytan fullopin. Hönnunarrennsli um fleytu er 40 m^3/s. Þar sem lónið verður rekið í því sem næst fastri hæð og inntak í fleytu er um yfirfall, er rennslið um fleytuna undir venjulegum aðstæðum óháð innrennsli í lónið. Utan þess tíma sem vænta má göngu seiða er gert ráð fyrir að fleytan sé lokuð.

Líkanprófanir benda til að seiðafleyta nái yfirborðsrennsli í Heiðarlóni í streymi sem liggur að inntaki véla og því má ætla að seiði fari ekki um straumvélar svo lengi sem þau eru við yfirborð lónsins. Um 10 m frá yfirfallsþröskuldi fleytu á mörkum uppgötvunar- og ákvörðunarsvæðis er þykkt lagsins sem fer á fleytu meiri en 1 m.

Miðað við langæi miðlaðs rennslis í Heiðarlón sem byggir á mælingum frá 1950 til 2005 yrði ekkert rennsli um flóðgáttir 59 % tímans sem fleytan er opin og öll seiði færu þá um hana. Sé reiknað með að fjöldi seiða sé í réttu hlutfalli við rennsli og að þau gangi allan tímann sem fleytan er opin færu um 12 % seiða að flóðgáttum og 88 % um seiðafleytu.

Hér er meginforsenda að seiði gangi í réttu hlutfalli við rennsli, þannig gangi fleiri seiði í flóðum en í venjulegu rennsli. Þetta er afar varfærin nálgun, þ.e. fjöldi seiða sem ekki kemst í seiðafleytu er ofmetinn.

Sé reiknað með að seiði skiptist jafnt á tímabilið sem opið er, þ.e. að jafn mörg seiði fari á degi hverjum um lónið verður skiptingin þessi: 91 % um fleytu og 9 % að gáttum. Þessi forsenda er einnig varfærin þar sem seiði ganga almennt þegar vorflóðum lýkur og áin tekur að hlýna. Miðlun Þjórsár getur þó haft áhrif á þessa hegðun.

Við hönnun mannvirkja er lögð áhersla á að seiði tefjist ekki í Heiðarlóni og óæskilegt að þau verði innlyksa eins og t.d. við gáttir. Óhjákvæmilegt er að í miklu rennsli fari hluti seiða um gáttir og veltuþró en niðurstöður líkanprófana benda til að aðstæður við þær verði ólíkar eftir rennsli.

- Sé ekkert rennsli um flóðgáttir er svæði með straumleysu ofan við þær, finni seiði yfirborðsstraum leiðir hann þau að seiðafleytu,
- Sé rennsli minna en um 150 m^3/s um flóðgátt myndast straumleysa eða dautt svæði upp við hana sem seiði gætu orðið innlyksa í, þ.e. næsti yfirborðsstraumur leiðir þau aftur upp að gáttinni, straumur á meira dýpi liggur hins vegar undir gátt í veltuþró,
- Sé rennsli á bilinu 150 – 400 m^3/s myndast straumleysa upp við gátt, en skv. líkani sogast agnir í yfirborði þar undir gáttina með hvirflum,
- Sé rennsli meira en um 400 m^3/s um flóðgátt liggur allur straumur að gáttinni undir hana og í veltuþró.

Ef allar gáttir væru jafnt opnar á seiðagöngutíma má reikna með að 8 - 11 % seiða gætu orðið innlyksa við gáttir en um 1 % færu um gáttir í veltuþró.

Minnst hlutfall seiða verður innlyksa ef tíminn sem minna rennsli en 150 m^3/s er um hverja gátt verður lágmarkaður. Við slíka stýringu væri hægt að minnka hlutfall seiða sem gætu orðið innlyksa við gáttir úr 8 – 11 % í 4-5 %. Þeim sem eftir eru mætti mögulega koma úr lóninu með öðrum aðgerðum, s.s. aukafleytu frá gátt næst fleytu og inn í fleytustokk.

Verkís hf.
Ármúla 4, 108 Reykjavík
422 8000
verkis.is | verkis@verkis.is

Starfstöðvar:
108 Reykjavík, Ármúla 4-6
108 Reykjavík, Suðurlandsbraut 4

300 Akranes, Stillholti 18
310 Borgarnes, Bjarnarbraut 8
400 Ísafjörður, Hafnarstræti 1

603 Akureyri, Austursíðu 2
700 Egilsstaðir, Kaupvangi 3b
800 Selfoss, Austurvegi 10

Eftirfarandi takmarkanir á stýringum flóðvirkja væri æskileg frá 15. maí til 15. júní þegar seiðafleytan er opin:

1) **Allt rennsli umfram virkjað og fleytu fari um eina flóðgátt en hinar tvær verði lokaðar eins og kostur er,**
2) **ef umframrennsli er svo mikið að opna verður fleiri gáttir, verði minna en 150 m^3/s rennsli aðeins um eina gátt.**

Líkanprófanir sýna að vegna rennslisaðstæðna í veltuþró sé ekki æskilegt að meira en 200 m^3/s fari um gátt næst fleytu ef hinar tvær eru lokaðar.

Verði gerð aukafleyta frá einni gátt, ætti sú gátt að vera sú eina sem er með minna rennsli en 150 m^3/s á seiðafleytutíma. Útlit er fyrir að hentugast yrði að koma slíkri aukafleytu fyrir í gátt næst seiðafleytu.

1 Minna rennsli um fleytu

Með líkanprófum hefur verið sýnt fram á að seiðafleyta sem flytur 40 m^3/s uppfyllir hönnunarforsendur sem settar eru fram í minnisblaði 11036001-1-MB-0040 hvað varðar aðstæður í lóni. Jafnframt hefur verið sýnt fram á að fleyta með 20 m^3/s rennsli þar sem yfirfallsþröskuldur er áfram yfir öllu inntaki en dýpi minna á þröskuldinum virkar eins, en skilyrði um 2,5 m/s lágmarkshraða næst fleytunni yrði ekki uppfyllt.

Tilraunir sýna jafnframt að til að yfirborðsstraumur sem liggur í átt að vélum fari allur um seiðafleytu verða öll fjögur yfirfallsop fleytunnar að vera opin, þ.e. ef einu bili er lokað, fer hluti yfirborðsstraums í vélainntak.

Með minna rennsli um seiðafleytu en hönnunarrennsli gæti virkni hennar minnkað, hvort sem yfirfallsþröskuldur er hækkaður, lækkað er í lóni, eða lok sett fyrir eitt eða fleiri af yfirfallsopum.

2 Lengra opnunartímabil

Seiðafleytutímabilið miðast við líklegan göngutíma laxaseiða en ganga sjóbirtings hefst jafnan fyrr. Í árum þegar vatnsbúskapur Landsvirkjunar leyfir væri því æskilegt að seiðafleyta væri alveg opin eða að hluta allt frá byrjun apríl. Langæi miðlaðs rennslis er sýnt á mynd 1. Rennsli er umfram virkjað rennsli og sírennsli um 6 % aprílmánaðar, um 17 % fyrri hluta maí og 53 % á skilgreindum göngutíma laxaseiða 15. maí – 15. júní. Þannig er ekki mikið svigrúm fyrir fullopna seiðafleytu að jafnaði í apríl og fyrri hluta maímánaðar.

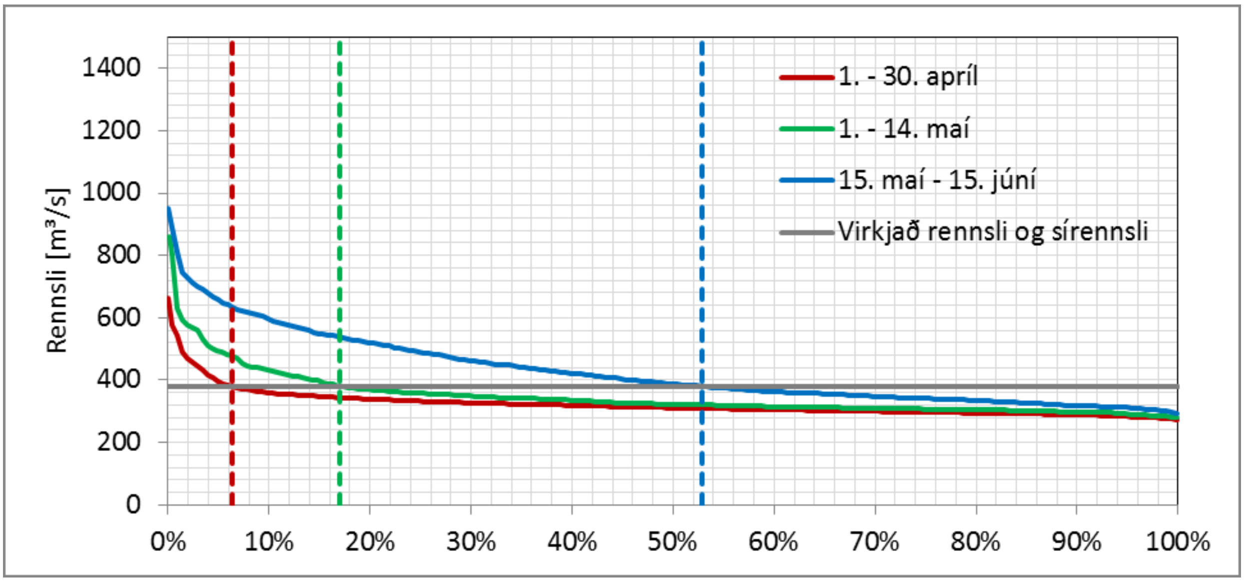

Mynd 1 Langæi miðlaðs rennslis í Heiðarlón byggt á mælingum frá 1950 – 2005. Brotalína sýnir hlutfall tímans sem rennsli er meira en virkjað rennsli og sírennsli

NTH-60 URRIÐAFOSSVIRKJUN

MINNISBLAÐ

VERKNÚMER:	11036-001	DAGS.:	2012-05-16
VERKÞÁTTUR:	308 - Seiðafleyta	NR.:	
HÖFUNDUR:	Ólöf Rós Káradóttir Verkís og Sigurður Guðjónsson Veiðimálastofnun		
DREIFING:	Helgi Jóhannesson Landsvirkjun		

Málefni: Seiðafleyta Urriðafossvirkjun - líkanprófanir

Hér eru endurskoðaðar hönnunarforsendur seiðafleytu sem settar voru fram í minnisblaði Verkíss og Veiðimálastofnunar árið 2009[1]. Endurskoðunin tekur m.a. mið af minnisblaði frá HÍ[2]. Einnig eru settar fram forsendur fyrir líkanprófanir á seiðafleytu í Urriðafossi sem lýst er nánar í drögum að samningi um líkanprófanir vegna virkjana í Neðri Þjórsá[3]. Ágúst Guðmundsson HÍ vinnur að gerð tölulegs líkans af Heiðarlóni sem nota má við frekari greiningar á rennsli en unnt er með líkanprófunum.

Mikilvægt er að seyðafleyta virki vel í Urriðafossvirkjun. Ofan virkjunarinnar eru um 88 % af öllum laxabúsvæðum árinnar eftir opnum laxastiga í Búðafossi. Með seiðafleytu er laxagönguseiðum og niðurgöngusilungi forðað frá því að fara í gegnum vélar sem veldur einhverjum afföllum en ekki síður frá því að tefjast eða verða innlyksa í inntakslóni Urriðafossvirkjunar, Heiðarlóni. Slík töf getur valdið miklum afföllum því seiðin viðhalda sjóþroska einungis í nokkrar vikur. Ef þau eru tafin lengur en sem því nemur að komast til sjávar er úti um flest þeirra.

Seiðafleyta fyrir laxfiska byggir á því atferli niðurgönguseiða og fisks að hann gengur í meginstraumi yfirborðsvatns. Sé hindrun á vegi hans reynir fiskur að fara yfir þá hindrun. Sé slíku yfirfalli komið fyrir ofan við inntak virkjunar, það er í sömu straumstefnu, eru miklar líkur á að yfirborðsvatni og fiski þar með sé fleytt yfir yfirfallið í seiðafleyturennuna og þaðan niður í ána fyrir neðan.

Kappkostað verður að hönnun lóns, stíflumannvirkja, vatnsinntaks virkjunar og seiðafleytu verði sem best verður á kosið fyrir niðurgönguseiði og fisk.

Eftir virkjun er mikilvægt að gera mælingar á raunvirkni seiðafleytu með merkingum seiða (útvarpsmerki, hljóðmerki, segulmerki) sem fara í gegnum lón og niður fyrir virkjun.

1 Hönnunarforsendur seiðafleytu

Við hönnun Urriðafossvirkjunar er reynt með seiðafleytu að komast hjá því að seiði fari um vélar eða verði innlyksa í lóni. Inntak fleytunnar er staðsett yfir inntaki virkjunarinnar og á að ná yfirborðsstraumi í lóninu þar sem talið er að seiðin haldi sig. Reynt verður að tryggja að sem mest af seiðunum úr efsta lagi meginstraumsins fari um fleytuna. Í flóðum rennur einnig um flóðgáttir, liggur þá straumur þangað og hluti seiðanna fer um þær áfram í farveginn.

Aðrennsli að seyðafleytu er skipt í aðkomusvæði (e. approach zone) sem er 100 – 1000 m frá inntaki í fleytuna, uppgötvunarsvæði (e. discovery zone) 10 - 100 m frá inntaki og ákvörðunarsvæði (e. decision zone) 1 – 10 m frá inntaki[4].

---

1 Minnisblað ME-VST/ÓRK-008, dags. 2009-01-16. Málefni: Fiskvegir við Urriðafossvirkjun. Höfundar: Ólöf Rós Káradóttir og Sigurður Guðjónsson.

2 Drög að minnisblaði, dags. 2011-11-08. Málefni: Hönnunarforsendur seiðafleytu í Urriðafossvirkjun. Höfundar: Ágúst Guðmundsson og Sigurður Magnús Garðarsson.

3 Verkís og Mannvit, drög 2010-01-22. Lower Þjórsá Hydroelectric Projects. Contract documents NTH-81. Hydraulic model tests. Spillways at Hvammur and Urriðafoss. LV-2008/102.

4 Johnson et al., 2006. Surface Flow Outlets to Protect Juvenile Salmonids Passing Through Hydropower Dams. Reviews in Fisheries Science, 14:213-244.

Verkís hf.
Ármúla 4, 108 Reykjavík
422 8000
verkis.is | verkis@verkis.is

Starfstöðvar:
108 Reykjavík, Ármúla 4-6
108 Reykjavík, Suðurlandsbraut 4

300 Akranes, Stillholti 18
310 Borgarnes, Bjarnarbraut 8
400 Ísafjörður, Hafnarstræti 1

603 Akureyri, Austursíðu 2
700 Egilsstaðir, Kaupvangi 3b
800 Selfoss, Austurvegi 10

Forsendur hönnunar eru:

- meginyfirborðsstraumur innan aðkomusvæðis liggi að seiðafleytu
- gerð og stærð fleytuinntaks ræðst af því hversu djúpur og breiður inntaksþröskuldur þarf að vera til að allt rennsli innan uppgötvunar- og ákvörðunarsvæðis frá yfirborði niður í um 1 m dýpi fari í seiðafleytuna
- rennsli sé sem jafnast að seiðafleytu, hröðun jákvæð og að hámarki 1 m/s^2 innan ákvörðunarsvæðis[5]
- rennslishraði 0 – 1 m í lóni ofan yfirfalls sé ekki minni en 2,5 m/s
- ekki verði dauðir pollar eða svæði með iðustraumi í yfirborði þar sem seiði geti orðið innlyksa
- seiði og fiskur sem komin eru yfir yfirfall í seiðafleytu eigi ekki afturkvæmt upp í lónið
- vatnshraði í seiðafleytu sé sem jafnastur
- frítt rennsli sé í seiðafleyturennu
- engar fyrirstöður séu í seiðafleytu sem geti skaðað seiði.

2 Rennsli

Ganga seiða í Þjórsá hefst yfirleitt um miðjan maí og stendur fram í miðjan júní. Hún er háð hitastigi árinnar og er því oft á svipuðum tíma og vorleysingar með tilheyrandi flóðum. Á mynd 1 er sýnt áætlað langæi miðlaðs rennslis við Urriðafoss fyrir tímabilið frá 15. maí til 15. júní, byggt á mælingum frá 1950 til 2005. Með röðinni má finna líklegustu dreifingu rennslis á þessu tímabili inn í lónið, hún sýnir ekki útmörk rennslis s.s. hönnunarflóð, sem ekki hafa mælst í ánni á því tímabili sem liggur til grundvallar.

Bent er á að flóð geta orðið stærri og innrennsli minna en langæi gefur til kynna. Ætla má að um 41 % tímabilsins sem seiðafleytan er opin verði rennsli um flóðgáttir og 1 % tímabilsins verði meira rennsli um flóðgáttir en um vélar.

Reiknað er með að rennsli um seiðafleytu verði mest um 40 m^3/s og sírennsli um sérstaka rás í stíflu og laxastiga verði samtals 10 m^3/s.

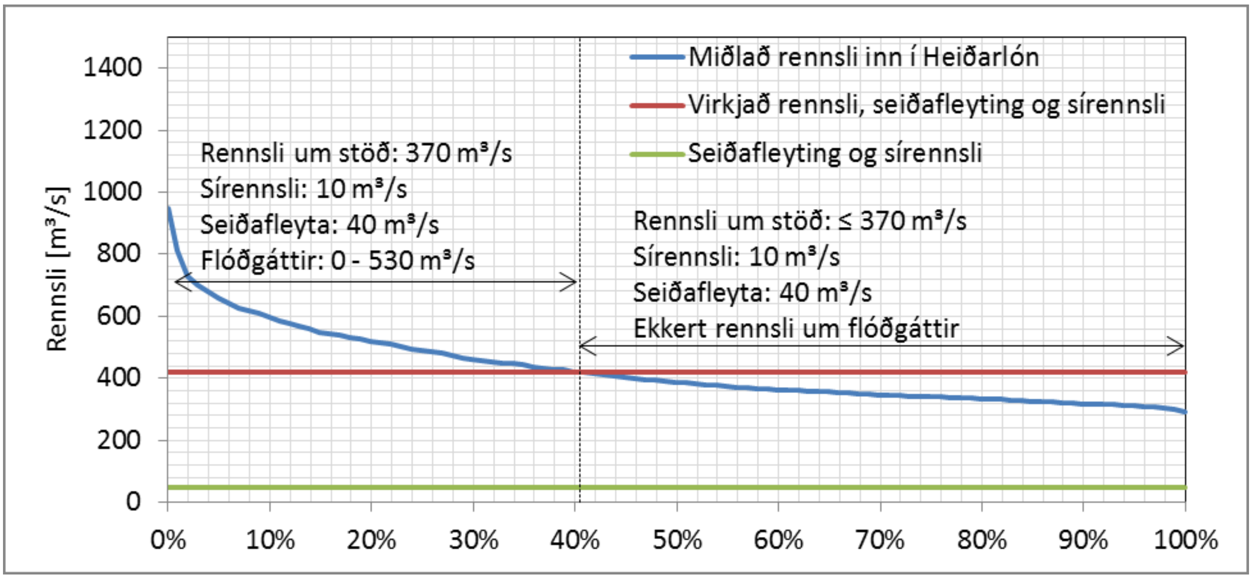

Mynd 1 Langæi miðlaðs rennslis í Heiðarlón frá 15. maí til 15. júní – byggt á mælingum frá 1950 til 2005

[5] Sweeney et al., 2007. Surface Bypass Program. Comprehensive Review Report. ENSR/AECOM.

3 Líkanprófanir

Í köflum 0 til 3.3 í þessu minnisblaði er lýst líkanprófunum þar sem rennslisaðstæður eru skoðaðar við mismunandi rennsli um yfirfall og vélar.

Hvorki er gert ráð fyrir að sírennsli um veitu, sem liggur djúpt í vesturenda meginstíflu, né rennsli um laxastiga, sem opnast við yfirborð á svipuðum stað, hafi áhrif á yfirborðslag straums. Samtals er rennsli þar um 10 m^3/s. Sírennsli er því dregið frá langæiskúrfu á myndum 3 – 6.

Ganga þarf þannig frá s.k. „flow straighteners“, sem ætlað er að jafna og beina flæði í líkaninu sem réttast að flóðvirkjum, að áhrifa frá þeim gæti ekki við efsta mælisnið (um 200 m frá inntaki við austurenda).

Rennslisprófanir fara fram með litarefni en lagt er til að jafnframt verði fljótandi agnir settar í líkanið til að kanna mögulega staði þar sem seiði gætu tafist verulega eða orðið innlyksa, sér í lagi nálægt flóðgáttum.

Gert er ráð fyrir að fulltrúi Veiðimálastofnunar og hönnuða fylgist með líkanprófunum á seiðafleytu og rennslisaðstæðum þar og viðbótarpróf verði framkvæmd óski þeir þess.

Í prófunum þar sem seiðafleyta er opin (kaflar 0 - 3.3) er eftirfarandi athugað og mælt eftir atvikum og eftir því sem hægt er, staðsetning mælisniða eru sýnd á mynd 1:

- Rennsli inn í seiðafleytu (m^3/s)
- Hversu djúpt og vítt er yfirborðslagið sem fer um seiðafleytuna (m x m) og hver er straumhraði þar (m/s)
    - innan aðkomusvæðis, um 200 m frá inntaki við austurenda aðrennslisrásar að mannvirkjum
    - á mörkum aðkomusvæðis og uppgötvunarsvæðis, 100 m frá inntaki
    - innan uppgötvunarsvæðis, 20 m frá inntaki.
    - á mörkum uppgötvunarsvæðis og ákvörðunarsvæðis, 10 m frá inntaki
    - innan ákvörðunarsvæðis, 1 m frá inntaki.
- Hversu djúpt og vítt er yfirborðslagið sem fer um flóðgáttir (m x m) og hver er straumhraði þar (m/s)
    - innan aðkomusvæðis, um 200 m frá inntaki við austurenda aðrennslisrásar að mannvirkjum
    - á mörkum aðkomusvæðis og uppgötvunarsvæðis, um 100 m frá inntaki.
- Eru svæði með iðum eða dauð svæði þar sem seiði gætu orðið innlyksa?
    - skoða sérstaklega aðstæður við flóðgáttir
    - skoða sérstaklega aðstæður á milli flóðgátta og seiðafleytuinntaks.
- Eru svæði með snöggum hraðabreytingum?
    - skoða sérstaklega aðstæður í aðrennsli ofanvert við inntak í seiðafleytu.

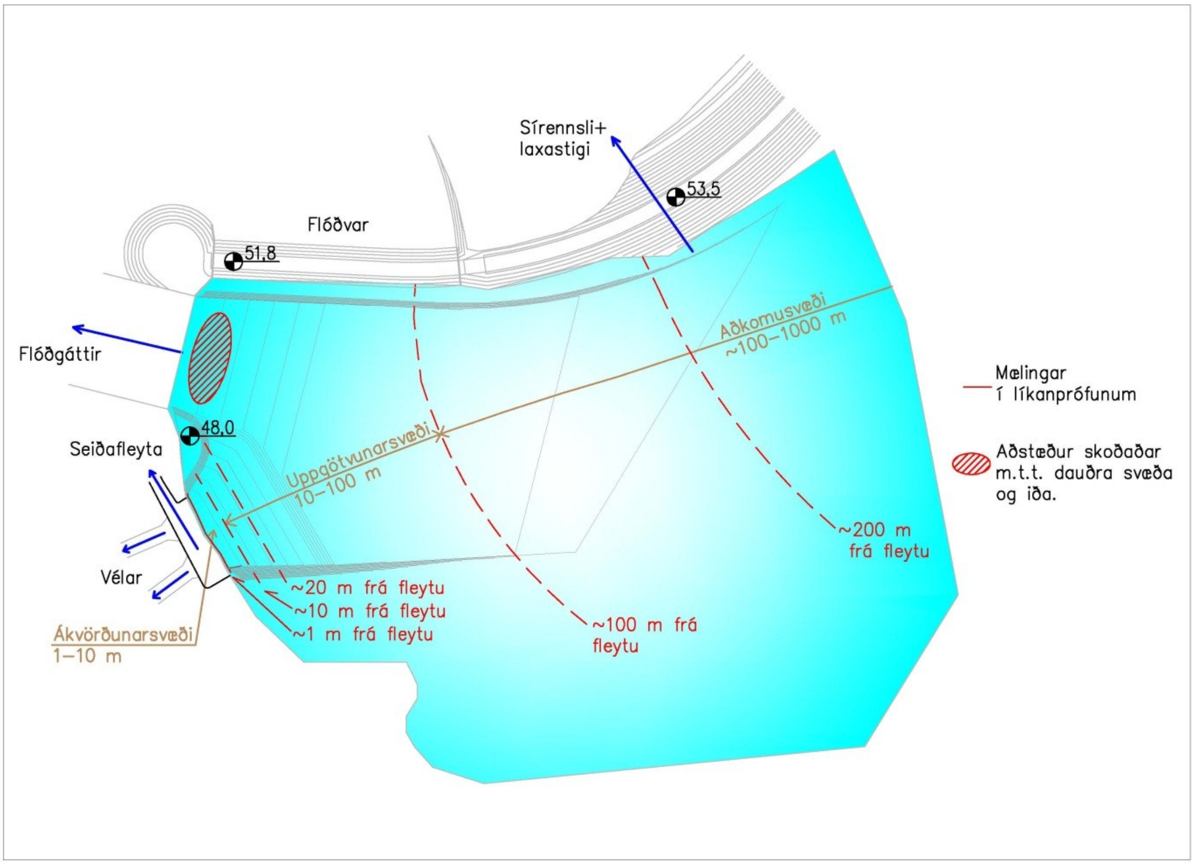

Mynd 2 Heiðarlón við rennslisvirki – mælisnið í líkanprófunum sýnd með rauðu

3.1 Venjulegur rekstur

Hér eru skoðaðar rennslisaðstæður við venjulegan rekstur á göngutíma seiða, þ.e. þegar aflvélar eru í gangi og lón er í 50,0 m y.s.

3.1.1 Fast:

Lónhæð 50,0 m y.s. (u.þ.b. 40 m^3/s um seiðafleytu)

3.1.2 Breytilegt:

Rennsli um vélar 370 m^3/s eða minna ef innrennsli ekki nægilegt
Rennsli um flóðgáttir

Nr.	Rennsli um vélainntak	Rennsli um flóðgáttir	Heildarrennsli	Hlutfall tímans sem rennsli er jafnt eða meira	Hlutfall heildarrennslis um seiðafleytu
	[m^3/s]	[m^3/s]	[m^3/s]		
1.1	240	0	280	99,9%	14%
1.2	370	0	410	41%	10%
1.3	370	70	480	25%	8%
1.4	370	235	645	5%	6%
1.5	370	515	925	0,1%	4%

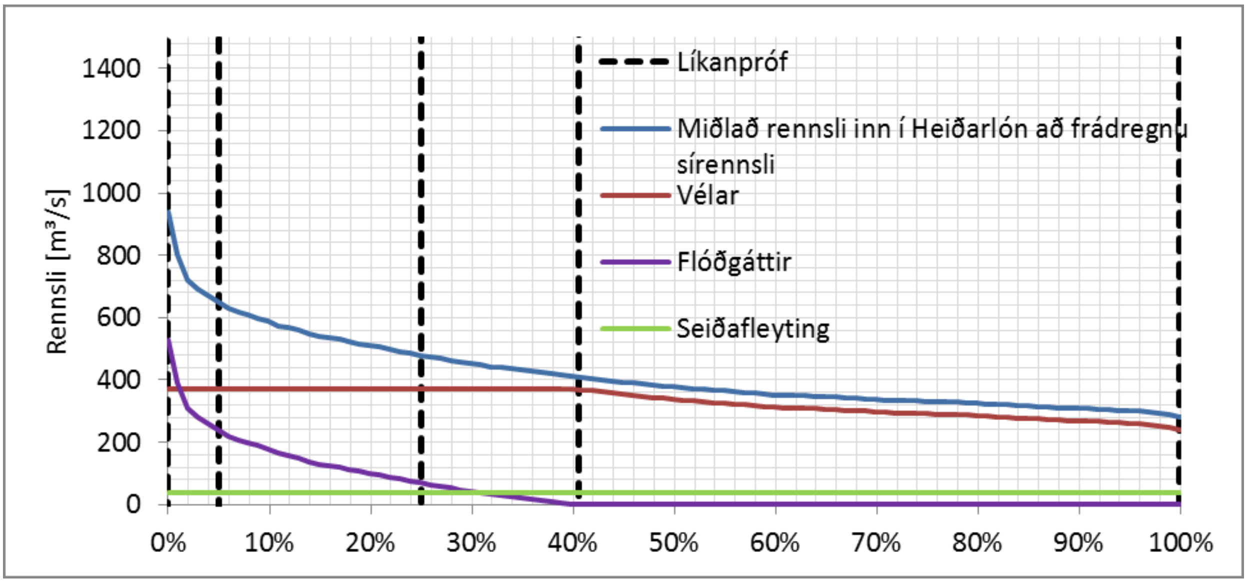

Mynd 3 Líkanprófanir 1

3.2 Bilun

Hér eru skoðaðar rennslisaðstæður þegar vélar eru ekki í gangi og flóðgáttir opnar. Viðhald á vélum verður ekki leyft á niðurgöngutíma seiða. Því væri um bilun að ræða og þessar aðstæður því fremur ólíklegar.

3.2.1 Fast:

Lónhæð 50,0 m y.s. (rennsli um seiðafleytu um 40 m^3/s)

3.2.2 Breytilegt:

Rennsli um flóðgáttir

Nr.	Rennsli um flóðgáttir	Heildarrennsli	Hlutfall tímans sem rennsli er jafnt eða meira	Hlutfall heildarrennslis um seiðafleytu
	[m^3/s]	[m^3/s]		
2.1	260	300	95%	13%
2.2	335	375	50%	10%
2.3	605	645	5%	6%

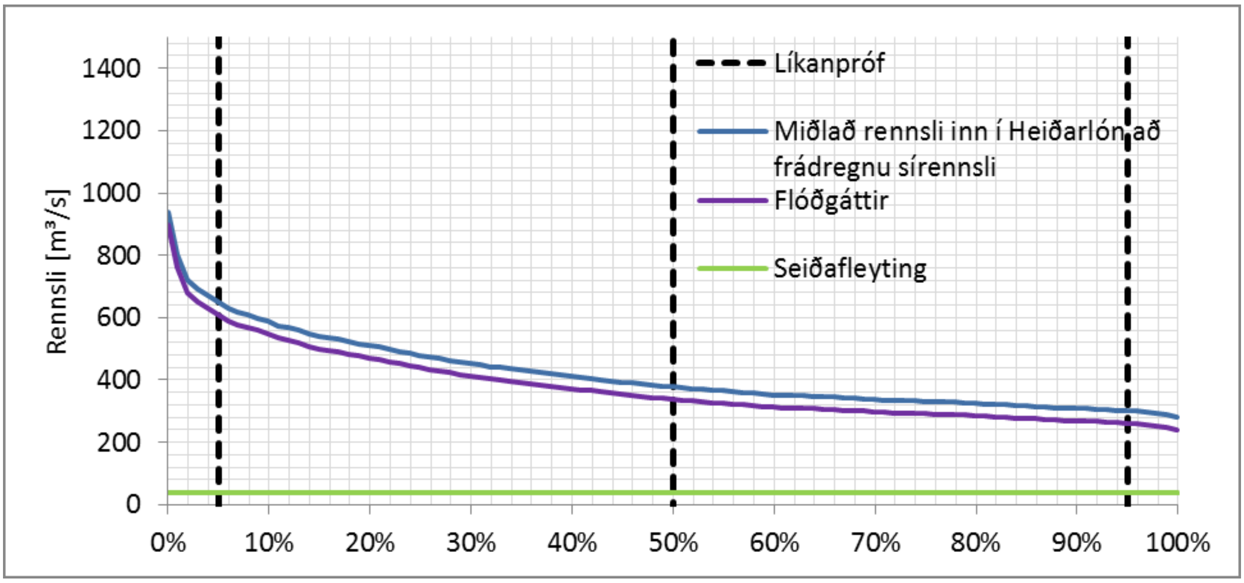

Mynd 4 Líkanprófanir 2

3.3 Lægra í lóni og aflvélar í gangi

Til greina kemur að lækka í lóninu við lítið innrennsli og minnka þannig rennsli um seiðafleytu. Hér eru skoðaðar rennslisaðstæður þegar vélar eru í gangi, minna rennsli fer um seiðafleytu og ekkert um flóðlokur.

3.3.1 Fast:

Lónhæð 49,7 m y.s. og yfirfallsþröskuldur í 49,1 m y.s. (rennsli um seiðafleytu u.þ.b. 20 m^3/s)
eða
lónhæð í 50,0 m y.s. og yfirfallsþröskuldur í 49,4 m y.s. (rennsli um seiðafleytu u.þ.b. 20 m^3/s)

3.3.2 Breytilegt:

Rennsli um vélar

Nr.	Rennsli um vélainntak	Heildarrennsli	Hlutfall tímans sem rennsli er jafnt eða meira	Hlutfall heildarrennslis um seiðafleytu
	[m^3/s]	[m^3/s]		
3.1	260	280	99,9%	7%
3.2	370	390	46%	5%

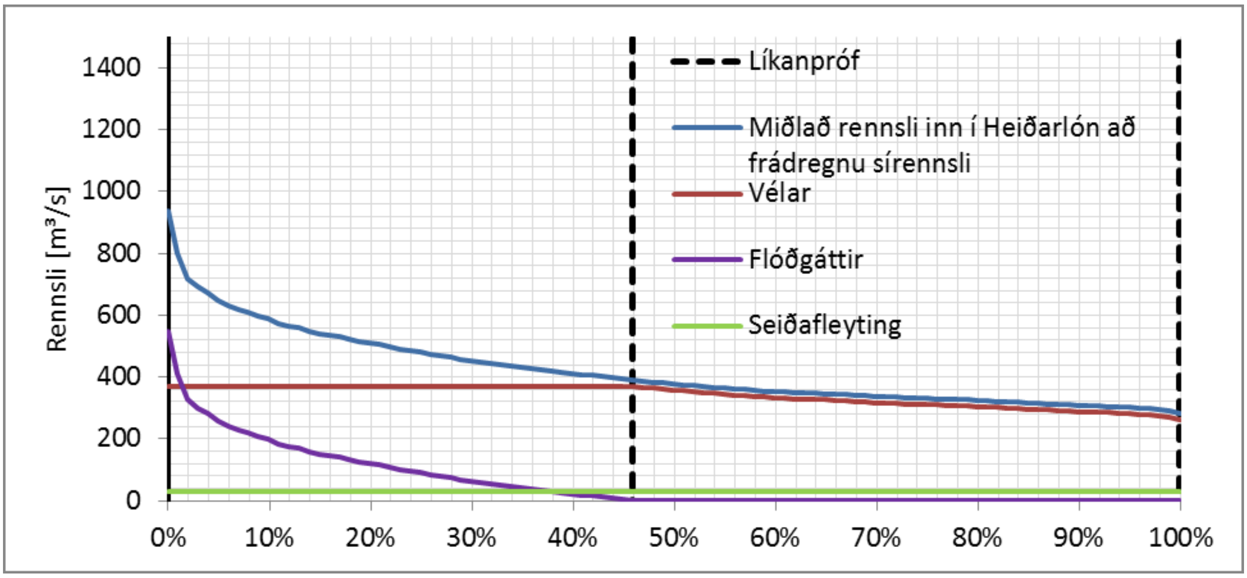

Mynd 5 Líkanprófanir 3

3.4 Seiðafleyta lokuð

Þar sem seiðafleytu verður lokað með geiraloku í rennu neðanvert við inntak utan niðurgöngutíma seiða, er vatn í fleytunni neðan yfirfalls og ofan loku stærstan hluta ársins. Rennslisaðstæður eru skoðaðar til að ákveða hvort verja þurfi mannvirki sérstaklega þegar fleyta er lokuð.

Hér eru skoðaðar aðstæður inni í seiðafleytu neðanvert við inntak við lónhæð 50,0 m y.s. og 49,7 m y.s.

3.4.1 Fast:

Lónhæð 50,0 m y.s.

Rennsli um vélar 370 m^3/s

3.4.2 Breytilegt:

Rennsli um flóðgáttir

Nr.	Rennsli um vélainntak	Rennsli um flóðgáttir	Heildarrennsli	Hlutfall tímans sem rennsli er jafnt eða meira
	[m^3/s]	[m^3/s]	[m^3/s]	
4.1	370	0	370	53%
4.2	370	275	645	5%

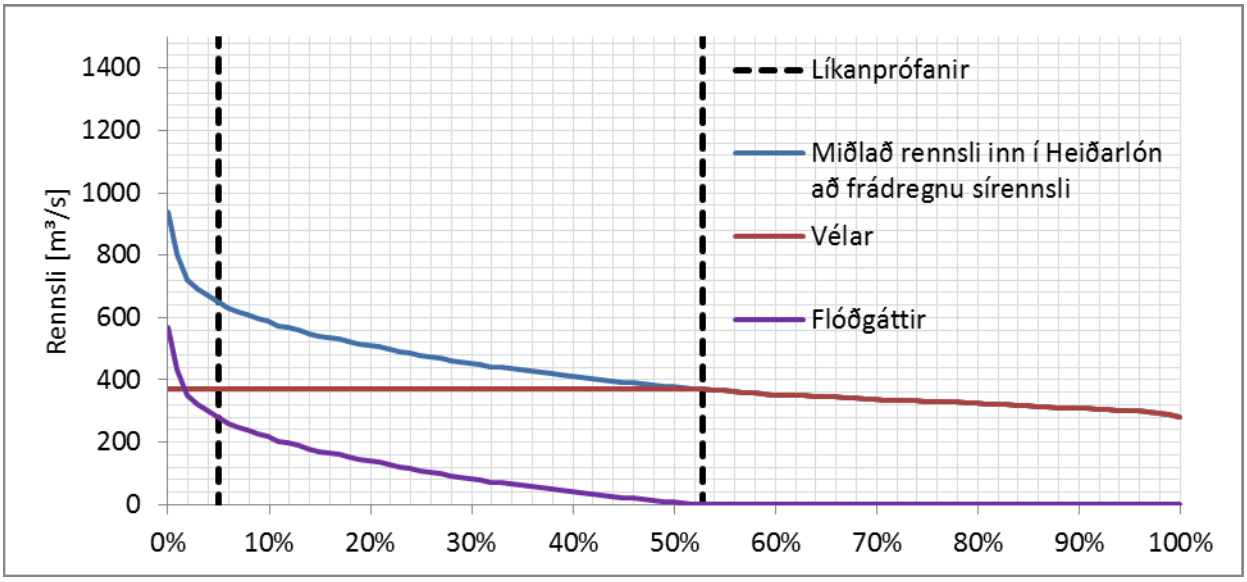

Mynd 6 Líkanprófanir 3

3.5 Sírennsli við flóðgáttir

Leiði líkanprófanir í ljós s.k. dauð svæði við flóðgáttir þar sem seiði gætu tafist eða orðið innlyksa verða gerð próf þar sem sírennsli sem flytti allt að 5 m^3/s væri komið fyrir við annan enda flóðgátta.

Landsvirkjun

Háaleitisbraut 68
103 Reykjavík
landsvirkjun.is

landsvirkjun@lv.is
Sími: 515 90 00